# HUWE1 coordinates RNAPII-dependent ATM signaling at collisions with replication forks

**Dissertation**

der Mathematisch-Naturwissenschaftlichen Fakultät

der Eberhard Karls Universität Tübingen

zur Erlangung des Grades eines

Doktors der Naturwissenschaften

(Dr. rer. nat.)

vorgelegt von

Elias Einig

aus Tübingen

Tübingen

2023

Gedruckt mit Genehmigung der Mathematisch-Naturwissenschaftlichen Fakultät der Eberhard Karls Universität Tübingen.

| | |
|---|---|
| Tag der mündlichen Qualifikation: | 18.10.2023 |
| Dekan: | Prof. Dr. Thilo Stehle |
| 1. Berichterstatter/-in: | Prof. Dr. Boris Maček |
| 2. Berichterstatter/-in: | Prof. Dr. Nikita Popov |
| 3. Berichterstatter/-in: | Prof. Dr. Jennifer Ewald |

# Table of contents

# 1 Summary

Oncogenic signaling deregulates RNA polymerase II (RNAPII) dependent transcription programs, which can lead to collisions of the transcription machinery with DNA replication complexes (transcription replication conflicts, TRCs). Although encounters of both machineries are thought to be frequent events at very long genes and may be readily resolved in healthy cells, perturbation of transcription or TRC-coordinating mechanisms can result in deleterious DNA damage. TRC-induced DNA damage is thought to underlie genomic instability in cancer cells. Both, transcription and replication, involve ubiquitin-dependent regulation of effector proteins. Previous studies highlighted the importance of the ubiquitin ligase HUWE1 in controlling RNAPII-dependent transcription through regulation of transcription factors, including MYC, TP53 and β-catenin. Furthermore, HUWE1 is involved in the control of DNA replication through interaction with the DNA sliding clamp PCNA, the replication factor CDC6 and it facilitates recovery from replication stress. In this study, I characterize the effect of the HUWE1 ubiquitin ligase function on conflicts between the transcription and DNA replication machineries and the influence of HUWE1 on DNA damage response (DDR) signaling and maintenance of genome integrity. Genetic inhibition of the ubiquitin ligase by mutation of the catalytic cysteine in the HUWE1-HECT domain shows that HUWE1 is required for the resolution of TRCs and suppression of DDR signaling via the ATM kinase. I identify the ATPase WRNIP1 is a novel interaction partner of HUWE1 and as critical effector protein to protect stalled replication forks at TRCs from collapse into severe double strand breaks. Catalytic activity of HUWE1 promotes the association of WRNIP1 with elongating RNAPII. Inactivation of HUWE1 or depletion of WRNIP1 results in elevated levels of TRCs without physical DNA breaks, but induces activation of ATM. Interestingly, the MRN complex, that is required for ATM recruitment to DNA double strand breaks, associates with elongating RNAPII in unperturbed cells. Consequently, elongating RNAPII is poised for ATM recruitment and activation at encounters with stalled replication forks or at TRCs. Upon induction of replication stress or catalytic mutation of HUWE1, WRNIP1 transfers from RNAPII to bind to the DNA replication machinery. This transfer likely enables ATM recruitment to RNAPII and protection of replication forks. Inhibition of RNAPII prior to induction of replication stress diminishes TRCs, impairs ATM signaling, abolishes DNA repair and results in severe growth defects.

Taken together, the HUWE1 ubiquitin ligase and its effector WRNIP1 coordinate transcription and DNA replication to jointly resolve TRCs and redundantly stabilize replication forks. This coordination maintains genome integrity and facilitates cell proliferation. Further, this work suggests that contrary to the common perception of TRCs as a cause of genome instability, a conflict may provide a rescue mechanism in response to replication stress, since it enables RNAPII-dependent, preemptive ATM signaling to facilitate DNA repair.

# 2 Zusammenfassung

Onkogene Signalwege deregulieren die Transkription durch die RNA-Polymerase II (RNAPII), was zu Kollisionen der Transkriptionsmaschinerie mit DNA-Replikationskomplexen (Transkriptions-Replikations-Konflikte, TRCs) führen kann. Obwohl davon ausgegangen wird, dass das Zusammentreffen beider Komplexe bei sehr langen Genen häufig vorkommt und in gesunden Zellen leicht aufgelöst werden kann, führt eine Störung der Transkription oder Mechanismen zur Prävention von TRCs zu toxischen DNA-Schäden. Es wird angenommen, dass TRC-induzierte DNA-Schäden der genomischen Instabilität in Krebszellen zugrunde liegen. Sowohl Transkription als auch Replikation werden durch Ubiquitinierung von Effektorproteinen reguliert. Frühere Studien haben die Bedeutung der Ubiquitin-Ligase HUWE1 für die Kontrolle der RNAPII-abhängigen Transkription durch die Regulierung von Transkriptionsfaktoren wie MYC, TP53 und β-Catenin verdeutlicht. Darüber hinaus reguliert HUWE1 die DNA-Replikation, beispielsweise durch Interaktion mit der DNA-Klemme PCNA und dem Replikationsfaktor CDC6 und erleichtert damit die Erholung von Replikationsstress. In dieser Studie charakterisiere ich die Auswirkungen der HUWE1-Ubiquitin-Ligase Funktion auf die Konflikte zwischen den Transkriptions- und Replikationskomplexen und ihren Einfluss auf die DNA-Schadenssignalantwort und damit die Aufrechterhaltung der Genomintegrität. Die genetische Hemmung von HUWE1 durch Mutation des katalytischen Cysteins in der HUWE1-HECT-Domäne zeigt, dass HUWE1 für die Auflösung von TRCs und die Hemmung der ATM-abhängigen DNA-Schadenssignalantwort erforderlich ist. Die ATPase WRNIP1 ist ein neu identifizierter Interaktionspartner und Effektor von HUWE1, welcher entscheidend dazu beiträgt blockierte Replikationsgabeln und TRCs vor dem Zusammenbruch zu DNA Doppelstrangbrüchen zu schützen. Die katalytische Aktivität von HUWE1 fördert die Assoziation von WRNIP1 mit aktiver RNAPII. Die Inaktivierung von HUWE1 oder die Depletion von WRNIP1 führen zu einer erhöhten Menge von TRCs ohne physische DNA-Brüche, jedoch wird die DNA-Schadenssignalkinase ATM aktiviert. Interessanterweise assoziiert der MRN-Komplex, der für die Rekrutierung von ATM zu DNA-Doppelstrangbrüchen erforderlich ist, auch in ungestörten Zellen mit transkribierender RNAPII. Folglich ist die aktive RNAPII in der Lage ATM zu rekrutieren und zu aktivieren während möglicher Kollisionen mit Replisomen oder an TRCs. Replikationsstress oder katalytische Mutation von HUWE1 führt zum WRNIP1-Transfer von RNAPII zur DNA-Replikationsmaschinerie. Diese Ergebnisse weisen darauf hin, dass der WRNIP1-Transfer die Rekrutierung von ATM zu RNAPII und den Schutz von Replikationsgabeln ermöglicht. Die Hemmung von RNAPII gefolgt von Replikationsstress vermindert TRCs, beeinträchtigt die ATM-Signalkaskade, hemmt die DNA-Reparatur und führt zu schweren Zell-Wachstumsdefekten.

Alles in allem koordinieren die HUWE1-Ubiquitin-Ligase und ihr Effektor WRNIP1 die Transkription und die DNA-Replikation, um gemeinsam TRCs aufzulösen und einen möglichen Konflikt redundant zu stabilisieren, damit die Integrität des Genoms erhalten bleibt und effiziente Zellproliferation möglich ist. Darüber hinaus zeigt diese Arbeit, dass, entgegen der allgemeinen Auffassung von TRCs als Ursache von Genominstabilität, ein Konflikt möglicherweise einen Rettungsmechanismus als Reaktion auf Replikationsstress darstellen kann, da TRCs eine RNAPII-abhängige, präventive ATM-Aktivierung zur Erleichterung der DNA-Reparatur ermöglichen.

# 3 Introduction

## 3.1 Cancer development

With an estimated prevalence of more than 19 million cases worldwide and about 10 million fatalities in the year 2020, cancer is a leading cause of death in the majority of countries (Sung et al., 2021). A major challenge in cancer research, as well as for clinical treatment options is the daunting plasticity of cancer regarding its origin, course of disease, severity and treatment escape capabilities.

Even though virtually any tissue in the human body may serve as an origin of cancerous cells, most, if not all cancers share a similar set of acquired capabilities and enabling characteristics (Hanahan and Weinberg, 2000, Hanahan and Weinberg, 2011, Hanahan, 2022). Cancerous cells of a single tumor are thought to originate from one progenitor cell possessing an altered or mutated genome, enabling the cell to avoid apoptosis, proliferate limitless and progress independent of inhibitory signals, metabolic challenges and the presence of immune cells. Therefore, a key characteristic of cancer cells compared with its tissue of origin is an elevated growth rate, requiring a higher synthesis rate of biomolecules such as DNA, RNA and proteins. A growing tumor further shapes its microenvironment through signaling molecules, attraction of vasculatures, nutrient and oxygen depletion, as well as tumor promoting inflammation. A solid tumor therefore does not only persist as an agglomeration of similar cancerous cells, but consists of a variety of different cell types interacting with each other (Whiteside, 2008). Through genome instability-induced mutations or alterations in gene expression programs based on endogenous or exogenous stimuli, existing tumor cells may further develop novel traits to get adapted to their surrounding for even faster and independent proliferation, apoptosis resistance, senescence induction or mobilization of metastasizing cells. This process is termed tumor evolution and whether it follows entirely the Darwinian principles remains subject of discussions (Cahill et al., 1999, Ling et al., 2015, Laukien, 2021).

The nature of mutation at an evolutionary scale is an inherent process of any cell or organism and is required to adapt to changing environments on the long run. Advantageous or non-harmful characteristics remain, whereas harmful traits are negatively selected (Darwin, 1859). Somatic mutations without any impact on cellular phenotypes occur throughout the lifespan and follow the principle of clonal expansion. Accumulation of somatic mutations and DNA damage is also considered to underlie the process of ageing (Franco and Eriksson, 2022). Surprisingly, somatic cells may accumulate a heavy mutational burden, including cancer driver mutations, without developing into tumor cells as shown for sun-exposed tissues (Martincorena et al., 2015). On the contrary, few key driver mutations may be sufficient to initiate the formation of a dormant cancer cell and promote its progression to a malignant clone

(Balmain, 2022). To date, more than 500 driver mutations are considered to play a role in cancer development (Martinez-Jimenez et al., 2020). Since decades, an increasing body of studies focuses on understanding the molecular mechanisms and effects of these mutations in various cancer types, but a universal understanding is still missing.

Impactful genetic alterations include the activation of proto-oncoproteins. Proteins playing key regulatory roles for cellular processes such as transcription factors, transducers of signaling events or growth factors may function as proto-oncoproteins. Uncontrolled activation of oncoproteins has a strong influence on transcriptional programs, cell proliferation and phenotype (Kontomanolis et al., 2020). Events that activate oncoproteins include for instance single point mutations as in the RAS genes (Gimple and Wang, 2019) or gene amplifications as shown for MYC (Schaub et al., 2018). Gene translocation may result in functional fusion proteins, such as BCR-ABL (Hantschel and Superti-Furga, 2004), or localization of a non-transcribed proto-oncogene proximal to an active promotor region as shown for MYC (Duffy et al., 2021). Further events for oncoprotein activation include an altered protein turnover rate or the insertion of an active promotor sequence adjacent to an oncogene due to a virus infection.

Oncogenic events are counteracted by tumor suppressors that maintain homeostasis, genome integrity, dampen cell proliferation and lead to the induction of apoptosis or senescence, if cellular abnormalities reach a severe level. Therefore, the inactivation of tumor suppressor functions complements the hallmarks of cancer (Hanahan, 2022). For instance, the tumor suppressor TP53 is evolutionary conserved since the development of multi-cellular organisms and is involved in maintenance of DNA, as well as cell fate decision towards cell cycle arrest or apoptosis following severe DNA damage (Aubrey et al., 2016). Few driver mutations leading to either activation of proto-oncoproteins or inactivation of tumor suppressors may accelerate the accumulation of mutational burden, resulting in a plethora of dispensable mutations. However, a higher mutation rate gives rise to an increased chance of altering other safeguarding mechanisms, further fueling a long term positive forward loop for tumor development.

Tumor cells may become resistant to apoptosis and DNA damage induced cell cycle arrest. To tolerate the increased level of DNA damage and maintain single cell survival, tumor cells require efficient DNA repair mechanisms. Concomitant, uncontrolled cell proliferation leads to elevated levels of DNA replication and transcription. Both processes are an intrinsic source of DNA damage. Hence, fast growing tumor cells require tight coordination of transcription and DNA replication to efficiently proliferate and keep potential DNA damage at tolerable levels. The ubiquitin system is an integral regulation network for cellular protein function, abundance and localization, and is therefore crucial for coordination of DNA replication and transcription machineries. Moreover, ubiquitination shapes the effects of a huge

variety of cellular factors, including tumor suppressors and oncoproteins, to safeguard genome integrity and control transcriptional programs for maintaining cellular identity (Mansour, 2018).

This study focuses on the ubiquitination-dependent coordination of transcription and DNA replication. Transcription replication conflicts (TRCs) are thought to underlie genome instability in cancer cells. Therefore, investigating how DNA damage response (DDR) signaling is initiated and conveyed following the induction of TRCs or replication stress may provide valuable mechanistic insight of how tumor cells cope with transcription and DNA replication challenges. In particular, colorectal carcinoma cells are a useful model system, since colorectal cancers may frequently harbor genome instability and hypermutation phenotypes.

## 3.2 Colorectal carcinoma

Cancer development in tissues of the colon or rectum affects 4 – 5% of the global population. Since genetic predispositions are rarely inherited in a family, tumor development rather depends on age, sex, adiposity and lifestyle choices (Marmol et al., 2017). A unique property of colorectal carcinomas is the exposure of affected tissues to the gut content and the interaction with the gut microbiome (Clay et al., 2022). Therefore, dietary preferences have a strong influence on the risk to develop colorectal carcinomas. Pathogenic microbes, dysbiosis, as well as increased levels of visceral adipose tissue, support an inflammatory environment that favors cancer development (Clay et al., 2022).

Importantly, factors governing the development of colorectal carcinomas include aberrant molecular mechanisms that lead to genomic instability. For a subset of colorectal carcinoma patients this results in a hypermutation phenotype (Forgo et al., 2020, Bourdais et al., 2017). Depending on the molecular subtypes of colorectal cancer, distinct cases may be classified based on chromosomal instability (CIN), CpG island methylator phenotype (CIMP) and microsatellite instability (MSI) properties (Marmol et al., 2017). Integration of these categories with data of deep sequencing experiments from patient material yields a taxonomy of colorectal cancer subtypes (Guinney et al., 2015). Within these tumors, important pathways such as WNT, MYC and TGF-β were deregulated and genes, including BRAF and KRAS, were mutated. Furthermore, copy number alterations, gene translocations and alterations of non-coding RNAs contribute to deregulated transcription programs and therefore to the pathogenesis of colorectal carcinomas (Guinney et al., 2015). To deepen the understanding of molecular factors, colorectal carcinoma cell lines are a well-established and widely used model system. A cell line system enables specific perturbation of protein functions to investigate molecular mechanisms that support tumor cell survival in the context of genome instability, transcription and DNA replication challenges, as well as DNA damage response signaling.

## 3.3 DNA damage response signaling

Genome instability is a hallmark of cancer cells and arises from DNA damage (Hanahan, 2022). DNA damage may result from a multitude of sources, including ionizing radiation, UV light, environmental toxins, reactive oxygen species, mechanical stress or simply by endogenous processes, such as transcription or replication and conflicts of both. Organisms developed mechanisms to monitor genome integrity in order to ensure transmission of unaltered genetic information to their progeny (Blackford and Jackson, 2017). The DNA damage response (DDR) is a complex signaling network involved in cell fate decisions. Activation of DDR signaling leads to activation and recruitment of DNA repair factors to alleviate DNA damage. However, excessive DNA damage may drive cells into programmed cell death (apoptosis) or to permanently exit the cell cycle (senescence). This prevents the accumulation of heavily mutated cells that would eventually lead to cancer development or age-related pathologies (Schmitt et al., 2007, Jackson and Bartek, 2009).

The DNA damage response initiates with the detection of a DNA lesion by sensor proteins, followed by a cellular signaling cascade and subsequent recruitment of repair factors that alleviate DNA damage, pause the cell cycle, or initiate senescence or apoptosis. All eukaryotes encode at least one member of the phosphoinositide 3-kinase (PI3K)-related kinase (PIKKs) family with key roles in DDR signal transduction (Blackford and Jackson, 2017). In humans, the three serine/threonine kinases ATM, ATR and DNA-PK are the major DDR signaling kinases. Phosphorylation of a large number of downstream effector proteins results in recruitment of DNA repair factors, chromatin remodeling and the activation of cell cycle checkpoint dependent growth arrest (Yang et al., 2004). ATR activation mainly results from single strand DNA breaks, whereas double strand breaks (DSBs) are a well characterized trigger for ATM and DNA-PK activation (Figure 1) (Shiloh and Ziv, 2013, Awasthi et al., 2015).

The DNA-dependent protein kinase catalytic subunit (DNA-PKcs) is recruited to DSBs by Ku heterodimers that tether both DNA ends at a DSB. DNA-PK recruitment initiates non-homologous end joining (NHEJ) by the recruitment of the core NHEJ factors XRCC4, XLF, LIG4 and PAXX. DNA-PK disassembles upon autophosphorylation and DNA ends are ligated by the NHEJ factors (Graham et al., 2016).

ATM recruitment to DNA double strand breaks requires the MRN complex, which consists of the exonuclease MRE11, the ATPase RAD50 and NBS1 (Marechal and Zou, 2013). Following recruitment to DSBs, activated ATM phosphorylates its target proteins including itself, tumor suppressor TP53, tumor suppressor BRCA1, transcriptional regulator KAP1, histone H2AX, the histone reader 53BP1 and the effector kinase CHK2 (Bakkenist and Kastan, 2003, Shiloh and Ziv, 2013, Panier and Boulton, 2014, Blackford and Jackson, 2017). At DSBs, ATM-dependent phosphorylation of 53BP1 favors DNA repair via NHEJ similar to DNA-PK.

However, BRCA1 phosphorylation counteracts the recruitment of 53BP1 effectors and favors DNA repair via homology-directed DNA repair (HR) (Hustedt and Durocher, 2016). ATM signaling is also involved in stabilization of stalled DNA replication forks and therefore plays a role in facilitating the recovery from replication stress (Trenz et al., 2006, Syed and Tainer, 2018, Schleicher et al., 2022).

In contrast to ATM and DNA-PK, ATR is recruited to extended tracks of RPA-bound single-stranded DNA (ssDNA) via the ATR interacting protein ATRIP. Therefore, ATR is the major kinase in response to replication fork stalling and other DNA lesions that result in ssDNA (Blackford and Jackson, 2017). Activated ATR phosphorylates itself, the checkpoint kinase CHK1, the helicase SMARCAL1 and other effectors (Zou and Elledge, 2003, Zhao and Piwnica-Worms, 2001, Couch et al., 2013). CHK1 activation promotes the degradation of CDC25A, reduces CDK activity and therefore slows or arrests cell cycle progression, as well as origin firing. This avoids premature entry into mitosis (Bartek et al., 2004). The inhibitory phosphorylation of SMARCAL1 prevents the remodeling and processing of the stalled replication fork. Further, ATR activity leads to the upregulation of the ribonucleotide reductase subunit RRM2, which is required to maintain the cellular pool of available dNTPs (Lopez-Contreras et al., 2015).

A common endpoint of DNA-PK, ATM and ATR activation is the transient inhibition of cyclin-dependent kinases (CDKs) in order to stall the cell cycle at respective checkpoints. Both, ATM and ATR, are proposed to cooperatively activate the intra-S and G2/M checkpoints, since ATM-dependent DNA resection at DSBs provides binding sites for ATR at RPA-bound ssDNA (Cuadrado et al., 2006).

In cancer cells, DDR factors are frequently mutated, which leads to higher levels of DNA damage and genome instability. This contributes to the development of apoptosis resistance and underlies the ability to proliferate uncontrolled and to metastasize (Groelly et al., 2023). Compromised DDR signaling renders tumor cells susceptible to DNA damaging treatments as for instance radiotherapy. Inhibitors of the DDR kinases are applied to increase the sensitivity of DNA-damaging cancer treatments or to selectively kill tumor cells harboring synergistic mutations (Groelly et al., 2023).

All in all, DDR signaling prevents the accumulation of detrimental mutations derived from exogenous or endogenous influences and leads to the restoration of genome integrity. An intact genome is required for expression of essential genes and the generation of functional gene products.

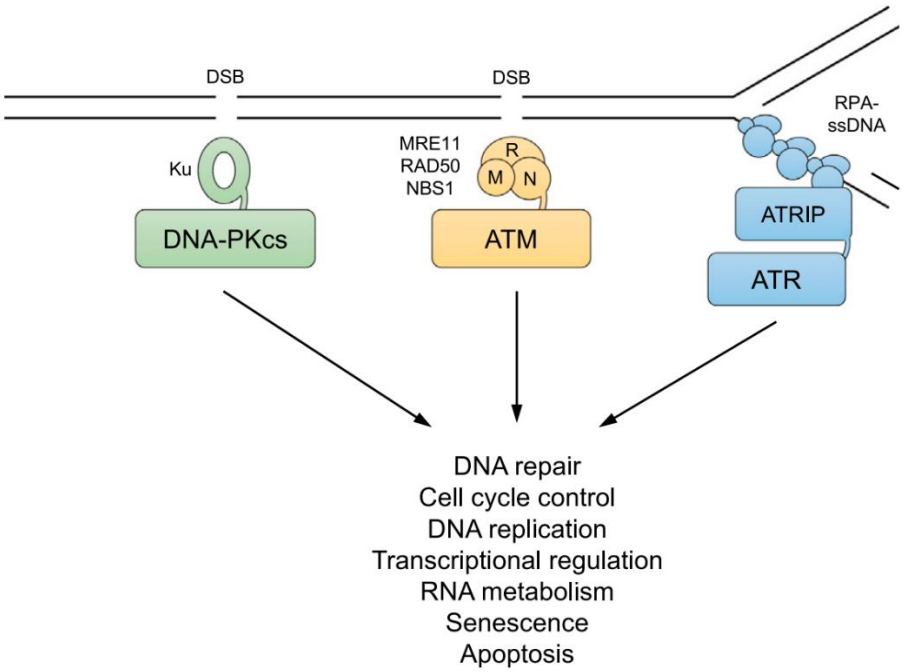


***Figure 1: DNA damage response signaling pathways.***

*DNA lesions, such as DNA double strand breaks or ssDNA, recruit sensors of DNA damage to activate the three major DDR signaling kinases DNA-PKcs, ATM and ATR. The DDR contributes to maintain cellular homeostasis. This figure was adapted from Blackford and Jackson (2017). This article was published in Molecular Cell, Volume 66, Blackford et al., ATM, ATR, and DNA-PK: The Trinity at the Heart of the DNA Damage Response, Pages 801-817, Copyright Elsevier (2017).*

## 3.4 RNAPII-dependent transcription

RNA polymerase II (RNAPII) dependent transcription is responsible for the expression of protein coding genes, as well as other regions of the eukaryotic genome and is therefore a centerpiece for all aspects of life, including proliferation, differentiation and cellular responses to environmental stimuli. Increasing knowledge about functions and dependencies of involved factors in health and disease deciphers the complex regulation of transcription.

Eukaryotic transcription initiates by assembly of the 12-subunit RNAPII complex with general transcription factors (GTFs) TFIIA, -B, -D, -E, -F, and -H, constituting the pre-initiation complex (PIC) (Osman and Cramer, 2020, Schier and Taatjes, 2020). Throughout the transcription cycle, binding, dissociation and post-translational modifications of various RNAPII interaction partners govern the generation of a mature mRNA. Upon recruitment to promoter sequences, the PIC unwinds DNA, initiates template-dependent RNA synthesis of a short RNA fragment and remains paused proximal to promoters. At this stage, the 5’-cap is attached to nascent pre-mRNA, which stabilizes the RNA molecule and enables subsequent recruitment of splicing factors (Ramanathan et al., 2016). Upon integration of activating signals on RNAPII at the promotor, processive elongation is initiated. This pause release of RNAPII leads to

synthesis of pre-mRNA, which is readily processed by RNAPII-bound factors during ongoing transcription. Reaching the transcription termination site (TTS) at the end of a gene, RNA is cleaved, polyadenylated and mature mRNA is released for nuclear export into the cytoplasm followed by translation into proteins (Osman and Cramer, 2020, Schier and Taatjes, 2020). In general, a transcription cycle lasts for a few minutes per gene on average (Figure 2), but depending on the gene size may last longer than the cell doubling time or even up to 16 hours at the longest human gene (Tennyson et al., 1995).

### *3.4.1 Transcriptional regulation via the RNAPII C-terminal repeat domain*

Gene transcription at the correct location, time and intensity requires a multilevel regulatory system. Signaling events to initiate, pause, promote and terminate transcription are mainly integrated at the C-terminus of the catalytic RPB1 subunit of RNAPII (C-terminal domain, CTD). The human CTD consists of 52 heptapeptide repeats with the consensus sequence YSPTSPS. The CTD forms a tail-like extension of the core RNAPII close to the RNA exit tunnel (Cramer et al., 2001, Osman and Cramer, 2020). Aside from the two prolines, the other five residues of the heptapeptide repeats are readily phosphorylated or modified with other post-translational modifications (PTMs) (Figure 2) (Lyons et al., 2020). The CTD therefore allows the recruitment of effector proteins to RNAPII depending on its post-translational modification pattern. Interactors include RNA processing factors, chromatin readers and remodelers, as well as writers of PTMs, which modulate RNAPII functions. Throughout the transcription cycle these modifications are following a canonical pattern. Transcription initiation at promotors coincides with S5 phosphorylation of RNAPII, which is maintained during promotor-proximal pausing. S5 phosphorylation enables recruitment of RNA capping factors (Komarnitsky et al., 2000, Sims et al., 2004). Actively transcribing RNAPII loses S5 phosphorylation and is predominantly phosphorylated at S2 residues of the CTD. This contributes to the recruitment of RNA processing factors, such as the splicing machinery (Cho et al., 2001, Heidemann et al., 2013). Y1 phosphorylation is involved in antisense transcription (Descostes et al., 2014). T4 and S7 phosphorylation are proposed to be involved in non-essential functions, however these modifications are less well understood and remain to be characterized in a comprehensive manner (Eick and Geyer, 2013, Kempen et al., 2023).

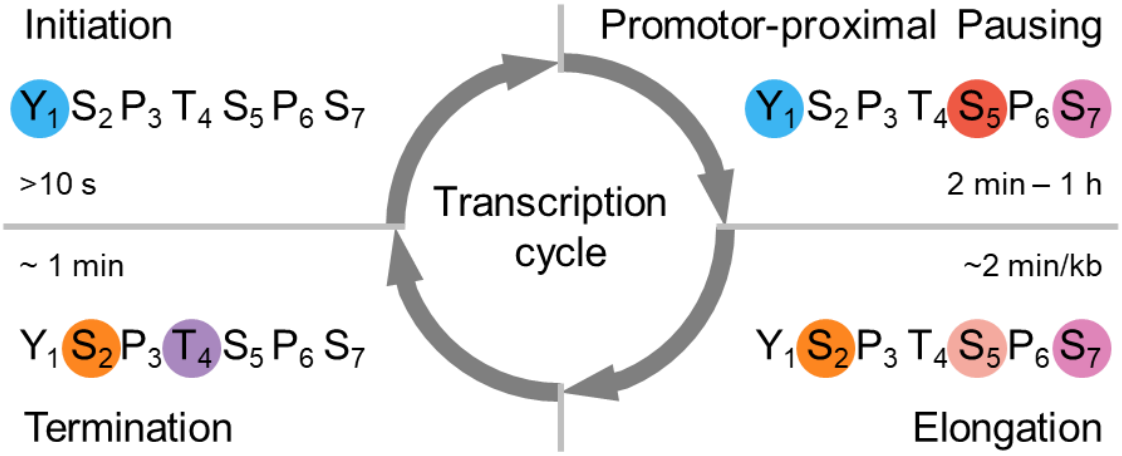


***Figure 2: The CTD repeat code during the transcription cycle.***

*Eukaryotic transcription cycles can be divided in distinct major phases preferentially harboring different PTMs at the RNAPII hexapeptide repeats in the CTD. Following transcriptional initiation, RNAPII is phosphorylated at S5 residues and paused proximal to promotor regions. Elongation initiates upon phosphorylation of S2 residues, while S5 phosphorylation decreases. Transcription termination results in the eviction of RNAPII from chromatin, which can then be reused for subsequent transcription cycles. Circles indicate phosphorylation events. This figure was adapted from Lyons et al. (2020).*

### *3.4.2 RNAPII pause release*

Promotor proximal pausing of RNAPII is balanced between factors inhibiting RNAPII progression and signaling events supporting its productive elongation throughout the gene body. Shortly after transcription initiation, binding of the NELF and DSIF complexes to RNAPII keeps RNAPII in a paused state (Adelman and Lis, 2012). Binding of NELF restricts RNAPII mobility and sterically interferes with the active site of RNAPII, rendering the polymerase incompatible for RNA elongation (Figure 3) (Vos et al., 2018). RNAPII-pausing is supported by phosphatases such as PP2A and PP4, which directly counteract the activating phosphorylation of the SPT5 subunit in the DSIF complex (Parua et al., 2020). To overcome the paused state, RNAPII is phosphorylated at its S2 residue by the cyclin dependent kinase CDK9 that is part of the positive transcription elongation factor b (p-TEFb) together with cyclin T (Peterlin and Price, 2006). CDK9 does not only phosphorylate RNAPII but also NELF, resulting in its dissociation from RNAPII. Further, CDK9 phosphorylates SPT5 and inactivates PP4 which results in NELF dissociation and a switch for DSIF to function as a positive elongation factor for transcription (Cheng and Price, 2007, Egloff, 2021). Active elongation requires the histone chaperone SPT6 that loosens the DSIF-RNA clamp (Osman and Cramer, 2020) and polymerase associated factor complex (PAF1c) serving as a hub to recruit further transcription modulators (Yu et al., 2015, Vos et al., 2018). SPT5 phosphorylation by CDK9 promotes recruitment of PAF1c to active RNAPII (Yamada et al., 2006, Qiu et al., 2012). Interestingly,

PAF1c and NELF binding to RNAPII is mutually exclusive, suggesting that after pause release binding of PAF1c ensures that the inhibitory NELF complex is not able to bind elongating RNAPII and transcription proceeds efficiently (Vos et al., 2018). PAF1c is involved in recruitment of CDK12, which targets pS2 residues in the RNAPII-CTD to keep the pS2 modification of the CTD at sufficiently high levels throughout gene bodies. (Davidson et al., 2014, Yu et al., 2015). All in all, promotor proximal pausing of RNAPII serves as a time window for signal integration, pre-mRNA capping and dampens the rate of new and unscheduled initiation events.

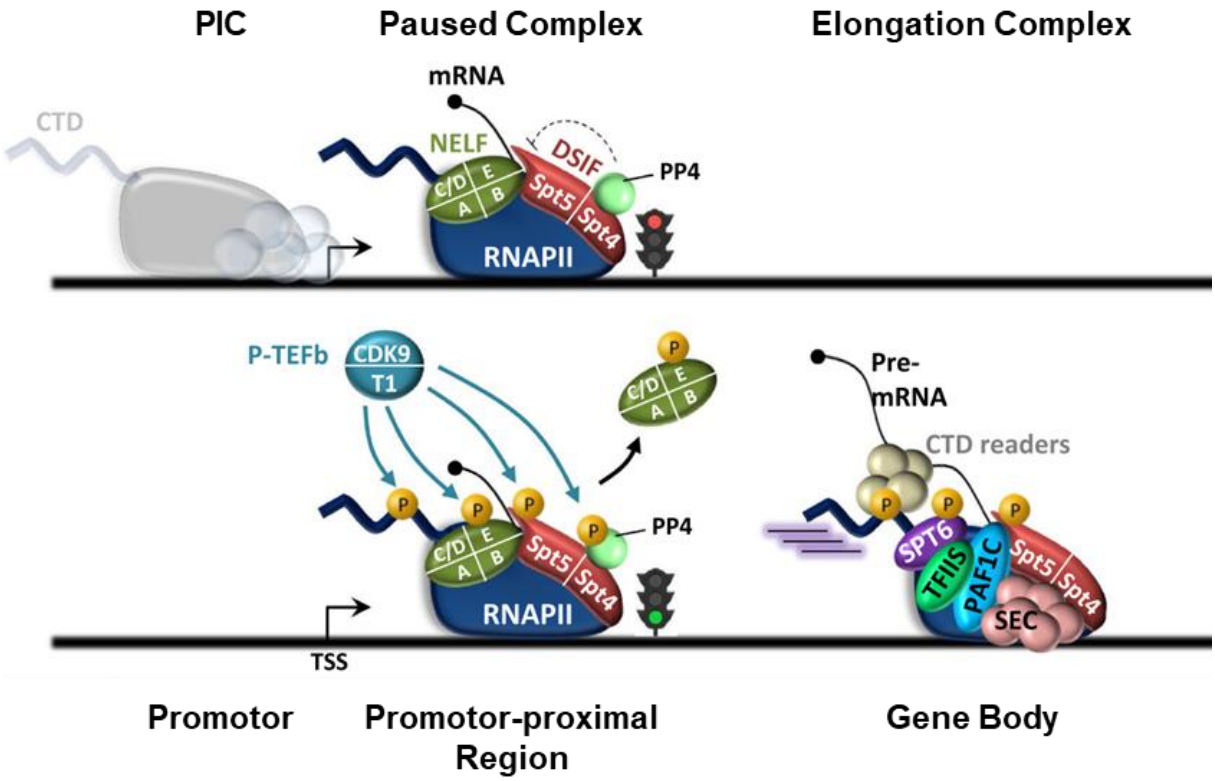


***Figure 3: Mechanism of RNAPII pause release.***

*Recruitment of RNAPII to active promotors is followed by promotor proximal pausing of the transcription machinery. Integration of inhibitory and supportive signaling events keep a balance to maintain the pausing status and allow pause release at a desired gene, time and intensity. One major factor to release RNAPII into the gene is the cyclin dependent kinase CDK9. Upon pause release, the interactome of RNAPII is altered towards factors promoting processive RNA elongation, including the spliceosome and chromatin remodelers. CTD: carboxyl-terminal domain, PIC: pre-initiation complex, DSIF: DRB-sensitivity inhibitory factor, NELF: negative elongation factor, SEC: Super elongation complex, TSS: transcription start site. This figure was adapted from Egloff (2021). This article was published under CC BY 4.0 (http://creativecommons.org/licenses/by/4.0/).*

### *3.4.3 Processive elongation, proofreading and backtracking*

Precise transcription of genetic information is the basis for production of functional proteins. To ensure the incorporation of the valid nucleotide triphosphate (NTP), RNAPII does not only preferentially select the cognate NTP, but is also able to correct the misincorporation of a falsely incorporated NTP (Sydow and Cramer, 2009, Osman and Cramer, 2020). A mismatch of an incorporated NTP with the template DNA results in a frayed base pairing, which overlaps with the NTP binding site and thereby inhibits the forward translocation of RNAPII. Stalled by this roadblock, RNAPII may backtrack by one position on DNA to hydrolyze the RNA backbone and release a dinucleotide from the RNA 3' end (Zenkin et al., 2006, Wang et al., 2009, Sydow and Cramer, 2009, Osman and Cramer, 2020). The presence of polymerase and hydrolase functions at the same active center are unique to the RNAPII protein and therefore ensure the high fidelity of transcription through both NTP selection and proofreading. The proofreading function results in transient transcriptional pausing, which varies in duration and is resolved by RNAPII itself upon insertion of the correct base (Osman and Cramer, 2020). Moreover, encounters of RNAPII with obstacles such as nucleosomes and DNA lesions can result in pausing of RNAPII, during which RNAPII can move backwards on the DNA template (Shilatifard et al., 2003, Bondarenko et al., 2006). This backtracking spans about 10 nucleotides and may lead to RNAPII arrest (Cheung and Cramer, 2011). Resuming transcription after an arrest requires cleavage of the nascent RNA and nucleosome remodeling by chaperones (LeRoy et al., 2019). Further obstacles for transcription include epigenetic marks such as methylated DNA bases (Wang et al., 2015, Wang et al., 2017). Although these challenges modulate the speed of transcription, integrity of the RNA transcript and the genome are maintained.

### *3.4.4 Transcription termination*

A successful transcription cycle ends with termination of RNA synthesis by RNAPII. Towards the 3'-end of genes, RNAPII passes the polyadenylation signal (PAS) in most protein coding genes. The nascent RNA molecule is cleaved at the desired 3'-position and polyadenylated, while RNAPII remains on the template DNA. RNAPII may travel further downstream for a few bases or up to millions of bases (Eaton and West, 2020).

Several models have been proposed to explain transcriptional termination. On the one hand, transcription of the PAS domain itself is thought to play a role in exchange of RNAPII bound factors that previously prevented termination throughout the gene body. Therefore, passing the PAS domain leads to dissociation of the anti-termination factors and/or conformational changes of RNAPII, resulting in transcription termination (Zhang et al., 2015). On the other hand, rapid 5'→3' degradation of the remnant RNA after PAS cleavage facilitates

transcription termination. In this model, the nuclear exonuclease XRN2 plays a key role in RNA degradation and is the integral component of the so-called torpedo model, favoring the idea that upon encounter of XRN2 with RNAPII, the transcription machinery is disassembled (West et al., 2004). The torpedo model is not limited to termination of RNAPII beyond the PAS domain, but can lead to premature termination of nascent RNA transcripts. XRN2-dependent pre-mRNA cleavage can be initiated by hybridization of antisense oligonucleotides with nascent RNA and therefore regulate transcript levels of specific genes via RNA interference (Lee and Mendell, 2020).

Most likely, transcriptional termination in cells involves elements of both models to efficiently terminate a transcription cycle, release RNAPII from DNA and enable its reuse (Eaton and West, 2020).

## 3.5 The role of RNAPII in genome integrity

RNAPII functions exceed the sole synthesis of high-fidelity RNA. The genome-wide association of RNAPII and its ability to recruit chromatin remodelers, signaling factors and scaffold proteins have a strong influence on genome stability. Although several mechanisms involve RNAPII to maintain genome integrity, strong transcription may also result in elevated levels of DNA damage and therefore threaten genome integrity.

### *3.5.1 RNAPII promotes genome integrity*

Transcription entails reorganization of chromatin contexts and therefore poses a mechanism to scan DNA for lesions. Simultaneously, RNAPII serves as a hub for effector protein recruitment. This includes mechanisms such as transcription-coupled DNA repair, homologous recombination (HR) and DSB end transcription.

DNA lesions appear to be repaired with higher efficiency in transcribed genes, indicating that RNAPII facilitates the repair pathways alongside transcription (Hanawalt and Spivak, 2008). This process is termed transcription-coupled nucleotide excision repair (TC-NER) and initiates with sensing a larger DNA lesion, crosslinked bases or crosslinked proteins. Sensing is achieved by either stalling and backtracking of RNAPII at the lesion site or by other DNA lesion sensors, including DDB1 and DDB2 (Hanawalt and Spivak, 2008). Either way, the transcription factor TFIIH is recruited alongside XPG to further open up the DNA helix (Compe and Egly, 2012). RPA2 binds and stabilizes single stranded DNA and the damaged DNA strand is cleaved at an upstream location by XPF-ERCC1 and a downstream position via XPG (Hanawalt and Spivak, 2008). Following the excision of DNA lesions, DNA replication factors, including PCNA and DNA polymerases, as well as DNA ligases are recruited to fill in the ssDNA gap (Lans et al., 2019).

Interestingly, also DNA double strand breaks are repaired with a higher efficiency in actively transcribed genes compared with other regions of chromatin. This observation extends the model towards transcription-dependent DSB repair. At DSBs, the non-homologous end joining pathway is supported by the nascent RNA as a template to ensure error-free DSB repair (Keskin et al., 2014, Chakraborty et al., 2016, Guha and Bhaumik, 2022). Next to nascent RNA transcripts covering the break site, the RNAPII-dependent DNA-RNA hybrids adjacent to a double strand break favor the recruitment of homologous recombination (HR) factors, including RAD52 and the processing factor XPG for HR mediated DSB repair (Yasuhara et al., 2018, Ui et al., 2020).

Moreover, RNAPII is actively recruited to sites of double strand breaks which enables the synthesis of damage induced long non-coding RNA (dilncRNA) at DSB sites (Michelini et al., 2017, Sharma et al., 2021). DSB transcription requires the MRN complex, which not only recruits RNAPII to the damaged site, but also unwinds the DNA double helix adjacent to the DSB. The exonuclease activity of the MRN complex is dispensable for this process. Independent of the source of DNA double strand break associated DNA-RNA hybrids, the hybrid structure supports the recruitment of 53BP1 to damaged sites and therefore facilitates the following recruitment of repair factors (Michelini et al., 2017, Sharma et al., 2021). Taken together, various mechanisms covering the role of RNAPII in maintaining genome integrity have been described.

### *3.5.2 RNAPII threatens genome integrity*

Contrary to its supportive functions, RNAPII can be a threat to genome integrity resulting in DNA lesions, breaks, faulty transcripts or chromatin aberrations. For instance, pervasive activation of oncogenic pathways disrupts the transcriptional programs of healthy cells and may lead to constitutive activation of RNAPII at many genes. Aberrant transcription leads to unbalanced unwinding and supercoiling of template DNA and may result in mechanical breakage (Bermejo et al., 2012, Ma and Wang, 2016). Topological stress of the DNA helix dampens the efficiency of transcription. Release of supercoiling involves the topoisomerases TOP1, TOP2 and TOP3, which transiently cleave the DNA helix and immediately re-ligate the lesion after topological stress release (Pommier et al., 2016). Interestingly, TOP2β induced double strand breaks at promotor regions are sufficient to induce transcription activation at certain genes (Trotter et al., 2015). However, when re-ligation by topoisomerases is perturbed, DNA lesions covalently bound to TOP proteins prevail. An increased need for the release of topological stress gives rise to a higher chance of DNA lesions or even chromosomal re-arrangements that may cause cancer (Haffner et al., 2010).

Beyond topological stress, small DNA lesions or abasic sites may lead to misincorporation of ribonucleotides, resulting in transcriptional mutagenesis. For instance, an 8-oxoguanine residue or 8,5-cyclo-2-deoxyadenosine residue or a missing base in the template strand may lead to misincorporation of AMP and therefore a faulty transcript sequence (Damsma and Cramer, 2009, Walmacq et al., 2015, Wang et al., 2018).

Aberrant regulation of RNAPII can result in excessive formation of DNA-RNA hybrids, termed R-loops, throughout genic areas. R-loops are secondary DNA structures in which the nascent RNA hybridizes with the complementary DNA strand resulting in a DNA-RNA hybrid strand and a displaced ssDNA strand. Although R-loops naturally occur at regions of transcriptional termination (Skourti-Stathaki et al., 2014), failure to resolve R-loops through HR factors causes DNA damage (Skourti-Stathaki and Proudfoot, 2014). R-loops constitute a roadblock for the replication machinery leading to transcription replication conflicts (TRCs) and are therefore considered a key factor of genome instability (García-Muse and Aguilera, 2016, Garcia-Muse and Aguilera, 2019, Crossley et al., 2019). DNA lesions result in the activation of the DNA damage response kinases ATM, ATR and DNA-PK, which lead to cell cycle arrest, recruitment of repair factors and therefore ensure genome maintenance (Blackford and Jackson, 2017).

Taken together, transcription is required to maintain cellular functions and survival but may simultaneously damage the genome. During transcription, concomitant repair mechanisms alleviate the threat to genome stability and enable the maintenance of cellular identity.

### *3.5.3 Transcription inhibition as targeted therapy approach*

Oncogenic signaling interferes with transcriptional programs. Therefore, targeting of the transcription machinery with small molecules could serve as a useful tool not only for basic research purposes, but also for therapeutic targeting in clinical applications. Modulation of transcriptional programs may be achieved at several levels since various proteins and therefore potential drug targets are involved in transcriptional initiation, pause release, elongation and termination. Activation and pause release of RNAPII can be prevented using inhibitors targeting cyclin dependent kinases (CDKs) either broadly with pan-CDK inhibitors such as flavopiridol, roscovitine or dinaciclib or with kinase specific inhibitors (Martin et al., 2020). For instance, THZ1 was identified as a potent inhibitor of CDK7. Moreover, the activating S2-phosphorylation in the CTD by CDK9 can be inhibited with 5,6-dichloro-1-beta-D-ribofuranosylbenzimidazole (DRB) and AZD4573 (Barlaam et al., 2020).

Aside from kinase inhibitors, transcription can be prevented by targeting the core transcription machinery using for example the plant derived toxin triptolide. Triptolide targets

the TFIIH subunit XBP that is required for transcription initiation by translocation of DNA into the catalytic site of RNAPII (Martin et al., 2020). Moreover, RNAPII can be targeted directly with compounds such as α-amanitin.

All in all, inhibition of transcription may counteract oncogenic signaling dependent transcription programs and thereby compromise tumor cell survival. However, global inhibition of transcription on an organism scale may induce severe implications far beyond its potential supportive influence.

## 3.6 Transcription replication conflicts

Due to the genome-wide association of RNAPII with chromatin that may last for hours and the necessity to replicate DNA in dividing cells, encounters of the transcription and replication machinery are considered unavoidable, frequent events. Transcription replication conflicts (TRCs) at low levels are likely resolved efficiently during normal cell cycle. However, perturbation of transcription programs or DNA replication may give rise to high levels of TRCs, underlying genome instability (Azvolinsky et al., 2009, García-Muse and Aguilera, 2016).

Several RNAPII complexes may transcribe a single gene simultaneously by consecutive initiation. In contrast, the DNA replication machinery comprises two catalytic sub-complexes with DNA polymerase activity and both act on ssDNA. Since DNA is expected to be replicated only once per cell cycle, ongoing replication forks are not followed by a second replisome complex (García-Muse and Aguilera, 2016). Encounters of the replication machinery with transcription complex therefore exclude the possibility to simply pass through each other and result in a supposedly transient conflict configuration with several potential outcomes (Lalonde et al., 2021). First, the replisome may simply skip an RNAPII bound DNA sequence and re-prime at a downstream position to proceed with replication. In the case of a co-directional encounter, RNAPII can be released from DNA and the ongoing replication machinery may use the remaining RNA as a primer for DNA replication. Second, an ongoing replication fork may evict the transcription complex or facilitate the proteasomal degradation of the entire transcription machinery and nascent RNA to proceed with replication (Poli et al., 2016, Lalonde et al., 2021). Third, the replication fork may stall and reverse and build a so-called ‘chicken-foot’ DNA structure at arrested RNAPII complexes, which may be resolved by skipping, re-priming or eviction of RNAPII. A reversed replication fork may be cleaved by endonucleases to relieve torsional stress. This enables the transcription machinery to pass through the replicated DNA. Upon re-ligation of the cleaved replication fork, replisome proteins may proceed with DNA replication (Lalonde et al., 2021). At last, failure to resolve a TRC may result in replication fork collapse and subsequent DNA damage. The relative orientation of the replisome and the transcription machinery at TRCs can lead to distinct DNA damage response

signaling events via the ATM and ATR kinases (Hamperl et al., 2017, Hamperl and Cimprich, 2016).

Mechanisms to avoid TRCs include the spatial and temporal uncoupling of both processes during the S-phase of the cell cycle (Meryet-Figuiere et al., 2014, Rivera-Mulia and Gilbert, 2016). Genes transcribed during early S-phase are replicated towards the end of S-phase and genes replicated early in S-phase are transcribed later. Moreover, the severity of a collision event in co-directional orientation is considered to be lower, since RNAPII may naturally terminate the transcription cycle and a previously slowed replication fork may proceed naturally. Interestingly, a global co-directional orientation is proposed for replication and transcription in non-transformed cells (Chen et al., 2019). Further mechanisms to avoid TRCs include replication arrest (Gerber et al., 1997), DNA damage response induced replication fork slowing and chromatin remodeling based on epigenetic modifications (García-Muse and Aguilera, 2016).

Both R-loops and torsional stress may be a cause and/or consequence of TRCs and are tightly connected with genome instability (García-Muse and Aguilera, 2016, Kemiha et al., 2021). Aberrant activation of RNAPII for instance through oncoproteins such as RAS and MYC causes TRCs, replication stress and DNA damage (Kotsantis et al., 2016, Kotsantis et al., 2018, Murga et al., 2011, Macheret and Halazonetis, 2018, Gaillard et al., 2015). Beyond the mentioned eviction of RNAPII, allowing replication fork progression (Poli et al., 2016), RNAPII promotes the recruitment of factors that enable efficient removal of R-loops and stabilization of replication forks. For example, spliceosome proteins (Tresini et al., 2015, Sherill-Rofe et al., 2022), the DNA helicase RECQ5 (Zheng et al., 2009, Aygun et al., 2008) or RNA helicase DHX9 (Chakraborty and Hiom, 2021), as well as the homologous recombination mediators BRCA1 and BRCA2 can be recruited by RNAPII (Lomonosov et al., 2003, Welcsh et al., 2000, Gruber et al., 2019, Shao et al., 2020). The transcription factor PAF1c and the spliceosome associate with elongating RNAPII based on its CTD phosphorylation at the S2 residues. Hence, the PAF1 complex and the spliceosome are not only involved in supporting transcriptional elongation, but also play a role in resolution of TRCs and promotion of DNA repair (Wood et al., 2003, Tresini et al., 2015, Poli et al., 2016, Francette et al., 2021). Therefore, RNAPII is not simply the cause of TRCs but serves as a scaffold protein to recruit repair factors based on its functional status and thereby impacts the resolution of TRCs.

## 3.7 DNA replication

Spatial and temporal coordination of transcription and DNA replication facilitates cell survival and proliferation. Since a plethora of factors is involved in carrying out both processes on a genome-wide scale, an imbalance in the coordination may have a severe effect in cellular phenotypes. Recent studies suggest that transcription shapes DNA replication during the entire replication cycle, starting with initiation followed by processive replication and termination (Azvolinsky et al., 2009, Brison et al., 2019, Blin et al., 2019, Chen et al., 2019, Liu et al., 2021). On the one hand, oncogenic signaling deregulates both, transcription and DNA replication and aberrant transcription interferes with DNA replication. On the other hand, intense transcription of genomic areas results in reorganization of epigenetic markers, rendering the DNA more accessible and thereby facilitates loading of DNA replication factors. Moreover, the global orientation of transcription is proposed to be co-directional with DNA replication in order to avoid severe DNA lesions (Chen et al., 2019). Beyond transcription replication conflicts and oncogenic signaling, DNA alterations may give rise to replication stress through various processes (Primo and Teixeira, 2019, Cybulla and Vindigni, 2023).

### *3.7.1 The DNA replication machinery*

Complete and accurate duplication of the eukaryotic genome is a prerequisite for cell proliferation. During S-phase of the cell cycle, functional replisomes are assembled on chromatin to replicate DNA (Figure 4). First, the origin recognition complex (ORC) marks sites to load two DNA helicase hexamers on dsDNA, each consisting of six subunits that are termed MCM2-7 (Ticau et al., 2015, Burgers and Kunkel, 2017). Second, several accessory factors including DNA polymerase epsilon, CDC45 and GINS associate with the inactive MCM double hexamer and will remain associated during ongoing DNA replication. Third, the pre-initiation complex is re-modelled and the helicase function activated by MCM10 and RPA2 (Heller et al., 2011, Perez-Arnaiz et al., 2016). Activation of the MCM hexamers results in two diverging DNA replication forks that encircle ssDNA. Movement of the helicase complex along the leading strand generates downstream ssDNA, which is coated by RPA2. This ssDNA is primed by the DNA polymerase alpha-DNA primase complex to enable leading strand synthesis (Burgers and Kunkel, 2017). The DNA Polymerase epsilon complex performs subsequent leading strand synthesis, whereas lagging strand synthesis is achieved by DNA polymerase delta and repeated priming by the polymerase alpha complex (Figure 4). The DNA sliding clamp PCNA travels alongside polymerases alpha and epsilon to enhance processivity for both DNA strands to comparable levels (Chilkova et al., 2007, Burgers and Kunkel, 2017). PCNA comprises a homotrimer that encircles dsDNA and functions as a binding hub for a variety of replication factors during ongoing DNA replication. A conserved sequence motif known as

PCNA Interacting Protein box (PIP-box) enables the interaction with PCNA at each of its three PIP-box binding sites (Gonzalez-Magana and Blanco, 2020). Ongoing DNA synthesis by the replisome requires the constant supply with sufficient amounts of dNTPs, which are provided by the enzymatic activity of the ribonucleotide reductase M2 (RRM2) (Zuo et al., 2022).

DNA replication during S-phase is orchestrated by a distinct timing and spatial organization of chromatin. Replication timing and chromatin architecture are set up during G1 phase of the cell cycle and differ between cell types. Epigenetic markers and DNA sequence-dependent mechanisms influence replication timing and the coordination with the transcription machinery (Marchal et al., 2019).

Perturbed DNA replication poses a threat to genome integrity in both normal and cancer cells (Saxena and Zou, 2022). In general, cancer cells show elevated levels of replication stress, which could serve as a useful handle for the selective inhibition of cancer cell proliferation (Berti et al., 2020, Cybulla and Vindigni, 2023).

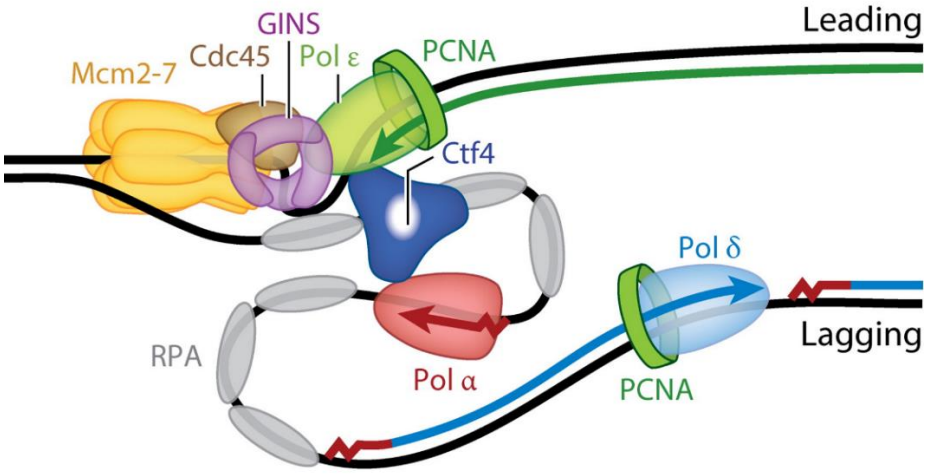


***Figure 4: The DNA replication machinery.***

*The replisome consists of the MCM2-7 helicase hexamer, the accessory factors CDC45 and GINS, as well as the DNA polymerases epsilon, delta and alpha. The DNA sliding clamp PCNA associates with polymerases epsilon at the leading strand and polymerase delta at the lagging strand. RPA coats and protects single stranded DNA. CTF4 is thought to tether polymerase epsilon with the RNA primase-containing polymerase alpha complex. This figure was adapted from Burgers and Kunkel (2017).*

### *3.7.2 DNA replication stress and damage response signaling by ATR and ATM*

Replication stress is defined as either slowing or stalling of the progressing replication fork and can result from DNA-crosslinked proteins or unusual DNA structures, including DNA supercoiling, G-quadruplexes, centromeres and telomeres. Moreover, DNA lesions, impaired origin licensing, disturbed origin firing or depletion of nucleotides can cause replication stress (Figure 5) (Gaillard et al., 2015, Primo and Teixeira, 2019, Cybulla and Vindigni, 2023).

Induction of replication stress is used for cancer treatment, exemplified by the use of the ribonucleotide reductase inhibitor hydroxyurea (HU) that leads to dNTP depletion (Madaan et al., 2012). Following replication stress, replication forks may reverse and build a stabilizing DNA structure, which is termed ‘chicken foot’ DNA (Rickman and Smogorzewska, 2019). Replication fork stalling or slowing results in the generation of single stranded DNA, since the synthesis of the coding strand is compromised. Single stranded DNA is bound and stabilized by RPA2, which in turn recruits ATRIP and ETAA1. This enables the recruitment and activation of the ATR kinase to initiate its damage response signaling cascade by phosphorylation of effector proteins, as described (see 3.3). Therefore, ATR signaling is initiated mainly upon ssDNA lesions or ssDNA/dsDNA junctions that are present at stalled or collapsed DNA replication forks. (Blackford and Jackson, 2017). ATR signaling limits replication origin firing, stabilizes stalled replication forks and maintains the dNTP pool through regulation of RRM2 (Costanzo et al., 2003, Couch et al., 2013, Toledo et al., 2014, Pfister et al., 2015, Buisson et al., 2015).

The ATR kinase is activated upon replication stress. However, replication stress also activates the ATM kinase, which is predominantly involved in signaling of DNA double strand breaks (Olcina et al., 2013). Nascent chromatin capture followed by mass spectrometry analysis showed that ATM, as well as the MRN complex is bound to newly synthesized DNA (Alabert et al., 2014). A mechanism to activate ATM includes the recruitment of the MRN complex to RPA2-coated ssDNA, which in turn enables ATM recruitment to stalled replication forks (Robison et al., 2004). ATM signaling results in the phosphorylation in its downstream targets, including KAP1, CHK2, TP53 and H2AX. This facilitates the efficient restart of replication forks by activating the homologous recombination based repair pathway (Mazouzi et al., 2014). Moreover, collapse of a stalled replication fork forms double strand breaks, which potently induce ATM-dependent DNA damage response signaling that can result in non-homologous end joining or homologous recombination-based DNA repair.

Both ATR and ATM signaling pathways are interconnected, since the downstream effectors of ATM and ATR, namely CHK2 and CHK1 may phosphorylate each other and it has been shown that ATM can directly phosphorylate ATR (Ronco et al., 2017). Inhibition of these DNA damage response signaling kinases sensitizes a variety of tumor cells to DNA damaging treatments and may therefore serve as therapeutic strategy (Ronco et al., 2017, Weber and Ryan, 2015).

Mechanisms of replication fork restart include the rescue of a stalled fork through firing of an adjacent origin, re-priming the template DNA downstream of a lesion, translesion synthesis (TLS), template switching or reversal of the replication fork followed by fork restoration (Conti and Smogorzewska, 2020). The DNA sliding clamp PCNA is an integral factor of the replisome and travels with replication forks. In response to DNA-damage induced

replication stress, PCNA is ubiquitinated on chromatin either by a single ubiquitin moiety or polyubiquitinated through different E3 ligases (Yang and Zou, 2009). Ubiquitination of PCNA functions as component for the choice of repair pathways either favoring damage bypass using the error prone translesion synthesis or the template switching-based homology directed repair (HR) pathway, which is considered to be error-free (Masuda and Masutani, 2019, Ripley et al., 2020). PCNA ubiquitination shapes its interactome by blocking or providing interaction surfaces leading to the recruitment of ubiquitin binding domain (UBD) containing interaction partners (Shen et al., 2021). One of the interaction partners binding to PCNA upon replication stress-induced ubiquitination is the ATPase WRNIP1, which interacts with PCNA via its N-terminal ubiquitin zinc finger (UBZ) domain (Saugar et al., 2012).

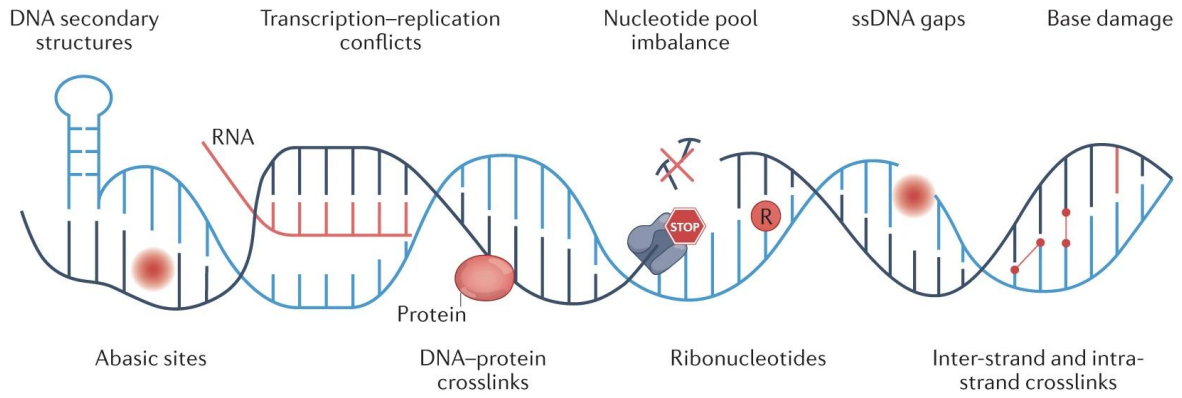


***Figure 5: Sources of DNA replication stress.***

*Replication stress originates from various sources, including single nucleotide aberrations such as DNA inter- and intra-strand crosslinks, abasic sites, the incorporation of ribonucleotides into DNA, base damage induced by alkylating drugs and ssDNA gaps. Moreover, proteins crosslinked to DNA, transcription-replication conflicts, DNA secondary structures and depletion of nucleotides are considered sources of replication stress. This figure was adapted from Cybulla and Vindigni (2023).*

### *3.7.3 The role of WRNIP1 in the replication stress response*

The Werner helicase interacting protein 1 (WRNIP1) localizes to sites of replication stress and interferes with the function of DNA polymerase delta in order to stabilize stalled replication forks (Hishida et al., 2006, Crosetto et al., 2008, Saugar et al., 2012, Jiménez-Martín et al., 2020). Recruitment of WRNIP1 to the replisome and its nuclear localization requires the UBZ domain, with which it binds to ubiquitinated PCNA. Replication fork stabilization through WRNIP1 is mediated by its collaboration with RAD51 and BRCA2 to prevent the MRE11 and SLX4 nuclease activity and therefore maintain the stalled fork (Leuzzi et al., 2016, Porebski et al., 2019). During drug-induced replication stress with hydroxyurea (HU) treatment, WRNIP1 safeguards the replication fork and upon treatment release, facilitates the restart of previously stalled replication forks via its ATPase function (Leuzzi et al., 2016).

Moreover, WRNIP1 is considered to be involved in promoting DNA damage response signaling pathways following replication stress (Kanu et al., 2016). A proposed model implicates WRNIP1 as a linker between ubiquitinated PCNA and the ATM interaction partner ATMIN. According to this model, replication stress induces the recruitment of WRNIP1 to focal structures, which co-localize with ATMIN in the presence of WRNIP1. ATMIN in turn is required for 53BP1 focus formation and activation of the DNA damage response signaling kinase ATM. Therefore, WRNIP1 is considered to bridge ubiquitinated PCNA and ATM/ATMIN to promote DNA damage response signaling and maintain genome integrity (Kanu et al., 2016). However, opposing studies have demonstrated that ATM activation upon replicative stress induction in ATMIN-depleted cells is still functional (Liu et al., 2017), showing that ATMIN is dispensable for ATM activation. Hence, the connection of WRNIP1 and replication stress induced ATM signaling is yet unknown, but may be important to understand cellular mechanisms to respond to replication stress. Moreover, the fact that WRNIP1 has a UBZ domain, with which it can bind to ubiquitinated PCNA proposes a crucial role for the ubiquitin system in the WRNIP1-mediated DNA damage response pathway.

## 3.8 The ubiquitin system

The post-translational modification by ubiquitin regulates protein functions involved in various processes, ranging from transcription, DNA replication, differentiation and apoptosis to metabolic processes and autophagy. Protein turnover and ubiquitin-dependent protein regulation networks are frequently perturbed in cancer cells. Ubiquitination of a given target protein follows a cascade of sequential actions (Figure 6) (Sluimer and Distel, 2018). First, a ubiquitin molecule covalently binds to a ubiquitin activating enzyme (E1), which transfers ubiquitin to a ubiquitin conjugating enzyme (E2) in a second step. Transfer of ubiquitin from an E2 enzyme to a target protein requires a ubiquitin ligase (E3). Several classes of E3 ligases have been characterized in human cells, including the really interesting new genes (RING), RING-between-RINGs (RBR) and homologous to E6AP C-terminus (HECT) ubiquitin ligases. While the molecular structures of these classes differ profoundly from each other (Zheng and Shabek, 2017), a common property is that ubiquitin ligases catalyze the transfer of a ubiquitin molecule mostly to a lysine residue or the N-terminus of a desired target protein. Importantly, RING E3 ligases catalyze the direct transfer of ubiquitin to its target molecule, whereas HECT (and RBR) E3 ligases require an intermediate step during which ubiquitin is covalently bound to a catalytic cysteine in the active center of the ligase via a thioester bond (Figure 6) (Sluimer and Distel, 2018). Therefore, genetic inhibition of HECT E3 ligases only requires a single point mutation to alter the catalytic cysteine in the respective gene.

Transfer of ubiquitin to target proteins may be performed at several lysine residues of a given target protein. Since several lysine residues are available in the ubiquitin molecule itself, polyubiquitin chains with distinct linkage types or even branched ubiquitin chains can be attached to target proteins (Figure 6). Depending on the nature of ubiquitination and facultative linkage specificities, the function of a target protein can be affected in different ways (Komander and Rape, 2012). Post-translational modifications, such as phosphorylation and acetylation, can be added to ubiquitin and ubiquitin chains, which further diversifies the potential modes of protein regulation through the ubiquitin system (Swatek and Komander, 2016).

K48- and K11-linked polyubiquitin are the best characterized linkage types that target a protein for proteasomal degradation. Therefore, these modifications play a key role in limiting protein levels of for instance oncoproteins, but also for tumor suppressors. Throughout unperturbed cell cycle, protein turnover is required to coordinate the level of checkpoint proteins (Zou and Lin, 2021) or remove stalled protein complexes from chromatin. Other linkage types can result in a change of protein function, localization and activity. Moreover, a single ubiquitin moiety placed at an interaction domain of a protein may interfere with its binding capacity or generate novel interaction domains and therefore regulate its dimerization or interactome (Sluimer and Distel, 2018).

The removal of ubiquitin modifications on proteins involves deubiquitinases (DUBs), which remove a ubiquitin modification via a cysteine protease, or to a lesser extent, metalloprotease function (Komander et al., 2009). Due to their nature of counteracting ubiquitination and the concomitant effect to reverse for instance a degradative K48-linked PTM on an oncoprotein, DUBs are considered potential targets for cancer drugs (Wei et al., 2015). This also accounts for targeted inhibition of ubiquitin ligases to exploit their potential to modulate protein levels of otherwise undruggable cancer associated proteins (Peter et al., 2014, Kunz et al., 2020). Exploitation of the ubiquitin system for cancer therapy is exemplified by the use of PROTACs, which target desired proteins for proteasomal degradation (Békés et al., 2022). Other strategies involve the use of proteasome inhibitors for the treatment of melanoma patients (Manasanch and Orlowski, 2017). In general, understanding of the ubiquitin system and its implications in cancer may give rise to novel strategies for targeting cellular diseases (Hoeller and Dikic, 2009, Duan and Pagano, 2021).

Further, ubiquitination is required to regulate transcription by either directly modifying RNAPII (Vidaković et al., 2020) or associated regulatory proteins, including site-specific or general transcription factors (Mark and Rape, 2021). For instance, transcriptional repression is achieved by H2A monoubiquitination, which promotes H3K27 methylation, resulting in chromatin compaction and the spread of the compaction signal (Mark and Rape, 2021). On the contrary, clearance of promotor regions from histones and therefore transcriptional

activation is achieved by polyubiquitination and subsequent extraction of histones via VCP (Mark and Rape, 2021). The size of the RNAPII pool available for transcription and the possibility to control this pool via ubiquitination directly influences functional transcription programs and therefore the role of RNAPII in the DNA damage response (Vidaković et al., 2020).

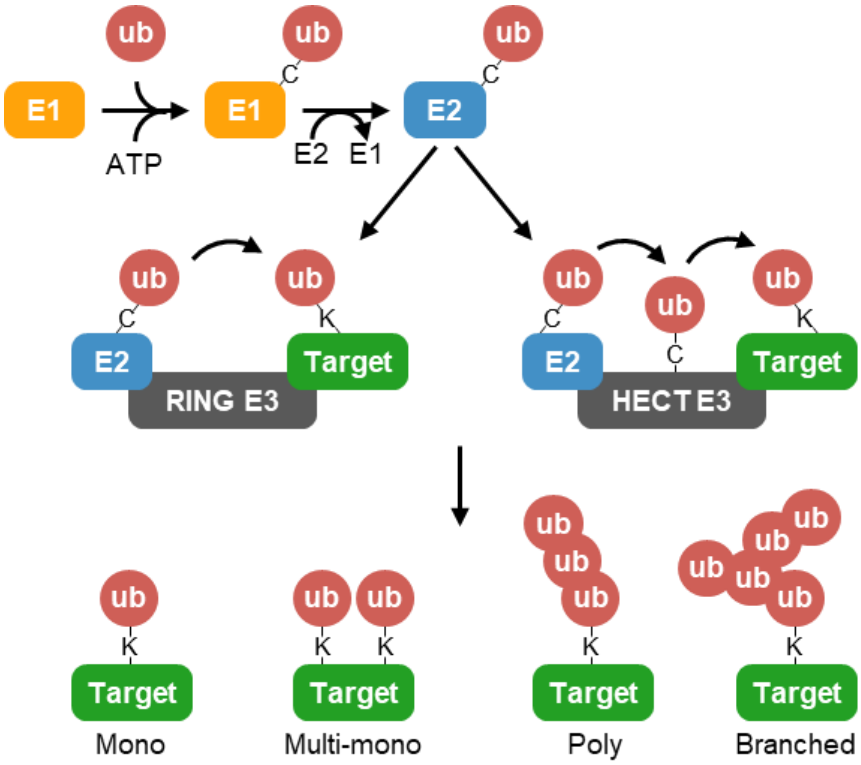


***Figure 6: The ubiquitin system.***

*Ubiquitination of target proteins requires three steps. First, ubiquitin is covalently bound by a ubiquitin activating (E1) enzyme, then transferred to a conjugating enzyme (E2) and finally transferred to a target protein by a ubiquitin ligase (E3). RING E3 ligases catalyze the direct transfer of ubiquitin from an E2 to a target protein, whereas HECT E3 ligases require an intermediate step during which ubiquitin is covalently bound by a catalytic cysteine residue. Different ubiquitination patterns and polyubiquitin linkage types may result in target protein regulation or degradation. This figure was adapted from Sluimer and Distel (2018).*

## 3.9 HUWE1 is a HECT E3 ubiquitin ligase

A large member (~480 kDa) of the HECT E3 ligases is HUWE1 (HECT, UBA, and WWE domain containing protein 1), which is comprised of several functional domains, including a solenoid scaffold structure, ubiquitin interaction motifs, substrate recognition surfaces and the catalytic HECT domain (Figure 7) (Hunkeler et al., 2021). Initially, HUWE1 was implicated in the turnover of MYC, TP53 and MCL1, as well as a growing list of substrates, including β-catenin, MIZ1 and histones. This elucidates the multifaceted roles of HUWE1 not only in

transcriptional regulation, but also in other processes such as DNA replication, DNA repair, apoptosis, stress responses, proliferation and differentiation (Choe et al., 2016, Adhikary et al., 2005, Chen et al., 2005, Zhong et al., 2005, Peter et al., 2014, Dominguez-Brauer et al., 2017, Kao et al., 2018, Qi et al., 2012, Jäckl et al., 2018, Gong et al., 2020).

HUWE1 targets its substrates not only for degradation via K48-linked polyubiquitination but can also regulate substrate functions via K6-, K11-, and K63-linked polyubiquitination, as well as monoubiquitination (Jäckl et al., 2018, Weber et al., 2019). Since HUWE1 plays a broad role in regulating complex protein networks, a key question in the field is whether and how it modulates transcription and replication and therefore enables or prevents tumor development.

On one hand, HUWE1 overexpression in prostate cancer cells slows down cell proliferation (Qu et al., 2018). In line with this finding, depletion of HUWE1 in mice leads to development of colonic tumors, potentially by the upregulation of MYC signaling once HUWE1-dependent degradation of MYC is abolished (Myant et al., 2017).

On the contrary, a growing body of evidence suggests that HUWE1 is required for efficient cell proliferation and thereby promotes tumor growth. The majority of conducted CRISPR/Cas9 KO and RNAi screens revealed that HUWE1 promotes cell proliferation (Tsherniak et al., 2017, Vazquez and Boehm, 2020, Pacini et al., 2021). Also, small-scale studies show that perturbation of HUWE1 function diminishes cell proliferation in several cancer types (Adhikary et al., 2005, He et al., 2021). Depletion or inhibition of HUWE1 in tumor cells and xenograft mouse models results in growth retardation of cancer cells, since it is involved in maintaining the DNA repair capacity (Peter et al., 2014, Yang et al., 2018, Kunz et al., 2020). The tumor promoting functions of HUWE1 identify HUWE1 as an interesting drug target for cancer therapy under the condition that the tumor repressing functions are maintained (Crawford et al., 2020, Qi et al., 2022).

HUWE1-dependent phenotypes can be partially explained by the ability of HUWE1 to modulate transcriptional programs via the mentioned substrates. However, HUWE1 is also involved in maintaining genome integrity upon DNA damage and replication stress through the modification of the replisome members PCNA, the initiation factor CDC6 and histones H2AX, H2B and H1 (Choe et al., 2016, Mandemaker et al., 2017, Kao et al., 2018). This suggests that HUWE1 is likely involved in the coordination of transcription and replication in a localized or global manner, but its actual impact on these processes are yet unclear. Therefore, investigating the ubiquitin ligase function of HUWE1 in the context of transcription replication conflicts and DNA damage response signaling may play an important role in understanding the HUWE1-dependent maintenance of genome integrity.

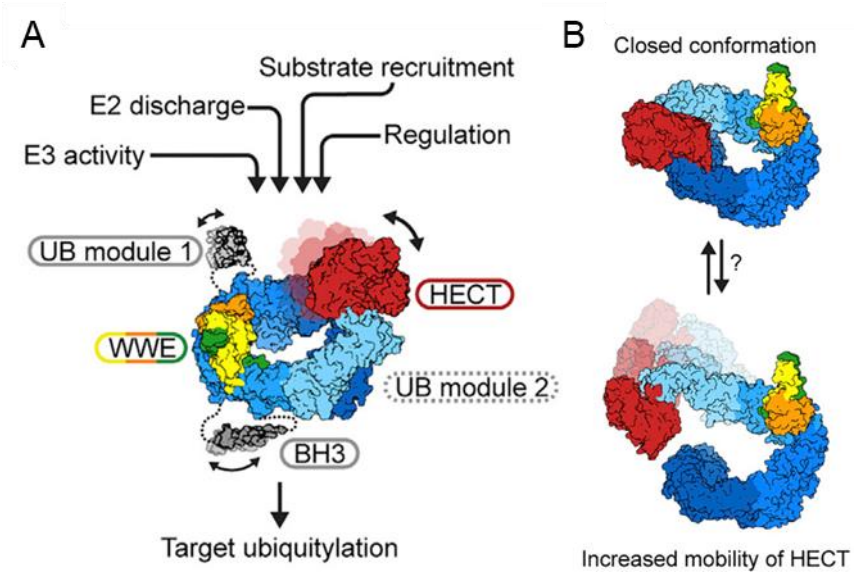


***Figure 7: Structure of the HUWE1 ubiquitin ligase.***

*A) The structure of the HUWE1 ubiquitin ligase is comprised of a solenoid architecture and several functional domains required for target protein interactions and ubiquitin transfer. The domains include ubiquitin interaction motifs (UB modules), substrate recognition surfaces (WWE, BH3, HWA) and the catalytic HECT domain. B) The solenoid scaffold may appear in closed or opened conformation that favors the mobility of the HECT domain. However, the functional outcome of this shift has not been characterized yet. This figure was adapted from Hunkeler et al. (2021). This article was published in Molecular Cell, Vol 81, Hunkeler et al., Solenoid architecture of HUWE1 contributes to ligase activity and substrate recognition, Page 3468-3480, Copyright Elsevier (2021). The article was published under CC BY-NC-ND 4.0 (https://creativecommons.org/licenses/by-nc-nd/4.0/) and the figure adapted with permission.*

## 3.10 Aim of the study

Key mechanisms by which the catalytic activity of HUWE1 maintains genome integrity and supports cell proliferation are yet unknown. This study aims to investigate

1. The effect of the HUWE1 ubiquitin ligase function on transcription, DNA replication and transcription replication conflicts
2. Effector proteins that are involved in HUWE1-dependent coordination of TRCs
3. The role of the transcription machinery in resolution of TRCs and DDR signaling
4. HUWE1- and WRNIP1-dependent DNA damage response signaling following the induction of TRCs and replication stress
5. The link between DNA damage and DNA damage response signaling at TRCs
6. HUWE1-dependent effects on tumor cell proliferation and synergistic treatment combinations for efficient killing of colorectal cancer cells.

# 4 Materials

All reagents and materials were purchased from the companies Thermo Fisher Scientific, Carl Roth, Sigma-Aldrich, Roche, Cell Signaling, New England BioLabs, Merck, Promega, Cayman, Sarstedt and Hartenstein if not stated otherwise (Einig et al., 2023).

## 4.1 Materials and chemicals

***Table 1: List of materials, chemicals and commercial buffers.***

| Product name | Catalog number | Supplier |
|---|---|---|
| 1,4-Dithiothreitol (DTT) | 6908.3 | Carl Roth |
| 10x EX Taq Buffer | RR01AM | Takara |
| 2-Propanol | 33539 | Sigma-Aldrich |
| 3M™ Empore™ C8 and C18 Extraction Disks | 14-386-2 | Empore |
| 4-(2-hydroxyethyl)-1-piperazineethanesulfonic acid (HEPES) | H3375 | Sigma-Aldrich |
| 5-Chloro-2'-deoxyuridine (CldU) | 18155 | Cayman |
| 5-Ethynyl-2'-deoxyuridine (EdU) | 61135-33-9 | Cayman |
| 5-Iodo-2′-deoxyuridine (IdU) | 20222 | Cayman |
| Acetic acid | ARK 2183 | Sigma-Aldrich |
| Acetonitrile (ACN) | 271004 | Merck |
| Agarose Low Melt | 6351.1 | Carl Roth |
| Agarose Standard | 3810.3 | Carl Roth |
| Albumin Fraktion V (BSA) | 8076.4 | Carl Roth |
| Ammonium bicarbonate (ABC) | 9830 | Merck |
| Ampicillin sodium salt | A9518 | Sigma-Aldrich |
| BIS-TRIS | B9754 | Sigma-Aldrich |
| Blasticidin | ant-bl-1 | InvivoGen |
| Bromophenol Blue | B0126 | Sigma-Aldrich |
| Buffer O (10X) | BO5 | Thermo Fisher |
| Buffer R (10X) | BR5 | Thermo Fisher |
| Calcium chloride dihydrate (CaCl2) | T885.2 | Carl Roth |
| cOmplete™, Mini, EDTA-free Protease Inhibitor Cocktail | 11836170001 | Roche |

| Product name | Catalog number | Supplier |
|---|---|---|
| Copper(II) sulphate pentahydrate (CuSO4) | 8175.1 | Carl Roth |
| Crystal violet solution | V5265 | Sigma-Aldrich |
| Deoxynucleotide (dNTP) Solution Mix | N0447 | New England BioLabs |
| Dimethylsulfoxid (DMSO) | A994.2 | Carl Roth |
| DNA Gel Loading Dye (6X) | R0611 | Thermo Fisher |
| dNTP-Set 1, 4 x 25 µmol (250 µl), 100 mM | K039.1 | Carl Roth |
| Doxycycline hyclate | D5207 | Sigma-Aldrich |
| Dulbecco's Modified Eagle's Medium - high glucose (DMEM) | D6429 | Sigma-Aldrich |
| Ethanol | K928.4 | Carl Roth |
| Ethidiumbromide | 2218.1 | Carl Roth |
| Ethylenediaminetetraacetic acid (EDTA) | ED | Sigma-Aldrich |
| Fetal Bovine Serum (FBS) | P30-3306 | PAN-Biotech |
| Formic acid (FA) | 111670 | Merck |
| GeneRuler™ 1 kb DNA-Ladder | SM0312 | Thermo Fisher |
| Glycerol | G5516 | Sigma-Aldrich |
| Glycine | G7126 | Sigma-Aldrich |
| GlycoBlue™ Coprecipitant | AM9516 | Thermo Fisher |
| Hexadimethrine bromide | 107689 | Sigma-Aldrich |
| Hydrochloric acid | 1099110001 | VWR Chemicals |
| Hydroxylamine | 438227 | Sigma-Aldrich |
| Hygromycin B Gold | ant-hg-1 | InvivoGen |
| InstantBlue™ | | Expedeon |
| Iodoacetamide (IAA) | I6125 | Sigma-Aldrich |
| LB-Medium (Lennox) | X964.2 | Carl Roth |
| Magnesium chloride hexahydrate (MgCl2) | 2189.1 | Carl Roth |
| Manganese(II) chloride monohydrate | 4320.1 | Carl Roth |
| MEM Non-essential Amino Acid Solution (100×) | M7145 | Sigma-Aldrich |
| Methanol | 8388.6 | Carl Roth |
| MOPS | M1254 | Sigma-Aldrich |

| Product name | Catalog number | Supplier |
|---|---|---|
| N,N,N′,N′-Tetramethylethylenediamine | T9281 | Sigma-Aldrich |
| NEBNext® dA-Tailing Reaction Buffer | B6059S | New England Biolabs |
| NEBuffer™ 2 | B7002S | New England Biolabs |
| N-Lauroylsarcosine sodium salt | 8.14715 | Sigma-Aldrich |
| Opti-MEM™ | 31985062 | Thermo Fisher |
| PageRuler™ Prestained Protein Ladder | 26617 | Thermo Fisher |
| Paraformaldehyde | P6148 | Sigma-Aldrich |
| PBS, pH 7.4 | 10010-056 | Thermo Fisher |
| Penicillin-Streptomycin | P4333 | Sigma-Aldrich |
| Phosphatase Inhibitor Cocktail 3 | P0044 | Sigma-Aldrich |
| Poly(ethyleneimine) solution | P3143 | Sigma-Aldrich |
| Potassium chloride | P9333 | Sigma-Aldrich |
| Potassium phosphate monobasic | P5655 | Sigma-Aldrich |
| Protease Inhibitor Cocktail | P8340 | Sigma-Aldrich |
| Protein A Agarose | 20333 | Thermo Fisher |
| Protein A Magnetic Beads | S1425S | New England BioLabs |
| Protein G Agarose | gel-agg-5 | InvivoGen |
| Protein G Magnetic Beads | S1430S | New England BioLabs |
| Puromycin | ant-pr-1 | InvivoGen |
| Quant-iT™ PicoGreen™ dsDNA-Reagent | P7581 | Thermo Fisher |
| rCutSmart Buffer (10x) | B6004 | New England Biolabs |
| ReproSil-Pur C18-AQ 1.9 µm resin | | Dr. Maisch |
| RiboLock RNase Inhibitor (40 U/µl) | EO0381 | Thermo Fisher |
| ROTI®Phenol/Chloroform/Isoamyl alcohol | A156.1 | Carl Roth |
| ROTIPHORESE®Gel 30 (37,5:1) | 3029.1 | Carl Roth |
| Sodium ascorbate | 3149.1 | Carl Roth |
| Sodium chloride | 3957.2 | Carl Roth |
| Sodium dodecyl sulfate (SDS) | 2326.5 | Carl Roth |
| Spermidine | 7161.1 | Carl Roth |
| Streptavidin Magnetic Beads | S1420S | New England BioLabs |
| Sulfo-Cyanin-3-azid | A1330 | Lumiprobe |

| Product name | Catalog number | Supplier |
|---|---|---|
| T4 DNA Ligase Reaction Buffer | B0202S | New England BioLabs |
| Tango-Buffer (10X) | BY5 | Thermo Fisher |
| TRI Reagent® | 93289 | Thermo Fisher |
| Trifluoroacetic acid (TFA) | 108262 | Merck Millipore |
| TRIS hydrochloride | 9090.2 | Carl Roth |
| Triton™ X-100 | X100 | Sigma-Aldrich |
| Trizma® base | T1503 | Sigma-Aldrich |
| Trypsin-EDTA (0.05%) | 25300054 | Thermo Fisher |
| TWEEN® 20 | P1379 | Sigma-Aldrich |
| VECTASHIELD HardSet Antifade Mounting Medium with DAPI | VEC-H-1500 | Biozol |

## 4.2 Commercial kits

***Table 2: List of commercial kits.***

| Product name | Catalog number | Supplier |
|---|---|---|
| Blunt/TA Ligase Master Mix | M0367 | New England Biolabs |
| Colorimetric Cell Viability Kit I | PK-CA705-CK04 | PromoKine |
| Con-A Sepharose® 4B | GE17-0440-03 | Sigma-Aldrich |
| Duolink® In Situ Detection Reagents Red | DUO92008 | Sigma-Aldrich |
| Duolink® In Situ PLA® Probe Anti-Mouse PLUS | DUO92001 | Sigma-Aldrich |
| Duolink® In Situ PLA® Probe Anti-Rabbit MINUS | DUO92005 | Sigma-Aldrich |
| Duolink® In Situ Wash Buffers, Fluorescence | DUO82049 | Sigma-Aldrich |
| FuGENE® HD Transfection Reagent | E2311 | Promega |
| GenElute™ HP Plasmid Miniprep Kit | NA0150 | Sigma-Aldrich |
| GenElute™ HP Plasmid Midiprep Kit | NA0200 | Sigma-Aldrich |
| HighPrep™ PCR Clean-up System | AC-60050 | MagBio Genomics |
| Immobilon Western HRP Substrat | WBKLS0500 | Merck Millipore |
| KAPA2G Robust HotStart ReadyMix | KK5701 | Sigma-Aldrich |
| KAPAHiFi™ Hot-Start ReadyMix (2X) | KM2605 | Roche |

| Product name | Catalog number | Supplier |
|---|---|---|
| Monarch® DNA Gel Extraction Kit | T1020S | New England Biolabs |
| Mycoplasma PCR Detection Kit | G238 | abm |
| NEB® 10-beta Competent E. coli (High Efficiency) | C3019I | New England BioLabs |
| NEBNext® Ultra™ II DNA Library Prep Kit for Illumina® | E7645S | New England BioLabs |
| NEBNext® Ultra™ II RNA Library Prep Kit for Illumina® | E7770S | New England BioLabs |
| NEBNext® Poly(A) mRNA Magnetic Isolation Module | E7490S | New England BioLabs |
| NEBNext® Ultra™ II End Repair/dA-Tailing Module | E7546S | New England BioLabs |
| NEBNext® Ultra™ II Q5® Master Mix | M0544 | New England BioLabs |
| Pierce™ BCA Protein Assay Kit | 23225 | Thermo Fisher |
| Quick-DNA Midiprep Plus Kit | D4075 | Zymo Research |
| TMTsixplex™ Isobaric Label Reagent Set | 90062 | Thermo Fisher |

## 4.3 Buffer recipes

***Table 3: List of buffer recipes used in this study.***

| Name | Recipe |
|---|---|
| 10x Oligo annealing buffer | 1 M NaCl, 100 mM Tris pH 7.4 |
| 10x Transfer buffer | 250 mM Tris, 1.92 M glycine |
| 10x Tris buffered saline (TBS) | 250 mM Tris-HCl, 1.4 M NaCl, pH 7.6 |
| 1x MOPS running buffer | 50 mM MOPS, 50 mM Tris, 0.1% SDS, 1 mM EDTA, 1 mM Na2S2O5 |
| 1x TE buffer | 1 mM EDTA, 10 mM Tris pH 8 |
| 1x Transfer buffer | 25 mM Tris, 192 mM glycin, 10% methanol |
| 20x MOPS running buffer | 1 M MOPS, 1 M Tris, 2 % SDS, 20 mM EDTA |
| 4x DTT sample buffer | 250 mM Tris-HCl pH 6.8, 4 % SDS, 25 % glycerol, 100 mM dithiothreitol, 0.02 % (w/v) bromophenol blue |
| 50x TAE buffer | 2 M Tris base, 1 M acetic acid, 50 mM EDTA |
| BisTris buffer pH 6.8 | 1.25 M BisTris pH 6.8 |
| Blocking buffer | 5% BSA in TBST |

| Name | Recipe |
|---|---|
| ChIP B&W buffer | 10 mM Tris-HCl pH 8.0, 1 M NaCl, 0.5 mM EDTA, 0.02 % Triton X-100 |
| Cut&Run binding buffer | 20 mM HEPES, 10 mM KCl, 1 mM CaCl2, 1 mM MnCl2 |
| Cut&Run incubation buffer | 3.5 mM HEPES, 10 mM CaCl2, 0.1% TritonX-100 |
| Cut&Run low salt buffer | 20 mM HEPES, 0.5 mM spermidine, 0.1% TritonX-100 |
| Cut&Run stop buffer | 150 mM NaCl, 20 mM EDTA, 0.1% TritonX-100, 50 µg/ml RNAseA |
| Cut&Run wash buffer | 20 mM HEPES, 150 mM NaCl, 0.5 mM spermidine |
| Permeabilization buffer | 0.3% TritonX-100 in 1x TBS |
| TBST | 50 mM Tris-HCl pH 7.6, 150 mM NaCl, 0.1% Tween20 |
| TNT-0 | 25 mM Tris-HCl pH 7.4, 1 % TritonX-100 |
| TNT-300 | 25 mM Tris-HCl pH 7.4, 1 % TritonX-100, 300 mM NaCl |

## 4.4 Oligonucleotides

***Table 4: List of primers and oligonucleotides used in this study.***

| Name | Sequence |
|---|---|
| shWRNIP1 #1 TRCN0000436158 F | CCGGATGATGTGCGAGATGTCATAACTCGAGTTATGACATCTCGCACATCATTTTTTG |
| shWRNIP1 #1 TRCN0000436158 R | AATTCAAAAAATGATGTGCGAGATGTCATAACTCGAGTTATGACATCTCGCACATCAT |
| shWRNIP1 #2 TRCN0000436134 F | CCGGGTGACATTATCTGCAACAAATCTCGAGATTTGTTGCAGATAATGTCACTTTTTG |
| shWRNIP1 #2 TRCN0000436134 R | AATTCAAAAAGTGACATTATCTGCAACAAATCTCGAGATTTGTTGCAGATAATGTCAC |
| shWRNIP1 #3 TRCN0000004527 F | CCGGCGCTGTCGAGTGATTGTTCTTCTCGAGAAGAACAATCACTCGACAGCGTTTTTG |
| shWRNIP1 #3 TRCN0000004527 R | AATTCAAAAACGCTGTCGAGTGATTGTTCTTCTCGAGAAGAACAATCACTCGACAGCG |
| shMYC TRCN0000039642 F | CCGGCCTGAGACAGATCAGCAACAACTCGAGTTGTTGCTGATCTGTCTCAGGTTTTTG |
| shMYC TRCN0000039642 R | AATTCAAAAACCTGAGACAGATCAGCAACAACTCGAGTTGTTGCTGATCTGTCTCAGG |
| shHUWE1 F (Peter et al., 2014) | CCGGCCCGCATGATCTTGAATTTCTCGAGAAATTCAAGATCATGCGGGTTTTTG |
| shHUWE1 R (Peter et al., 2014) | AATTCAAAAACCCGCATGATCTTGAATTTCTCGAGAAATTCAAGATCATGCGGG |

| Name | Sequence |
|---|---|
| shCtrl F | CCGGAGGCTCGCATGTATACAGACTCGAGTCTGTATACATGCGAGCCTTTTTTG |
| shCtrl R | AATTCAAAAAAGGCTCGCATGTATACAGACTCGAGTCTGTATACATGCGAGCCT |
| sgRNA HUWE1 #1 (Endres et al., 2021) | AAGGCCCTGCCCAACTCCGT |
| sgRNA HUWE1 #2 (Endres et al., 2021) | CATGCTACTGTTGGCTATCC |
| HA-WRNIP1 cds pRRL F | TGAGTCGGCCGGTGGATCCAATGTACCCTTACGACGTGCCCGACTACGCCGAGGTGAGCGGGCCG |
| HA-WRNIP1 cds pRRL R | GAGGGGCGGATCCGTCGACATCAGCACCTCCTCTGCTTGAAG |
| HA-WRNIP1 trunc #1 pRRL F | TGAGTCGGCCGGTGGATCCAATGTACCCTTACGACGTGCCCGACTACGCCCTACAGGGCAAGCCGC |
| HA-WRNIP1 trunc #2 pRRL F | TGAGTCGGCCGGTGGATCCAATGTACCCTTACGACGTGCCCGACTACGCTGGGTTGAACGGACTGCAGC |
| HA-WRNIP1 trunc #3 pRRL R | GAGGGGCGGATCCGTCGACATCATCGGGCGTCACCGTCACTG |
| HA-WRNIP1 trunc #4 pRRL R | GAGGGGCGGATCCGTCGACATCACATCTGTCGGATCTCC |
| HUWE1 clone screen bsr F | GTTGGGATTCGTGAATTGCT |
| HUWE1 clone screen flank R | GGTGTCTTCTTCAGTTTAGTCCTG |
| Random hexamer | NNNNNN |
| pRRL seq F | CTTCTGCTTCCCGAGCTCTA |
| pLKO seq R | GAACGGACGTGAAGAATGTG |

## 4.5 Plasmids

***Table 5: List of plasmid backbones used in this study.***

| Plasmid | Purpose | Origin |
|---|---|---|
| plentiCRISPR_V2 | Constitutive lentiviral expression vector | (Sanjana et al., 2014) |
| pLKO.1 | Constitutive shRNA backbone for lentivirus | (Stewart et al., 2003) |
| pLKO-Tet-on | Tet-inducible shRNA backbone for lentivirus | (Wiederschain et al., 2009) |
| pMD2.G | Lentiviral packaging vector | Laboratory of Didier Trono |
| pRRL | Constitutive lentiviral expression vector | Laboratory of Martin Eilers |

| Plasmid | Purpose | Origin |
|---|---|---|
| psPAX2 | Lentiviral packaging vector | Laboratory of Didier Trono |
| pSpCas9(BB)-2A-Puro (PX459) V2.0 | CRISPR/Cas9 based gene editing | (Ran et al., 2013) |

## 4.6 Enzymes

***Table 6: List of enzymes used in this study.***

| Enzyme | Catalog number | Supplier |
|---|---|---|
| BamHI (10 U/µL) | ER0051 | Thermo Fisher |
| Benzonase® Nuclease | 70746 | Sigma-Aldrich |
| BshTI (AgeI) (10 U/µL) | ER1461 | Thermo Fisher |
| CUT&RUN pAG-MNase and Spike-In DNA | 40366 | Cell Signaling |
| DNA Polymerase I, Large (Klenow) Fragment | M0210S | New England BioLabs |
| DNase I, RNase-free (1 U/µL) | EN0521 | Thermo Fisher |
| EcoRI (10 U/µL) 5000U | ER0271 | Thermo Fisher |
| Exonuclease I (E. coli) | M0293S | New England BioLabs |
| Klenow Fragment (3'→5' exo-) | M0212S | New England BioLabs |
| Micrococcal Nuclease | M0247S | New England BioLabs |
| M-MLV Reverse Transcriptase | M170 | Promega |
| Proteinase K | EO0491 | Thermo Fisher |
| RNase A | EN0531 | Thermo Fisher |
| Shrimp Alkaline Phosphatase (rSAP) | M0371S | New England BioLabs |
| SpeI (Bcu) | ER1251 | Thermo Fisher |
| T4 DNA Ligase | EL0011 | Thermo Fisher |
| Terminal Transferase (TDT) | M0315S | New England BioLabs |
| XhoI | ER0691 | Thermo Fisher |

## 4.7 Antibodies

***Table 7: List of primary antibodies used in this study.***

| Antigen | Catalog number | Supplier |
|---|---|---|
| ATM | sc-377293 | Santa Cruz |
| ATR | 2790 | Cell Signaling |
| BrdU | BD347580 | BD |
| BrdU | ab6326 | Abcam |
| CHK2 | 2662T | Cell Signaling |
| H2AX | sc-517336 | Santa Cruz |
| HA-tag | 2367 | Cell Signaling |
| HA-tag | 3724 | Cell Signaling |
| Histone H2B | 2934 | Cell Signaling |
| Histone H3 | 96C10S | Cell Signaling |
| HUWE1 | A300-486A-A | Bethyl |
| KAP1 | 15202-1-AP | Proteintech |
| MCM2 | 3619S | Cell Signaling |
| MCM5 | ab17967 | Abcam |
| MRE11 | NB100-142 | Novus Biologicals |
| MRE11 | sc-135992 | Santa Cruz |
| MYC | 13987 | Cell Signaling |
| PCNA | sc-56 | Santa Cruz |
| pS139-H2AX | 9718 | Cell Signaling |
| pS139-H2AX | 517348 | Santa Cruz |
| pS1981-ATM | 47739 | Santa Cruz |
| pS1981-ATM | ab81292 | Abcam |
| pS2-RNAPII | 61083 | Active Motif |
| pS2-RNAPII | A300-654A-M | Bethyl |
| pS4/8-RPA2 | 54762S | Cell Signaling |
| pS428-ATR | 2853T | Cell Signaling |
| pS5-RNAPII | 39749 | Active Motif |
| pS824-KAP1 | ab243870 | Abcam |
| pT68-CHK2 | ab3501 | Abcam |
| RAD50 | sc-74460 | Santa Cruz |
| RBP1 (RNAPII) | 14958 | Cell Signaling |
| RNAPII | 101307 | Active Motif |

| Antigen | Catalog number | Supplier |
|---|---|---|
| RPA2 | sc-56770 | Santa Cruz |
| Vinculin | V9131 | Sigma |
| WRNIP1 | 377402 | Santa Cruz |
| WRNIP1 | A301-389A-T | Bethyl |

***Table 8: List of secondary antibodies used in this study.***

| Antigen | Catalog number | Supplier |
|---|---|---|
| Anti-mouse IgG (Alexa Fluor® 488 Conjugate) | 4408 | Cell Signaling |
| Anti-mouse IgG (Alexa Fluor® 555 Conjugate) | 4409 | Cell Signaling |
| Anti-rabbit IgG (Alexa Fluor® 488 Conjugate) | 4412 | Cell Signaling |
| Anti-rabbit IgG (Alexa Fluor® 555 Conjugate) | 4413 | Cell Signaling |
| Anti-rat IgG (Alexa Fluor® 488 Conjugate) | 4416 | Cell Signaling |
| Anti-rabbit IgG, HRP-linked Antibody | 7074 | Cell Signaling |
| Anti-mouse IgG, HRP-linked Antibody | 7076 | Cell Signaling |
| Anti-rat IgG, HRP-linked Antibody | 7077 | Cell Signaling |

## 4.8 Cell lines

***Table 9: List of cell lines used in this study.***

| Cell line | Origin |
|---|---|
| HCT116 | Laboratory of Martin Eilers |
| HCT116 HUWE1-WT | Valentina Andrioletti, laboratory of Nikita Popov |
| HCT116 HUWE1-CS | Valentina Andrioletti, laboratory of Nikita Popov |
| HCT116 HUWE1-WT pLKO tet-on shCtrl | Elias Einig, this study |
| HCT116 HUWE1-CS pLKO tet-on shCtrl | Elias Einig, this study |
| HCT116 HUWE1-WT pLKO tet-on shWRNIP1 #1 | Elias Einig, this study |
| HCT116 HUWE1-CS pLKO tet-on shWRNIP1 #1 | Elias Einig, this study |
| HCT116 HUWE1-WT pLKO tet-on shWRNIP1 #2 | Elias Einig, this study |
| HCT116 HUWE1-CS pLKO tet-on shWRNIP1 #2 | Elias Einig, this study |
| HCT116 HUWE1-WT pLKO tet-on shWRNIP1 #3 | Elias Einig, this study |
| HCT116 HUWE1-CS pLKO tet-on shWRNIP1 #3 | Elias Einig, this study |

| Cell line | Origin |
|---|---|
| HCT116 pLKO tet-on shMYC | Elias Einig, this study |
| HCT116 pLKO tet-on shCtrl | Elias Einig, this study |
| HCT116 pLKO.1 shCtrl | Elias Einig, this study |
| HCT116 pLKO.1 shHuwe1 | Elias Einig, this study |
| HCT116 pRRL vector control | Elias Einig, this study |
| HCT116 pRRL HA-WRNIP1 FL | Elias Einig, this study |
| HCT116 pRRL HA-WRNIP1 ΔLZ | Elias Einig, this study |
| HCT116 pRRL HA-WRNIP1 UBZ | Elias Einig, this study |
| HCT116 pRRL HA-WRNIP1 ΔUBZ | Elias Einig, this study |
| HCT116 pRRL HA-WRNIP1 AAA | Elias Einig, this study |
| HCT116 pRRL HA-WRNIP1 LZ | Elias Einig, this study |
| HCT116 pRRL HA-WRNIP1 ΔAAA | Elias Einig, this study |
| HEK 293T | Laboratory of Lars Zender |
| Hep3B | Laboratory of Lars Zender |
| HuH7 | Laboratory of Lars Zender |
| HLF | Laboratory of Lars Zender |
| LentiX 293T | Laboratory of Michael Hudecek |
| MEF | Laboratory of Martin Eilers |

## 4.9 Equipment

***Table 10: List of instruments used in this study.***

| Instrument | Supplier |
|---|---|
| Centrifuge Micro Star 17R | VWR |
| ChemiDoc MP imaging system | Biorad |
| Column oven | Sonation |
| EASY-nLC 1200 | Thermo Fisher |
| Infinite M plex plate reader | Tecan |
| NanoDrop 1000 Spectrophotometer | Peqlab |
| NovaSeq 6000 | Illumina |
| Olympus BX63 microscope | Olympus |
| Olympus DP80 camera | Olympus |

| Instrument | Supplier |
|---|---|
| Q Exactive™ HFX Hybrid Quadrupole-Orbitrap™ mass spectrometer | Thermo Fisher |
| Spinning Carousel | A. Hartenstein |
| Stage-tip Centrifuge | Sonation |
| UP200St sonicator | Hielscher |
| Vacuum Centrifuge SpeedVac | Eppendorf |

# 5 Methods

*Parts of this chapter were adapted from EINIG, E., JIN, C., ANDRIOLETTI, V., MACEK, B. & POPOV, N. 2023. RNAPII-dependent ATM signaling at collisions with replication forks. Nature Communications.*

## 5.1 Cell culture

Cultured cell lines proliferated in Dulbecco's Modified Eagle's Medium with high glucose (DMEM; Sigma) supplemented with 1% (v/v) penicillin-streptomycin (Sigma), 10% (v/v) fetal bovine serum (FBS; PAN-Biotech), 1% (v/v) non-essential amino acids (Sigma) and 50 µM 2-mercaptoethanol. Cells were maintained in a humidified atmosphere at 37°C with 7.5% $CO_2$ and routinely tested for mycoplasma contamination using a Mycoplasma PCR Detection Kit (abm). The nature of HCT116 cells was confirmed by STR typing.

## 5.2 Cell viability assays

### *5.2.1 Crystal violet staining*

Following treatment, cell culture dishes were washed once with PBS and dried overnight. Aqueous solution of 1% (w/v) crystal violet (Sigma) was added to each well for 10 min prior to washing with water three times. Staining intensity was assessed via absorbance measurement at 595 nm with an Infinite M plex plate reader (Tecan) and 10x10 measurements per well.

### *5.2.2 WST-8 assay*

Cell viability was assessed using the tetrazolium salt WST-8 provided in the Colorimetric Cell Viability Kit I (PromoKine) according to the manufacturer's instructions. In brief, 10 µl of the WST-8 solution were added to each well of a 96-well plate containing cultured and treated cells in 100 µl media and incubated for 2 h in a humidified atmosphere at 37°C with 7.5% $CO_2$. Staining intensity was assessed via absorbance measurement at 450 nm with an Infinite M plex plate reader (Tecan).

### *5.2.3 Growth curve*

Indicated cell lines were treated with 50 µg/ml doxycycline for 7 days prior to seeding $10^4$ cells in a 6-well culture dish in triplicates. For the following 7 days, cells were not perturbed and cultivated under continuous doxycycline treatment. Every day, a set of triplicates was washed and dried followed by crystal violet staining.

### *5.2.4 Synergism of small molecule inhibitors*

Desired cells were treated with combinations of two small molecule inhibitors with up to five different inhibitor dilutions and a DMSO control. Cell viability was assessed as described for WST-8 assay (5.2.2). Potential synergism of treatments in relative growth inhibition was calculated with Synergy Finder 2.0 (Ianevski et al., 2020) using the ZIP synergy score model (Yadav et al., 2015).

## 5.3 Immunoblot

Cells were detached from culture dishes either with Trypsin-EDTA (0.05%) (Thermo) or with 1 mM EDTA in PBS for 3 min. Pelleting was performed by centrifugation at 500 g for 3 min prior to washing once with PBS and a second centrifugation step. Cell pellets were resuspended in PBS and lysed with 4x DTT Sample Buffer (250 mM Tris-HCl pH 6.8, 25% (v/v) glycerol, 4% (v/v) SDS, 100 mM dithiothreitol, 0.02% (w/v) bromophenol blue) supplemented with 1:1000 protease and phosphatase inhibitor cocktails (Sigma) and boiled at 95°C for 10 min. SDS-PAGE was performed with 9% Bis-Tris acrylamide gels in 1x MOPS running buffer for 1 h at 125 V. Separated proteins were transferred to PVDF membranes in transfer buffer (25 mM Tris, 192 mM glycine, 10% (v/v) methanol) for 2 h with 125 V at 4°C. Membranes were blocked using 5% (w/v) bovine serum albumin (BSA) in TBST (50 mM Tris-HCl pH 7.6, 150 mM NaCl, 0.1% Tween 20) for at least 1 h with horizontal shaking. Primary antibodies (1:1000 in TBST, see Table 7) were added to the membrane pieces overnight at 4°C followed by three washing steps with TBST for 5 min and incubation with HRP-linked secondary antibodies (Cell signaling; 1:7500 in TBST, see Table 8) for more than 2 h prior to blot development using Immobilon Western HRP Substrate (Merck) in a ChemiDoc MP imaging system (Biorad) and the ImageLab software version 5.2.1.

## 5.4 Cycloheximide assay

$2x10^5$ HCT116 cells were seeded in a 6 well plate 24 h prior to treatment. Cycloheximide was added at a final concentration of 50 µg/ml for 0, 1, 2, 4 and 8 h followed by detaching cells with EDTA in PBS and immunoblot analysis (see 5.3).

## 5.5 Immunofluorescence

Coverslips were sterilized with 70% ethanol for 20 min and dried in 24-well culture dishes. Cells were seeded on coverslips more than 24 h before fixation with a density that reaches about 70% confluence at the time of fixation. After washing with PBS, 1% paraformaldehyde (PFA) in PBS was added to each well for 10 min and coverslips were washed three times with

PBS. Permeabilization of cell membranes was performed with 0.3% (v/v) TritonX-100 in 1x TBS for 5 min followed by washing with blocking buffer (5% BSA (w/v) in TBST) once and blocking for 30 min at room temperature. Primary antibodies (Table 7) were diluted 1:200 in blocking buffer and added to coverslips for 2 h. Following three washing steps with PBS for 5 min each, fluorophore-linked secondary antibodies (Table 8) were added to the samples at a dilution of 1:200 in blocking buffer for 2 h at room temperature and protected from light. Samples were washed three times with PBS for 5 min and excess liquid was removed by careful contact with a paper towel at the edge of each coverslip. Cells were dried for 5 min and mounted on glass slides in 5 µl VECTASHIELD HardSet Antifade Mounting Medium with DAPI (Biozol) and kept at 4°C until analysis using an Olympus DP80 camera mounted to an Olympus BX63 microscope and the cellSens Dimension software version 1.17 (Olympus).

## 5.6 Proximity ligation assay

Formaldehyde-fixed slides were prepared as for immunofluorescence (see 5.5) and subsequently fixed with 90% methanol at -20°C overnight. Cells were re-hydrated in PBS for 5 min prior to blocking, permeabilization and primary antibody incubation with antibodies from two different host species as described for immunofluorescence (see 5.5). Proximity ligation assays (PLA) (Mendez and Banerjee, 2017) were performed by adding a mixture of two PLA probes (Duolink® In Situ PLA® Probe Anti-Mouse PLUS and Duolink® In Situ PLA® Probe Anti-Rabbit MINUS, Sigma) to the samples at a dilution of 1:20 in blocking buffer for 1 h at 37°C. The ligation reaction and signal amplification were performed using Duolink® In Situ Detection Reagents Red (Sigma) and Duolink® In Situ Wash Buffers following the manufacturer's instructions. In brief, samples were washed twice with PLA wash buffer A and the DNA ligase was added at a dilution of 1:40 in 1x ligation buffer for 1 h at 37°C in a humidified atmosphere. Cells were washed with PLA wash buffer A two times and signal amplification was performed by rolling-circle-amplification using a polymerase diluted 1:80 in 1x amplification buffer for 2 h at 37°C in a humidified atmosphere. At last, coverslips were washed twice with PLA wash buffer B for 10 min followed by washing with a 1:100 dilution of PLA wash buffer B in water. Samples were dried and mounted as described previously (see 5.5) and images of the dot-like PLA signals were acquired as Z-stacks.

Each Z-stack consisted of at least 5 frames with an z-increment of 1 µm. Images were processed with the free software FIJI/ImageJ version 1.53f (https://imagej.net/software/fiji/) (Schindelin et al., 2012). For image analysis and counting of PLA foci, z-layers were combined to a single image by maximum intensity projection prior to image segmentation based on nuclear areas stained with DAPI. Counts of PLA foci per cell nucleus were determined for each cell individually.

## 5.7 DNA fiber assay

Cultured cells were treated with 25 µM 5-Iodo-2′-deoxyuridine (IdU) followed by 250 µM 5-Chloro-2′-deoxyuridine (CldU) for 30 min at 37°C (Nieminuszczy et al., 2016). Detached cells were washed with PBS and 2000 – 3000 cells in 2 µl PBS were transferred to a glass slide. Lysis was performed by adding 7 µl 200 mM Tris pH 7.5, 0.5% SDS, 50 mM EDTA and stirring with the pipette tip followed by tilting the slide at a 15° angle to spread the DNA across the whole slide. DNA fibers were fixed and denatured with 33% acetic acid in 67% methanol for 10 min followed by 2.5 M HCl for 80 min. 5% BSA in PBS was used to block the slides for 20 min and primary antibodies to IdU (1:25) and CldU (1:300) in blocking buffer were added for 2 h. Following three washes with PBS, fibers were labeled with fluorophore-conjugated secondary antibodies diluted in blocking buffer (1:200) for 1 h protected from light. Images were acquired as described (see 5.5) and the length of symmetric fibers was measured using FIJI/ImageJ version 1.53f. The speed of replication forks was estimated based on the fiber length of which 1 µm roughly corresponds to 2.59 kb (Nieminuszczy et al., 2016, Jackson and Pombo, 1998).

## 5.8 EdU incorporation assay

HCT116 cells were cultivated on sterilized coverslips and treated with 25 µM 5-ethynyl-2′-deoxyuridine (EdU) for 30 min prior to fixation with 4% PFA in PBS for 5 min. Cell membranes were permeabilized with 0.3% TritonX-100 in TBS for 5 min. EdU incorporated in the genomic DNA was labeled via click-reaction with Cy3 by adding 2 mM CuSO4, 4 µM sulfo-Cy3-azide and 100 mM sodium ascorbate for 30 min at room temperature. Stained cells on coverslips were mounted on glass slides and picture acquisition was performed as described (see 5.5).

## 5.9 Single cell gel electrophoresis

For single cell gel electrophoresis under neutral conditions (neutral comet assay) (Boutet-Robinet et al., 2013), glass slides were coated with 1% (w/v) agarose and dried. Detached cells were pelleted and washed with PBS prior to embedding cells in 0.7% (w/v) agarose with low melting point (LMP agarose) at 37°C. The cell suspension in agarose was transferred to the pre-coated glass slides, spread out with a coverslip and chilled on ice for 3 s to solidify the LMP agarose. After removal of the coverslip, the cell layer was coated with a second layer of LMP agarose without cells. After complete gelation of the agarose, embedded cells were lysed with 10 mM Trizma base (pH 10), 2.5 M NaCl, 100 mM EDTA, 10% (v/v) DMSO, 1% (v/v) N-laurylsarcosine, 0.5% (v/v) TritonX-100 overnight at 4°C.

Samples were washed three times with 1x TAE buffer for 5 min each prior to electrophoresis at 18 V for 1 h. Glass slides were washed twice with PBS for 5 min followed by ethanol for 10 min twice and air drying for at least 2 h. Comets were stained by rehydration with 2 µg/ml ethidium bromide in water followed by image acquisition (see 5.5). DNA comet properties were quantified with the OpenComet v1.3.1 FIJI/ImageJ plugin (Gyori et al., 2014). The sample preparation for the neutral comet assays was performed by Chao Jin. Subsequent picture acquisition and data analysis was performed by Elias Einig.

## 5.10 Bacteria transformation and culturing

Competent 10-beta *E.coli* were transformed according to the manufacturer's instructions. In brief, 20 µl of bacteria cell suspension was thawed on ice and a maximum of 2 µl plasmid solution with up to 30 ng of plasmids were added. Suspensions were mixed by carefully flicking the reaction tube and incubated on ice for 30 min. Heat shock was applied at 42°C for 30 s and bacteria were immediately transferred back on ice for 5 min. Stable outgrowth medium (SOM) was pre-warmed at 37°C and 200 µl were added to each transformation mixture. Bacteria were allowed to grow without antibiotics for 1 h at 37°C with shaking at 800 rpm prior to spreading the solution on ampicillin (50 µg/ml) agar plates. Single colonies were formed overnight at 37°C and selected with a pipette tip to inoculate 4 ml cultures of LB Lennox medium. The mini-culture was rotated horizontally with 200 rpm at 37°C overnight. Resulting cell suspensions were either mixed 1:1 with 50% glycerol and stored at -80°C or centrifuged at 4000 rpm for 5 min and stored at -20°C for plasmid preparation (see 5.11).

## 5.11 Plasmid preparation

Plasmids were extracted from bacterial cell pellets using either the GenElute™ HP Plasmid Miniprep Kit for culture volumes up to 5 ml or the GenElute™ HP Plasmid Midiprep Kit for bacterial culture volumes up to 200 ml following the manufacturer's instructions. Alternatively, the buffers of respective kits were used to extract plasmids with a modified, faster extraction protocol lacking the need for spin columns. In brief, bacterial cell pellets derived from 4 ml cultures were resuspended in 130 µl resuspension buffer supplemented with RNAseA, lysed by addition of 130 µl lysis buffer and inverted six times followed by neutralization with 150 µl neutralization buffer. The suspension was centrifuged at 17000 g for 10 min and 400 µl of the supernatant was transferred to a new reaction tube containing 1 ml ethanol. After thorough mixing, precipitated plasmid DNA was pelleted by centrifugation at 17000 g for 20 min at 4°C and washed once with 80% ethanol. Purified plasmid DNA was stored in 10 mM Tris, pH 7.4.

## 5.12 HUWE1 gene replacement

The biallelic replacement of the genomic HUWE1 locus in HCT116 cells was performed by Valentina Andrioletti in the laboratory of Nikita Popov (Endres et al., 2021). In brief, HCT116 cells were transfected with a repair template and two sgRNAs targeting HUWE1 (Figure 8) using Fugene (Promega). The repair template contained the HUWE1 ORF sequence of amino acid residues 4277-4374 (Q7Z6Z7-1; ENST00000342160.7) with or without the C4341S mutation, P2A self-cleaving peptide, blasticidin resistance gene and flanking homology arms resembling genomic positions chrX:53561159-53561889 and chrX:53559367-53560269. HUWE1-targeting sgRNAs were cloned into the pSpCas9(BB)-2A-Puro (PX459) V2.0 vector (a gift from Feng Zhang, Addgene plasmid # 62988) (Ran et al., 2013) and co-transfected with the repair template. Following blasticidin and puromycin selection, single cell clones were propagated and validated by PCR and Sanger sequencing by the Microsynth Seqlab.

## 5.13 cDNA synthesis

RNA was purified from HCT116 cells using TRI Reagent® (Sigma) following the manufacturer's instructions and contaminating DNA was digested using DNAseI (Thermo) for 30 min at 37°C. RNA was precipitated and washed with 80% ethanol and quantified using a NanoDrop 1000 (Peqlab). Following cDNA synthesis was performed with 2 µg RNA and 1 µg random hexamer primer using M-MLV Reverse Transcriptase (Promega, M170) according to the manufacturer's instructions. In brief, the mixture of random primer and RNA was heated to 70°C for 5 min and immediately placed on ice. 200 U M-MLV reverse transcriptase, 50 U RiboLock RNase Inhibitor (Thermo), 200 µM dNTPs and a final concentration of 1x reaction buffer were added prior to incubation at 37°C for 1 h. Enzymes were heat inactivated at 70°C for 10 min and cDNA was stored at -20°C.

## 5.14 WRNIP1 expression plasmids and truncation variants

The WRNIP1 ORF sequence (ENST00000380773.9; Q96S55-1) was amplified from HCT116-derived cDNA (see 5.13) in PCR reactions using NEBNext® Ultra™ II Q5® Master Mix according to the manufacturer's suggestions. Similarly, WRNIP1 truncation variant sequences, encompassing the ubiquitin binding domain (UBZ, amino acid residues 1 - 222), the AAA-ATPase domain (AAA, amino acid residues 223 - 444), the leucine zipper containing domain (LZ, amino acid residues 445 - 665) or combinations of these domains, were amplified from cDNA with respective primers (Table 4). N-terminal primers consisted of an overlap sequence with the pRRL target vector backbone (TGAGTCGGCCGGTGGATCCA) and an HA-tag (ATGTACCCTTACGACGTGCCCGACTACGCC) prior to the WRNIP1 specific primer

sequence. Respectively, each C-terminal primer consisted of the pRRL overlap sequence (GAGGGGCGGATCCGTCGACA) linked to the reverse complement WRNIP1 C-terminal DNA sequence.

Amplified DNA sequences were purified via agarose gel electrophoresis (1.5 % agarose, 130 V, 35 min, TAE buffer) followed by gel extraction of desired bands with the Monarch® DNA Gel Extraction Kit. Purified DNA was cloned into lentiviral pRRL expression vector (a gift from Martin Eilers) (Wiese et al., 2015), digested with AgeI and SpeI in Tango buffer (Thermo) overnight, via the NEBuilder® HiFi DNA Assembly Master Mix following the manufacturer's instructions (50°C, 15 min). Resulting plasmids were transfected into NEB® 10-beta Competent *E. coli* according to the manufacturer's instructions and selected on ampicillin (50 mg/l) agar plates. Correct vector assembly was confirmed by restriction digestion with BamHI (Thermo) and subsequent Sanger sequencing performed by the Microsynth Seqlab with the pRRL forward sequencing primer (Table 4).

## 5.15 RNA interference

Oligonucleotides encoding forward and reverse MISSION® shRNA sequences (Sigma) or scrambled control sequences were annealed through heating to 95°C in 100 mM NaCl, 10 mM Tris pH 7.4 for 5 min followed by slowly ramping down to room temperature for 4 h. Annealed oligos were cloned into doxycycline inducible pLKO tet-on vector backbones (a gift from Dmitri Wiederschain, Addgene plasmid # 21915) (Wiederschain et al., 2009) or into constitutively expressing pLKO.1 vector backbones (a gift from Bob Weinberg, Addgene plasmid # 8453) (Stewart et al., 2003) following a published procedure (Wiederschain et al., 2009). In brief, plasmids were digested with AgeI and EcoRI in BufferO (Thermo) overnight and purified via agarose gel electrophoresis (1% agarose, 130 V, 30 min, 1x TAE buffer) and gel extraction of desired bands with the Monarch® DNA Gel Extraction Kit. Oligonucleotides were ligated into 10 – 20 ng digested vector backbones with T4 DNA ligase in 1x ligase buffer (Thermo) and a final concentration of 12.5 nM annealed oligonucleotides for 1 h at room temperature.

Alternatively, desired shRNA sequences were flanked with overhang sequences matching the ends of digested vector backbones and cloned using NEBuilder® HiFi DNA Assembly Master Mix following the manufacturer's instructions (50°C, 15 min). The overhang sequences for pLKO.1 were CTTGTGGAAAGGACGAAACA (5') and AATTCTCGACCTCGAGACAAATGG (3'), whereas the overhang sequences GTTCCCTATCAGTGATAGAGACA (5') and AATTCTCGACCTCGAGACAAATGG (3') were used for pLKO Tet-on respectively.

Resulting plasmids were transfected into NEB® 10-beta Competent *E. coli* according to the manufacturer's instructions and selected on ampicillin (50 mg/l) agar plates. Correct vector

assembly was confirmed by restriction digestion with XhoI in buffer R (Thermo) and subsequent Sanger sequencing performed by the Microsynth Seqlab with the pLKO.1 reverse sequencing primer (Table 4).

## 5.16 Lentiviral transduction

Desired lentiviral expression vectors (pRRL, pLKO.1 or pLKO Tet-on) were transfected alongside lentiviral packaging vectors pMD2.G (a gift from Didier Trono, Addgene plasmid # 12259) and psPAX2 (a gift from Didier Trono, Addgene plasmid # 12260) into LentiX 293T cells using polyethylenimine (PEI) (Longo et al., 2013). 30 µl of 1 mg/ml PEI were diluted with 670 µl Opti-MEM, as well as 1.4 µg psPAX2, 2.8 µg pVSV-G and 11.1 µg lentiviral expression vector in another 700 µl Opti-MEM. Both solutions were mixed and incubated for 10 min at room temperature prior to adding the entire solution dropwise to 6 million LentiX cells in 6 ml fresh culture media on a 10 cm cell culture dish overnight. The transfection mixture containing media was replaced with 6 ml fresh full media and lentiviral particles were produced for 48 hours. Virus containing supernatants were passed through 450 nm filters and cell-free suspensions were added to settled target cells seeded at 10% confluence in the presence of 8 µg/ml hexadimethrine bromide. After 72 h, target cells were passaged and selected with either 1 µg/ml puromycin (pLKO.1, pLKO Tet-on and pLentiCRISPR_V2) or 200 µg/ml hygromycin B (pRRL) for at least 48 h or until the vector-lacking control cells died.

Expression of HA-tagged WRNIP1 and its derivatives, as well as depletion of target proteins following pLKO.1 transduction was confirmed by immunoblot. Target cells transduced with pLKO Tet-on vectors were treated with 100 ng/ml doxycycline for at least 4 days prior to any experiment to induce shRNA expression, if not indicated otherwise. Likewise, target depletion was confirmed via immunoblot.

## 5.17 Immunoprecipitation

Reaching 80% confluence, cultured cells were washed and scraped on ice in PBS, centrifuged for 3 min with 500 g at 4°C and washed again. Cell pellets were lysed in TNT-300 (25 mM Tris pH 7.4, 300 mM NaCl, 1% (v/v) TritonX-100, supplemented with protease and phosphatase inhibitor cocktails) for 10 min on ice. Next, samples were diluted 1:1 with TNT-0 to a final concentration of 150 mM sodium chloride. Insoluble cell debris was pelleted by centrifugation at 17000 g for 10 min and supernatants were used to quantify protein content with the Pierce™ BCA Protein Assay Kit. Of each sample, 1 – 5% was separated serving as an input. 30 µl of agarose bead slurry (protein A or protein G) was washed three times with TNT-150 and added to the lysates, which were adjusted for equal protein content between samples (0.5 – 1 mg).

Target specific primary antibodies or non-targeting IgG control antibodies (0.5 – 2 µg) were added to the bead-lysate mixture and rotated overnight at 4°C. Samples were centrifuged at 700 g for 2 min and bead pellets washed three times with TNT-150. Bead pellets were resuspended in 30 µl 4x DTT sample buffer and boiled at 95°C for 5 min to retrieve precipitated proteins from beads followed by SDS-PAGE and analysis via immunoblot or LC-MS/MS.

Immunoprecipitation experiments shown in Figure 18C – G and in Figure 21B – D were performed by Nikita Popov.

### *5.17.1 Benzonase treatment*

For immunoprecipitation in the absence of nucleotides, cell pellets were resuspended in 20mM Tris, pH7.5, 100mM NaCl, 2mM CaCl2, 2mM MgCl2, 0.2% TritonX-100, supplemented with 0.2 µl benzonase per sample and incubated on ice for 1 h. Subsequently, 5 volumes of TNT-150 supplemented with 5 mM EDTA were added to each sample an immunoprecipitation was conducted as described in 5.17. This protocol was used for immunoprecipitation of pS2-RNAPII from MEF cells followed by LC-MS/MS analysis.

### *5.17.2 Paraformaldehyde crosslinking*

Harsh lysis or chemical properties of lysis buffers may prevent detection of transient or weak protein interactions. Therefore, cultured cells were washed with PBS once and mildly crosslinked with 0.2 % PFA for 4 min on a horizontal shaker prior to quenching the reaction by adding 200 mM glycine for 4 min. Crosslinked cells were washed three times with PBS and scraped followed by centrifugation with 500 g for 3 min. Washed cell pellets were lysed with TNT-150 and sonified for 3x 2 min with 30% amplitude, 2 W power and a 45 s on, 15 s off cycle with the UP200St sonicator (Hielscher). Lysates were cleared by centrifugation at 17000 g for 10 min and immunoprecipitation was performed as described (see 5.17). Boiling of precipitates was prolonged to 15 min to reverse crosslinks prior to SDS-PAGE and immunoblot.

## 5.18 In-gel digestion

Protein interactomes were analyzed by LC-MS/MS following immunoprecipitation (see 5.17). Therefore, eluted precipitates were boiled for 5 min at 95°C and subjected to a short SDS-PAGE using 9% Bis-Tris acrylamide gels for 20 min at 80 V in 1x MOPs buffer prior to staining proteins with InstantBlue™ for 10 min. Entire lanes were cut out of the gel and chopped to pieces of approximately 1 mm3. Gel pieces were washed with 5 mM ammonium bicarbonate (ABC) followed by 50% (v/v) acetonitrile (ACN) and a final wash with pure ACN

for 20 min each. Dehydrated gel pieces were soaked with 10 mM dithiothreitol (DTT) in 20 mM ABC and proteins were reduced for 45 min at 56°C prior to alkylation with 55 mM iodoacetamide (IAA) in 20 mM ABC for 45 min. Subsequently, gel pieces were dehydrated by washing with 5 mM ammonium bicarbonate (ABC) followed by 50% (v/v) acetonitrile (ACN) and a final wash with pure ACN for 20 min each.

To digest proteins, gel pieces were soaked with 12.5 ng/µl trypsin (Promega) in 20 mM ABC and incubated at 37°C overnight. Resulting tryptic peptides were extracted and acidified with subsequent washes using 50% ACN, 3% trifluoroacetic acid (TFA) prior to 80% ACN, 0.5% acetic acid and pure ACN for 30 min each. Supernatants of each washing step were pooled per sample and acetonitrile was evaporated by vacuum centrifugation in a SpeedVac for at least 45 min or until the sample volume reached the cumulative volume of aqueous buffers used for washing. Peptides were desalted via StageTips (see 5.19).

## 5.19 StageTips

Peptide solutions were acidified with TFA to a pH of 2 and desalted following the StageTip protocol (Rappsilber et al., 2007). In brief, two discs of C18 bonded silica (Empore) with an approximate size of 1 $mm^2$ were placed in a 200 µl pipette tip and carefully tightened at the tip of the tip. The C18 material was activated with 200 µl methanol prior to washing with 2% ACN, 1% formic acid (FA) without complete drying in a StageTip centrifuge. Aqueous samples with up to 10 µg of tryptic peptides were loaded on the StageTip and bound peptides were washed 0.1% FA followed by storage at 4°C.

To elute the peptides, 50 µl 80% ACN, 0.1% FA was pushed through the StageTip by air pressure and organic solvents were removed by vacuum centrifugation for 10 – 15 min.

## 5.20 TMT-labeling on StageTips

Peptides bound to StageTips were washed once with 10 mM HEPES pH 8 and labeled with TMTsixplex™ Isobaric Label Reagents (Thermo) by soaking the C18 material with 4 µl of a single TMT reagent dissolved in ACN for 1 h at room temperature. Afterwards, peptides were eluted two times with 20 µl 80% ACN. Remaining reactivity of the isobaric labeling reagents was quenched with 0.8 µl of 5% hydroxylamine for 15 min. Acetonitrile was evaporated during vacuum centrifugation and labeled peptides were concentrated via StageTips (see 5.19).

## 5.21 NanoLC-MS/MS analysis

To acquire mass spectra, eluted peptides were separated using an EASY-nLC™ 1200 HPLC system coupled to a Q Exactive™ HFX Hybrid Quadrupole-Orbitrap™ mass spectrometer (Thermo) through a nanospray ion source. HPLC-based peptide separation was performed using reverse-phase ReproSil-Pur C18-AQ 1.9 µm silica beads (Dr. Maisch GmbH) packed columns and a fragmented solvent gradient of solvent A (0.1% FA) and solvent B (80% ACN, 0.1% FA) for 90 min with a flow rate of 200 nl/min. Peptides were ionized via electrospray ionization (ESI) at 2.3 kV and a column temperature of 275°C in positive ion mode. Data-dependent spectrum acquisition consisted of scan cycles, each consisting of one full MS scan (60000 resolution at 200 m/z, 300 – 1650 m/z range) followed by selecting the top 12 most abundant precursor ions with an isolation window of 1.4 m/z for further HCD fragmentation with a normalized collision energy of 35%. Masses of sequenced precursor ions were dynamically excluded from MS/MS fragmentation for 30 s. Samples labeled with TMT reagents were measured individually using a 36 min gradient to assess labeling efficiency and mixed at equimolar ratios. Mixing ratios were confirmed by 36 min gradients and adjusted accordingly prior to data acquisition using a 90 min gradient.

## 5.22 Mass spectrometry data analysis

The MaxQuant software suite version 1.6.14.0 or version 2.0.3.0 (Tyanova et al., 2016a) and its integrated peptide search engine Andromeda (Cox et al., 2011) were used to process RAW data files. Peak lists were searched against the UniProt (Pundir et al., 2017) databases for *Mus musculus* (taxonomy ID 10090, release_2020-10-07) or *Homo sapiens* (taxonomy ID 9606, release_2019-12-11), where the mutated HUWE1-CS sequence was added manually. Additionally, a list containing 245 common contaminants was used to exclude potential misleading identifications. Two missed cleavages for tryptic peptides were allowed, as well as a minimum length of seven amino acids and carbamidomethylation (Cys) was set as fixed modification. Variable modifications contained oxidation of methionine and acetylation of N-termini. First search peptide mass tolerance was set to 20 ppm and to 4.5 ppm for the main search respectively. For TMT quantification, the isotopic distributions of additional masses for each label were provided by the manufacturer and set in MaxQuant to correct quantification errors. Protein and peptide identifications were filtered using a target-decoy approach with a false discovery rate of 0.01 (Elias and Gygi, 2007). The “match between runs” option was enabled.

Subsequent data analysis was conducted with Perseus version 1.6.14 (Tyanova et al., 2016b). First, reverse hits, contaminants and peptides only identified by the modified site were excluded from further analysis. Label free quantification (LFQ) ant TMT reporter ion intensities

were transformed with Log10 and protein groups lacking at least 2 valid values for one or more triplicate sample groups were excluded. Sample groups were compared using two-sample t-test. Data was deposited to the ProteomeXchange Consortium via the PRIDE (Perez-Riverol et al., 2022) partner repository with the dataset identifier PXD037677, PXD037680 and PXD037812.

## 5.23 RNA sequencing

Total RNA was extracted as described for cDNA synthesis (see 5.13). Poly(A)-tailed mRNA was enriched using the mRNA isolation module (NEB) from 0.5 µg of total RNA. Following reverse transcription and library preparation was performed using NEBNext® Ultra™ II RNA Library Prep Kit for Illumina® scaled down 1:2 at every step according to the manufacturer's instructions. In brief, NEBNext Oligo dT beads were washed with RNA binding buffer twice and added to the RNA sample prior to heating at 65°C for 5 min and cooling to 4°C. Poly(A) mRNA binding to the beads was facilitated by resuspending the magnetic beads twice for 5 min. Beads were washed twice with wash buffer and RNA was eluted at 80°C for 2 min in Tris buffer. By adding one volume of 2x RNA binding buffer, mRNA was bound again to the beads for 10 min at room temperature. After washing with mRNA wash buffer, bound nucleotides were eluted in a mixture of first strand synthesis buffer with random primers and fragmented at 94°C for 15 min. First strand cDNA synthesis was conducted by addition of murine RNase inhibitor and ProtoScript II reverse transcriptase at 25°C for 10 min followed by 42°C for 15 min and a final step of 70°C for 15 min. Second strand DNA synthesis was performed by adding the respective reaction buffer and second strand synthesis enzyme mix for 1 h at 16°C. Double stranded cDNA was purified using the HighPrep™ PCR Clean-up System (MagBio) with 1.8x volumes of bead suspension. Bound DNA was washed once with 80% ethanol and eluted in 10 mM Tris pH 8 buffer. End preparation of the cDNA libraries was performed using NEBNext End Prep Enzyme Mix with the respective buffer for 30 min at 20°C followed by 30 min at 65°C. NEBNext Illumina adaptors were ligated to the repaired cDNA library using the Blunt/TA Ligase Master Mix for 15 min at 20°C followed by digestion with USER enzyme for 15 min at 37°C. Non-ligated adaptors were depleted from libraries by purification with 1x volume of HighPrep™ PCR Clean-up solution (MagBio) twice. Adaptor-ligated cDNA libraries were amplified with 12 PCR cycles using unique pairs of i5 and i7 sequencing primers and the NEBNext® Ultra™ II Q5® Master Mix. The PCR program started with 30 s denaturation at 98°C for 30 s and amplification cycles consisting of 10 s denaturation and 75 s of annealing and extension at 65°C. Final extension lasted for 5 min at 65°C. Amplified libraries were purified with 0.9x volumes of HighPrep™ PCR Clean-up solution (MagBio). DNA amount of each library was determined using the Quant-iT™ PicoGreen™ dsDNA Assay-Kit (Thermo). In brief, 1 µl of

each library was diluted in 200 µl 1x TE buffer supplemented with 1:400 PicoGreen reagent prior to fluorescence measurement with an Infinite M plex plate reader (Tecan) at an excitation of 480 nm emission of 520 nm. Samples were pooled with equimolar ratios for each experiment prior to NGS analysis.

## 5.24 Chromatin Immunoprecipitation (ChIP)

Target cells were cultivated in 15 cm culture dishes and 4 – 6 x$10^7$ cells were crosslinked with 0.2% PFA in PBS for 4 min followed by quenching the reaction with a final concentration of 200 mM glycine for 4 min at room temperature. Fixed cells were washed and scraped in PBS, pelleted by centrifugation at 700 g for 3 min and washed again with PBS. To lyse the cells, 200 µl PBS 200, 0.5% (v/v) TritonX-100, 5 mM $CaCl_2$, 5 mM $MgCl_2$, 1 mM dithiothreitol and protease/phosphatase inhibitors were added for 10 min on ice. Further fragmentation of chromatin was achieved by adding 1 µl micrococcal nuclease (NEB) and shaking at 200 rpm for 3 in at 37°C. Chromatin fragmentation was terminated by addition of 20 µl 500 mM EDTA. Samples were diluted with 4 volumes of TNT-300 buffer (25 mM Tris pH 7.4, 300 mM NaCl, 1% (v/v) TritonX-100, supplemented with protease and phosphatase inhibitor cocktails) and sonified with an UP200St sonicator (Hielscher) for 3x 2 min on ice (30% amplitude, 2 W power and a 45 s on / 15 s off cycle). Centrifugation of lysates at 17000 g for 10 min at 4°C cleared the lysates of insoluble aggregates and supernatants were used to quantify and equalize the protein concentration based on BCA measurements with the Pierce™ BCA Protein Assay Kit. 2% of each sample was separates as input sample and 1.5 – 2 µg of target specific antibodies were added to each sample and mixed by end-over-end rotation overnight at 4°C. For precipitation of antibody bound target proteins, 10 µl magnetic protein A or protein B bead suspension (Thermo) was added to the lysates and rotated for 2 h at 4°C. Placed on a magnetic rack, beads settled at the reaction tube wall and the remaining supernatant was removed prior to three washing steps with TNT-300 supplemented with 0.1% SDS. Beads were resuspended in 200 µl 10 mM Tris pH 7.4, 250 mM NaCl, 1 mM EDTA, 0.5% (v/v) SDS and remaining RNA was digested with 1 µl RNAseA (Thermo) for 1 h at 50°C in all samples, including separated inputs. Subsequently, proteins were removed by adding 2 µl proteinase K (Thermo) in another 200 µl 10 mM Tris pH 7.4, 250 mM NaCl, 1 mM EDTA, 0.5% (v/v) SDS at 50 for 1 h followed by 65°C overnight. During digestion steps, magnetic beads were frequently resuspended in the solution by interval shaking for 25 s at 1300 rpm followed by 5 min off time. Captured DNA fragments were purified using 1 volume ROTI®Phenol/Chloroform/Isoamyl alcohol followed by centrifugation with 17000 g for 10 min at room temperature. Aqueous supernatants were transferred to a fresh reaction tube, supplemented with 2 µl GlycoBlue™ Coprecipitant (Thermo) and DNA was precipitated with 2.8 volumes ethanol at -20°C overnight.

Samples were centrifuged for 30 min at 4°C and DNA pellets were washed with 75% ethanol, dried for 5 min and dissolved in 10 mM Tris buffer, pH 8. Agarose gel electrophoresis of input samples confirmed the desired fragment size range of 100 – 800 bp and DNA yield was assessed with Quant-iT™ PicoGreen™ dsDNA Assay-Kit (Thermo) as described for RNAseq libraries (5.23). Sequencing library preparation was performed either following the “TELP” procedure (Peng et al., 2015) (5.25) or using the NEBNext® Ultra™ II DNA Library Prep Kit (5.26).

## 5.25 TELP library preparation

Fragmented DNA was dephosphorylated with rSAP (NEB) in 0.33x ExTaq buffer for 1 h at 37°C followed by 65°C for 10 min. Poly(C) tailing was performed by adding 35 µM dCTP (NEB), denaturing at 95°C for 5 min and addition of deoxynucleotidyl transferase (NEB) for 35 min at 37°C followed by 75°C for 20 min. KAPA2G Robust HotStart ReadyMix (Roche) was added to tailed DNA, as well as 250 nM biotinylated poly(G) anchor primer and C-tailed fragments were amplified with 16 PCR cycles (Initial denaturation at 95°C for 3 min, 47°C for 1 min, 68°C for 2 min and final extension at 72°C for 10 min). Excess primer was depleted with ExoI for 1 h at 37°C and biotinylated PCR products were captured on magnetic streptavidin beads (NEB) in 500 µl B&W buffer (10 mM Tris-HCl pH 8.0, 1 M NaCl, 0.5 mM EDTA, 0.02 % (v/v) TritonX-100) for 45 min at room temperature. Beads were washed once with B&W buffer followed by three washes with 10 mM Tris-HCl pH 8.0, 0.02% (v/v) TritonX-100 for 5 min each. Residual liquid was removed and beads were resuspended in 10 mM Tris.HCl prior to adding 500 nM annealed TELP adaptor oligos and Blunt/TA Ligase Master Mix (NEB). Adaptor ligation was performed at 16°C overnight. Again, beads were washed with B&W buffer and twice with 10 mM Tris-HCl pH 8.0, 0.02% (v/v) TritonX-100 for 5 min. To amplify the bead-bound DNA library with unique pairs of i5 and i7 sequencing primers, half of the bead suspension was transferred to new reaction tubes containing respective primers and KAPAHiFi™ Hot-Start ReadyMix (2X) (Roche) according to the manufacturer’s instructions. Amplification cycles started with 95°C for 5 min, followed by 22 cycles of 98°C for 20 s, 65°C for 15 s, 72°C for 30 s and a final extension step at 72°C for 7 min. Resulting NGS libraries were purified via agarose gel electrophoresis (2% agarose, 130 V, 25 min) and DNA fragment sizes ranging from 200 to 1000 bp were cut out of the gel prior to gel extraction using Monarch® DNA Gel Extraction Kit (NEB). DNA yield was determined with the Quant-iT™ PicoGreen™ dsDNA Assay-Kit (Thermo) as described for RNAseq libraries (5.23) and libraries were pooled at equimolar ratios prior to sequencing.

## 5.26 NEBNext Ultra II DNA Library Preparation

NGS libraries were prepared following the instructions of the NEBNext® Ultra™ II DNA Library Prep Kit for Illumina® (NEB) with 1:5 of material at each step. In brief, 200 ng of DNA was added to a reaction tube with 0.6 µl end preparation enzyme mix, 1.4 µl reaction buffer and pure water to a final volume of 12 µl. End preparation was performed at 20°C for 30 min followed by 65°C for ChIP or 50°C for Cut&Run for 30 min. For ligation of adaptors for Illumina sequencing, 0.5 µl adaptor oligo, 6 µl ligation master mix and 0.2 µl ligation enhancer were added to the repaired DNA and the reaction was incubated at 20°C for 15 min. Adaptor hairpins were digested with 0.6 µl USER enzyme at 37°C for 15 min. DNA fragments were purified with 17.37 µl (0.9x volumes) of HighPrep™ PCR Clean-up solution (MagBio) once as described for RNAseq libraries (5.23). Purified libraries for ChIPseq experiments were amplified with unique pairs of i5 and i7 sequencing primers and the KAPAHiFi™ Hot-Start ReadyMix (2X) with respective PCR parameters (described in 5.25). Libraries from other experiments including Cut&Run and DSBCapture were amplified with unique pairs of i5 and i7 sequencing primers and the NEBNext® Ultra™ II Q5® Master Mix. PCR cycles started with 30 s denaturation at 98°C for 30 s and 10 – 13 amplification cycles consisting of 10 s denaturation and 30 s of annealing and extension at 65°C. After final extension for 5 min at 37°C, libraries were purified via agarose gel electrophoresis (2% agarose, 130 V, 25 min). DNA fragments ranging from 200 to 1000 bp were extracted from the gel using Monarch® DNA Gel Extraction Kit (NEB). DNA yield was determined with the Quant-iT™ PicoGreen™ dsDNA Assay-Kit (Thermo) as described for RNAseq libraries (5.23) and libraries were pooled at equimolar ratios prior to sequencing.

## 5.27 Cut&Run

Chromatin profiling with Cut&Run assays was performed according to the published protocol (Meers et al., 2019) with modifications. Cultured cells were crosslinked with 0.2% PFA in PBS for 4 min prior to quenching the reaction with a final concentration of 200 mM glycine. Scraped cells were washed with PBS and 1 – 5 million cells were used for each experiment. Pellets were washed three times in Cut&Run wash buffer (20 mM HEPES, 150 mM NaCl, 0.5 mM spermidine) to remove free sugar and other cell debris. To activate concavalin A sepharose, 10 µl bead slurry per sample was washed in Cut&Run binding buffer (20 mM HEPES, 10 mM KCl, 1 mM $CaCl_2$, 1 mM $MnCl_2$) three times and added to washed cells in washing buffer and rotated for 5 min. Bead-bound cells were centrifuged with 600 g for 3 min and resuspended in wash buffer supplemented with 0.1% TritonX-100 and 2 mM EDTA and desired primary antibodies at a 1:100 dilution. Samples were incubated for 2 h up to overnight with interval shaking at 800 rpm. Excess antibodies were removed by washing two times with washing

buffer supplemented with 0.1% TritonX-100 and 1 µg/ml protein A/G-MNase fusion protein was added in the same buffer and incubated for 1 h at 4°C with shaking. After washing two times with wash buffer with 0.1% TritonX-100, low-salt buffer (20 mM HEPES, 0.5 mM spermidine, 0.1% TritonX-100) was added briefly and replaced with 200 µl incubation buffer (3.5 mM HEPES, 10 mM $CaCl_2$, 0.1% TritonX-100) for 30 min at 0°C. Cut&Run DNA fragments were released from cells following the addition of 200 µl stop buffer (150 mM NaCl, 20 mM EDTA, 0.1% TritonX-100, 50 µg/ml RNAseA) for 30 min at 37°C.

The DNA containing supernatants were used for phenol/chloroform extraction. First, 2 µl of 10% SDS and 5 µl Proteinase K was added to each sample for 1 h at 50°C. Second, 1 volume of ROTI®Phenol/Chloroform/Isoamyl alcohol was added and samples were centrifuged at 17000 g for 10 min at room temperature. The aqueous upper phase was transferred to a new reaction tube with 2 µl GlycoBlue™ Coprecipitant and 2.5 volumes of ethanol were added to precipitate the DNA at -20°C overnight. Samples were centrifuged at 17000 g for 30 min and washed with 75% ethanol. Precipitated DNA was dissolved in 10 mM Tris, pH 8 and yield was determined with the Quant-iT™ PicoGreen™ dsDNA Assay-Kit (Thermo) as described for RNAseq libraries (5.23). Sequencing libraries were prepared with the NEBNext® Ultra™ II DNA Library Prep Kit as described (5.26).

## 5.28 DSBCapture and sequencing

To quantify and map DNA double strand breaks, the DSBCapture protocol was used with modifications (Lensing et al., 2016). In brief, 5 million cells were either fixed with 0.2% PFA for 4 min followed by quenching the reaction with a final concentration of 200 mM glycine for 4 min or by detaching cells with trypsin-EDTA followed, washing with PBS and fixing cells with 90% methanol at -20°C overnight. Either way, cells were washed with PBS and permeabilized with Cut&Run wash buffer supplemented with 0.1% TritonX-100. Subsequently, fixed cells were bound to concanavalin A sepharose as described for Cut&Run (see 5.27).

Bound cells were washed once with 1x NEB buffer 2 and resuspended in 1x NEB buffer 2 with 33 µM dNTPs and 1 µl Klenow fragment (NEB) for 30 min at 25°C with interval shaking (25 s on, 1 min off, 1000 rpm). Subsequently, cells on beads were washed once with Cut&Run wash buffer, 0.1% TritonX-100 followed by washing with 1x NEBNext® dA-Tailing Reaction Buffer (NEB). To tail double strand breaks with an A-overhang, cells were resuspended in 1x dA tailing buffer with 1 µl Klenow Fragment (3'→5' exo-) (NEB) for 30 min at 37°C with interval shaking. Samples were washed with Cut&Run wash buffer, supplemented with 0.1% TritonX-100, followed by washing with 1x T4 DNA ligase buffer. Addition of 1 µl T4 DNA ligase per sample and 100 nM biotinylated anchor primers in 100 µl 1x T4 DNA ligase buffer for 1 h to overnight at 20°C was succeeded by a final washing step using wash buffer.

Proteins were digested using 2 µl proteinase K in 400 µl 10 mM Tris, 250 mM NaCl, 5 mM EDTA, 0.5 % SDS for 4 h to overnight at 50°C. Supernatants lacking sepharose beads were sonified for 5 min on ice (2 W power, 35 % amplitude, 40 s on 20 s off cycle). Fragmented DNA was purified using phenol/chloroform followed by ethanol precipitation as described for chromatin immunoprecipitation (see 5.24). 2 – 5% of each sample was separated as input sample. Biotinylated DNA fragments were captured with magnetic streptavidin beads (NEB) in B&W buffer as described (see 5.25). Bead-bound DSB DNA and input samples were used for end preparation and repair with the NEBNext® Ultra™ II DNA Library Prep Kit for Illumina® (NEB) as described (see 5.26). To remove excess adaptor after ligation, beads were washed six times with 10 mM Tris-HCl pH 8.0, 0.02% TritonX-100 and input samples were purified using the HighPrep™ PCR Clean-up system.

Final PCR using KAPAHiFi™ Hot-Start ReadyMix (2X) with unique pairs of i5 and i7 index primers, PCR product purification, quantification and pooling was performed as described for the TELP procedure (5.25).

## 5.29 Functional sgRNA screen

An sgRNA library screen targeting ~2300 genes with the gene ontology terms “DNA repair” (GO:0006281), “DNA replication” (GO:0006260), and “Cell cycle” (GO:0007049) was performed following a published protocol (Joung et al., 2017). In brief, respective oligos with 4 sequences per gene were cloned into the pLentiCRISPR_V2 vector backbone (a gift from Feng Zhang, Addgene plasmid #52961) (Sanjana et al., 2014) by Valentina Andrioletti. I used the resulting plasmid libraries to generate a pool of lentiviral particles as described (see 5.16). Resulting viral supernatants were added to two replicates of 1.6 $x10^7$ HUWE1-WT or HUWE1-CS cells each at a ratio of 1:1 with fresh cell culture media and a final concentration of 8 ng/ml hexadimethrine bromide and volume of 20 ml. This led to a 500-fold coverage of the sgRNA library and a MOI of 0.3. Transfected cells were selected with 1 µg/ ml puromycin for 4 days. At the first passage after puromycin selection, 10% of sgRNA expressing cells were transferred to fresh culture media and 90% of the cell population was harvested representing the first time point. Positive and negative selection of beneficial or respective disadvantageous sgRNAs was performed for 42 days including 19 passages (1:10) at which 90% of each population was harvested. Genomic DNA was extracted using Quick-DNA Midiprep Plus Kit (Zymo) following the manufacturer’s instructions. Eluted genomic DNA was concentrated by ethanol precipitation and 80 µg per sample were used for PCR amplification of retrieved sgRNA sequences using NEBNext® Ultra™ II Q5® Master Mix and unique pairs of i5 and i7 primers 28 cycles. Resulting PCR bands at approximately 320 bp were purified and from agarose gels (2% agarose, 130 V, 25 min) with the Monarch® DNA Gel Extraction Kit. DNA

yield was determined with the Quant-iT™ PicoGreen™ dsDNA Assay-Kit (Thermo) as described for RNAseq libraries (5.23) and libraries were pooled at equimolar ratios prior to sequencing.

## 5.30 Next Generation Sequencing and data analysis

Pooled libraries were sequenced on the Illumina NovaSeq 6000 platform using single or double end sequencing at CeGaT GmbH (Tübingen). Bioinformatic analysis of fastq files and metagenes was performed by Nikita Popov. Clustering of normalized read counts with Perseus (Tyanova et al., 2016b) and graphing of results was done by me. Sequencing reads were de-multiplexed with Illumina bcl2fastq (version 2.20) and adapter sequences were trimmed with Skewer (version 0.2.2). STAR (version 2.5.4) (Dobin et al., 2013) was used to map sequencing reads to the human genome assembly hg19 and differential gene expression analysis was performed with EdgeR (version 3.26.8) (Robinson et al., 2010). DSBCapture, ChIPseq and Cut&Run derived data was analyzed with Homer (version 4.10.3) and MAGECK (Li et al., 2014) was used to score sgRNAs from the respective sgRNA screen data. Raw fastq files and processed data files were submitted to NCBI's Gene Expression Omnibus (Edgar et al., 2002) and are accessible through GEO Series accession number GSE218240.

# 6 Results

*Parts of this chapter were adapted from EINIG, E., JIN, C., ANDRIOLETTI, V., MACEK, B. & POPOV, N. 2023. RNAPII-dependent ATM signaling at collisions with replication forks. Nature Communications.*

## 6.1 Catalytic mutation of HUWE1 induces TRCs

HUWE1 encompasses distinct functional domains including HECT, UBA, WWE and ARLD (Hunkeler et al., 2021). In order to study the ubiquitin ligase function of the HUWE1-HECT domain, the endogenous catalytic cysteine was replaced with either a serine (HUWE1-CS) or the wild type cysteine (HUWE1-WT) as control using a CRISPR/Cas9 based gene replacement strategy (Endres et al., 2021) (Figure 8A).

Correct gene targeting in human colorectal carcinoma cell lines (parental HCT116; HUWE1-P) was validated by PCR with primers matching the introduced blasticidin resistance gene and the adjacent flanking genomic DNA sequence, as well as by Sanger sequencing (Microsynth Seqlab) of genomic DNA (Figure 8B). HUWE1 protein levels were similar in all three cell lines (Figure 8C) and expected peptides carrying the mutation C4341S were identified by LC-MS/MS in HUWE1-CS cells, confirming that the mutation-carrying HUWE1 protein is expressed (Figure 8D) (Einig et al., 2023).

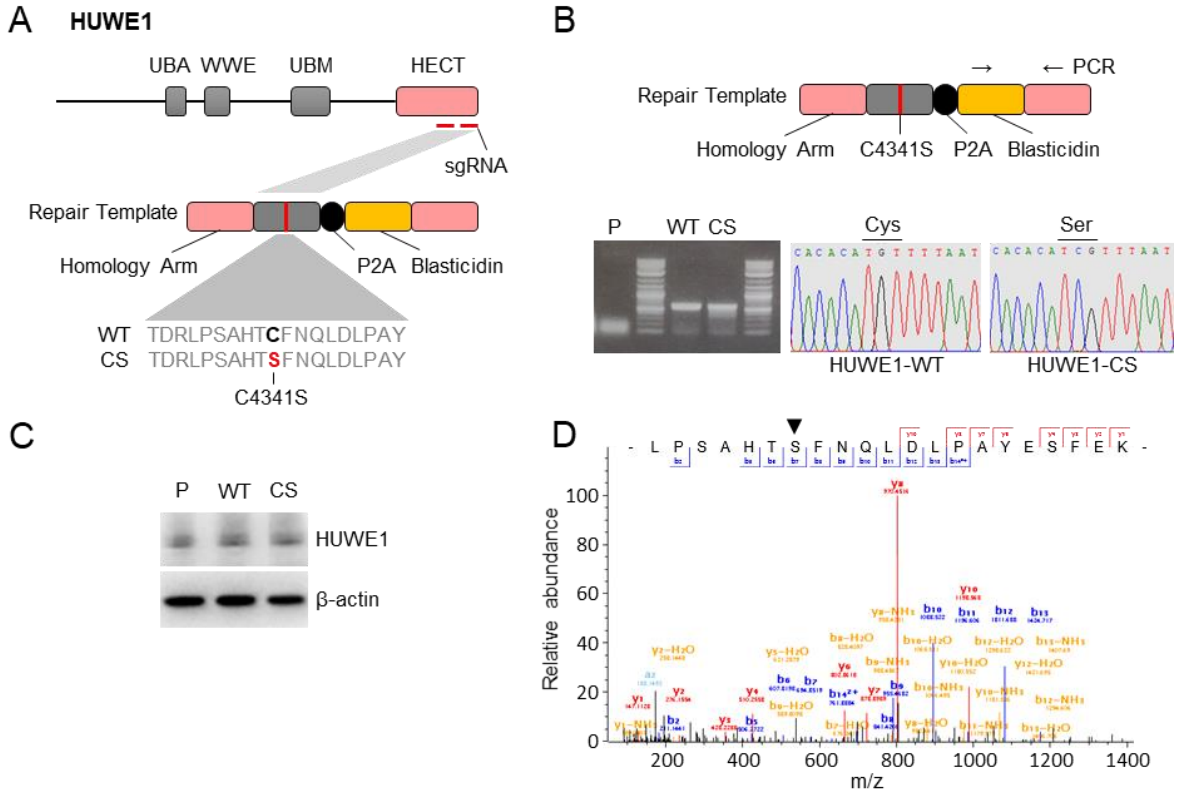


***Figure 8: Genetic model of HUWE1 inhibition.***

*A) Gene replacement strategy to exchange the catalytic cysteine of endogenous HUWE1 with either a*

*serine (CS) or cysteine (WT) in HCT116 cells (P). Specific sgRNAs targeting the HUWE1-HECT domain were used to cleave genomic DNA and a repair template encoding the flanking sequences, the P2A sequence and a blasticidin resistance gene was provided. Figure adapted from Endres et al. (2021) B) Validation of successful gene replacement by PCR and Sanger sequencing of the respective gene locus. The generation and validation of HUWE1-WT and HUWE1-CS cell lines was performed by Valentina Andrioletti. C) Immunoblot of cell lysates from parental HCT116 (P), HUWE1-WT and HUWE1-CS cells. D) Peptide spectrum of HUWE1 harboring the C4341S mutation after LC-MS/MS analysis of HUWE1-CS lysates. The black triangle indicates the mutated site. This figure was adapted from Einig et al. (2023).*

Catalytic mutation of HUWE1 resulted in a decreased DNA replication rate as shown by DNA fiber assays (Figure 9A, B), whereas the parental HCT116 compared with HUWE1-WT cells did not show any significant difference, validating the genetic model system. This agrees with previous studies (Choe et al., 2016). Moreover, loss of HUWE1 function significantly deregulated gene expression of more than 1900 genes as judged by RNAseq (Figure 9C, D). Principal component analysis shows that parental HCT116 and HUWE1-WT closely cluster, whereas HUWE1-CS cells are distinguished (Figure 9E). Gene set enrichment analysis (GSEA) of the RNAseq dataset revealed a HUWE1-dependent regulation of several hallmark gene sets including UV response, TP53 pathway and DNA repair, which were previously linked to the function of HUWE1 (Figure 9F) (Kao et al., 2018). Interestingly, MYC hallmark gene sets were not found among the top significant hits of the GSEA and MYC hallmark genes were not strongly enriched among HUWE1-dependent transcripts (Figure 9G). Furthermore, depletion of MYC in HCT116 cells deregulated the expected MYC hallmark gene set, which differs from HUWE1-dependent transcripts (Figure 9H, I), indicating that HUWE1 may regulate RNAPII-dependent transcription via other effectors (Einig et al., 2023).

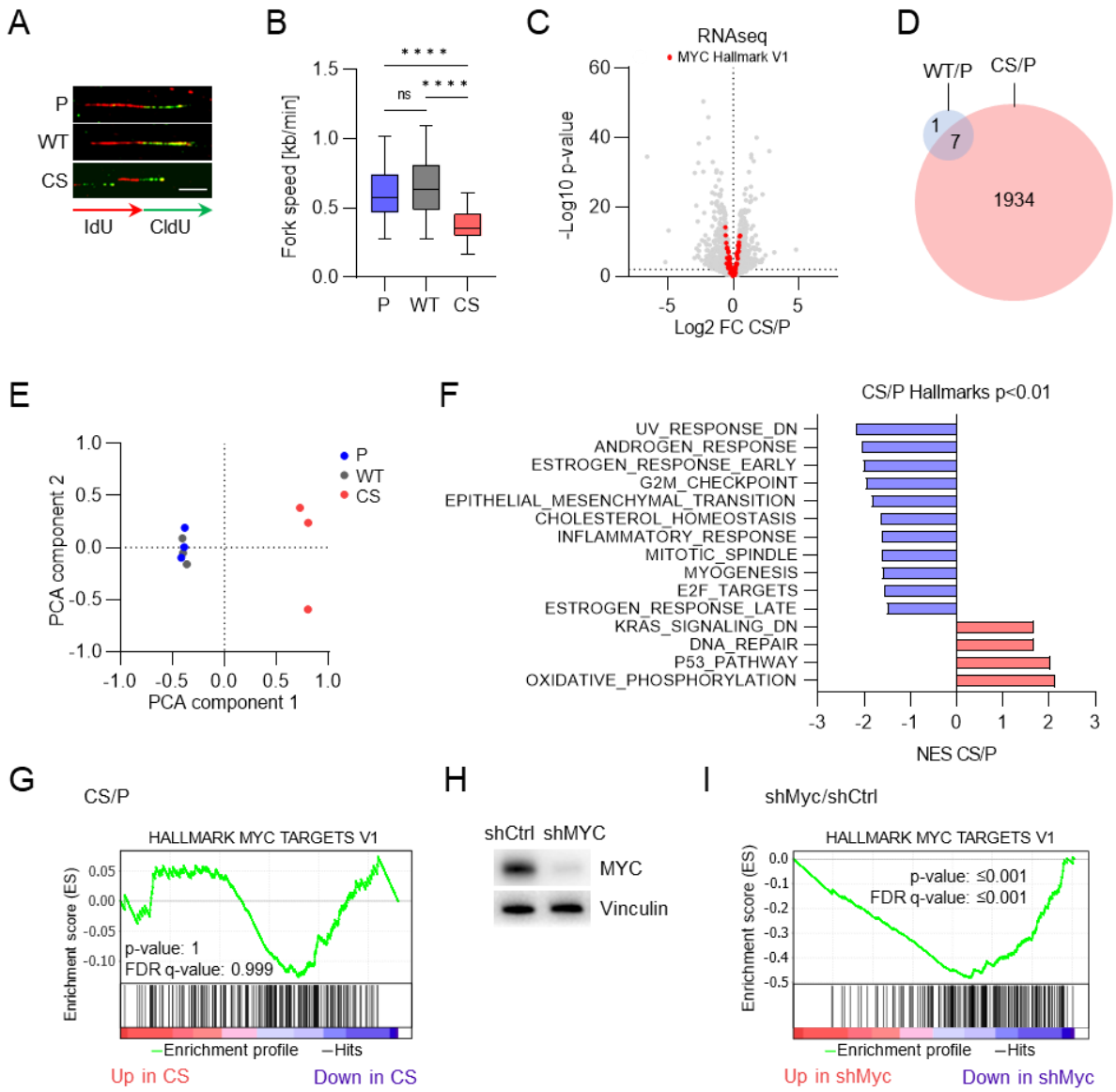


***Figure 9: HUWE1 ubiquitin ligase function promotes DNA replication and regulates transcription.*** *A) Representative images of single DNA fibers. Scale bar: 4 µm. B) Quantification of 50 fibers per group shown in (A). Boxplots represent the median ± quartiles according to the style of tukey. The non-parametric Kruskal-Wallis test followed by Dunn's multiple comparison was used to determine p-values. ****p ≤ 0.0001, ns: not significant. C) Transcriptome analysis of HUWE1-P, HUWE1-WT and HUWE1-CS cells. Hallmark gene set members of the MYC V1 gene set are highlighted in red. D) Overlap of genes significantly deregulated (p-value ≤ 0.01, FDR ≤ 0.01) in HUWE1-WT or HUWE1-CS cells relative to parental HCT116 (P) cells. E) Principal component analysis of RNAseq data. F) Enriched hallmark gene sets resulting from gene set enrichment analysis (GSEA) (Subramanian et al., 2005) of HUWE1-CS versus parental samples. NES: normalized enrichment score. G) Gene set enrichment analysis of hallmark MYC targets in HUWE1-CS cells compared with parental cells. H) Immunoblots of HCT116 cells expressing shMYC or shCtrl. I) GSEA for hallmark MYC targets in HCT116 cells expressing shMYC versus shCtrl. This figure was adapted from Einig et al. (2023).*

Taken together, mutation of HUWE1 results in deregulated transcription and DNA replication, which raises the question how transcription-replication conflicts (TRCs) are affected upon mutation of HUWE1. First, immunoprecipitation (IP) of RNAPII from formaldehyde-crosslinked and sonified HUWE1-WT and HUWE1-CS cells was performed. This approach was chosen to preserve transient protein interactions, such as TRCs, throughout the immunoprecipitation procedure and simultaneously disrupt chromatin to limit background signal from DNA-dependent interactions. The RNAPII-precipitates of HUWE1-CS cells showed increased levels of replisome proteins PCNA, MCM2 and MCM5 compared with HUWE1-WT cells (Figure 10A, B).

To further validate this result, an established proximity ligation assay (PLA) with antibodies targeting the proteins PCNA and RNAPII to score TRCs was used (Hamperl et al., 2017). Similar to the immunoblot, PLA signals increased in HUWE1-CS cells compared with HUWE1-WT cells (Figure 10C, D). Moreover, acute chemical inhibition of HUWE1 with BI-8622 (Peter et al., 2014) strongly induced the level of TRCs. The increase of TRCs in HUWE1-CS cells was rescued after inhibition of the CTD kinase CDK9 with AZD4573 or 5,6-dichloro-1-beta-D-ribofuranosylbenzimidazole (DRB), suggesting that collisions depend on transcription elongation (Titov et al., 2011, He et al., 2015, Bensaude, 2011). Inactivation of RNAPII with triptolide resulted in reduced levels of TRCs in both HUWE1-WT and HUWE1-CS cells (Figure 10C, D) (Einig et al., 2023).

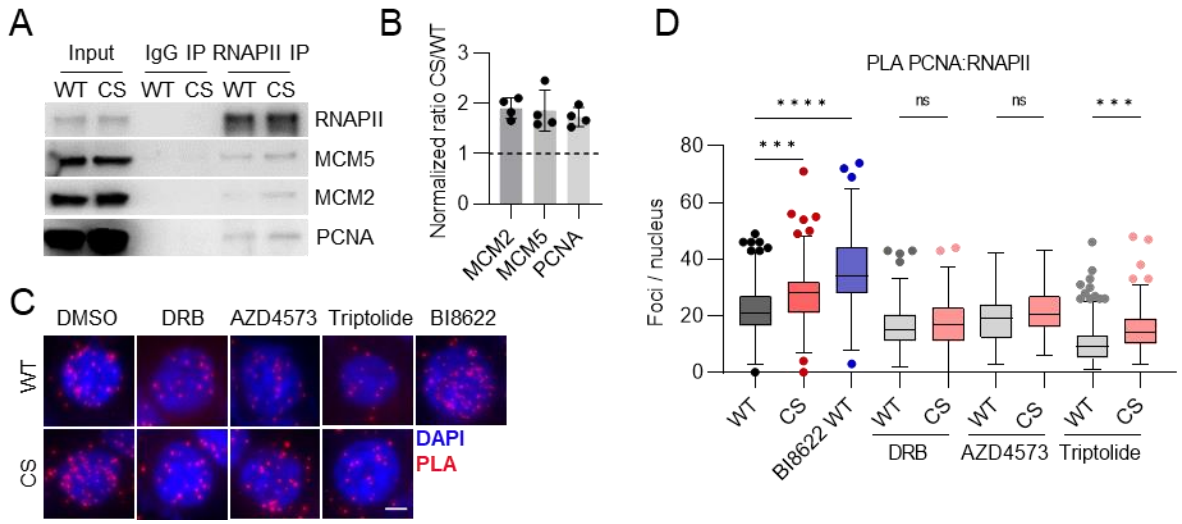


***Figure 10: HUWE1 prevents transcription-dependent TRCs.***

*A) Immunoprecipitation of RNAPII in formaldehyde-crosslinked and sonified HUWE1-WT and HUWE1-CS cells. A representative image and B) densitometry-based quantification of CS/WT ratio of precipitated protein level is shown (mean ± SD). C) Proximity ligation assay with antibodies to PCNA and RNAPII in HUWE1-WT and HUWE1-CS cells treated with 100 µM DRB, 10 nM AZD4573, 100 nM triptolide or the HUWE1 inhibitor BI-8622 (5 µM) for 7 h. Scale bar: 5 µm. D) Quantification of proximity pairs within nuclear areas shown in (C) for ≥ 140 cells per group. Boxplots represent the median ±*

*quartiles according to the style of tukey. The non-parametric Kruskal-Wallis test followed by Dunn's multiple comparison was used to determine p-values. ***p ≤ 0.001, ****p ≤ 0.0001, ns: not significant. This figure was adapted from Einig et al. (2023).*

## 6.2 HUWE1 and WRNIP1 co-regulate DNA replication and TRCs

In order to investigate how HUWE1 may affect RNAPII-dependent TRCs, I aimed to identify candidate effector proteins via Immunoprecipitation of HUWE1 prior to LC-MS/MS analysis. First, I analyzed HUWE1 precipitates by LC-MS/MS following a label-free approach with three technical replicates and found several known interactors including TP53 (Oughtred et al., 2021) and previously unknown interaction partners implicated in chromatin transactions such as the ATPase WRNIP1 in both HUWE1-WT and HUWE1-CS cells (Figure 11A). To validate this result, I repeated the experiment using three biological replicates for immunoprecipitation followed by a quantitative MS approach applying tandem-mass-tag (TMT) labeling. Again, among the top ten hits was the ATPase WRNIP1 (Figure 11B) that can bind and stabilize stalled replication forks upon inhibition of DNA synthesis (Kanu et al., 2016, Leuzzi et al., 2016, Crosetto et al., 2008). Catalytic activity of HUWE1 was not required for WRNIP1 binding. Next to WRNIP1, I identified previously unknown enzymes of the α-ketoglutarate dehydrogenase complex and proteins building the cytoskeleton as potential interaction partners of HUWE1 (Figure 11C).

WRNIP1 binding to HUWE1 was further validated by HUWE1-IP followed by Immunoblot (Figure 11D) and the nuclear co-localization of both proteins confirmed by immunofluorescence staining (Figure 11E). The nuclear association of WRNIP1 with HUWE1 was assessed using proximity ligation assays, showing a specific signal for HUWE1-WT and HUWE1-CS cells, which is absent in cells expressing an shRNA targeting HUWE1 (Figure 11F). Not only in HCT116 cells, but also in several other cell lines including HEK293T, Hep3B, HuH7 and HLF, WRNIP1 was found in immunoprecipitates of HUWE1 (Figure 11G).

To test whether the ubiquitin ligase function of HUWE1 affects the WRNIP1 degradation rate, I performed cycloheximide assays. WRNIP1 turnover rate remains unchanged upon mutation of HUWE1 (Figure 11H) (Einig et al., 2023).

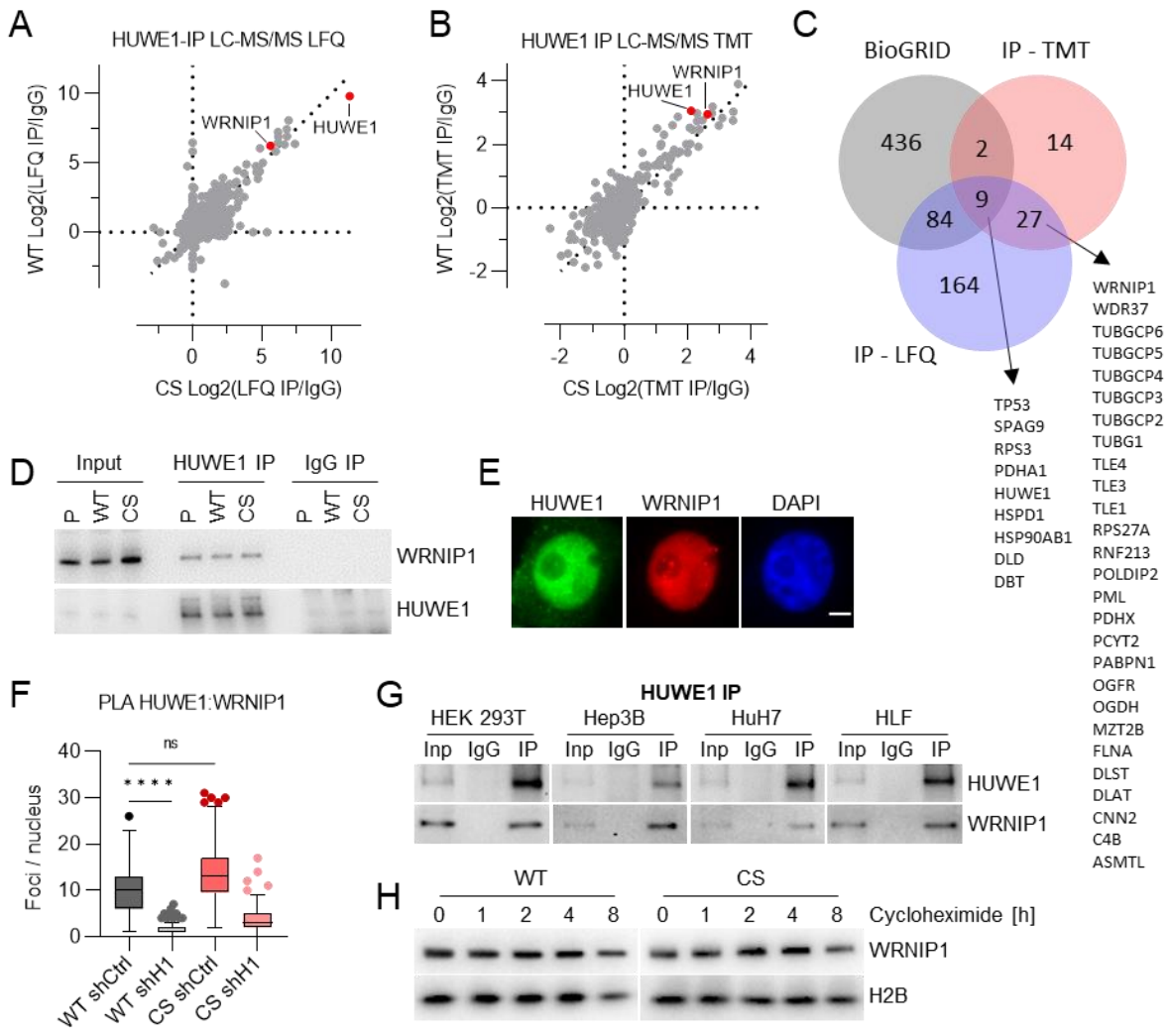


***Figure 11: HUWE1 binds WRNIP1 in the nucleus.***

*A) Immunoprecipitation of HUWE1 followed by LC-MS/MS in HUWE1-WT and HUWE1-CS cells. Axis show the log2 ratios of label-free quantification (LFQ) intensities between pulldowns with HUWE1-specific antibodies versus isotype control (IgG) antibodies of three technical replicates. B) Immunoprecipitation of HUWE1 followed by TMT labeling prior to LC-MS/MS in HUWE1-WT and HUWE1-CS cells. Axes show the log2 ratios of TMT reporter ion intensities between pulldowns with HUWE1-specific antibodies versus isotype control (IgG) antibodies of three biological replicates. C) Overlap of protein groups identified as putative HUWE1 interaction partners in both IP-MS experiments (A and B) and the BioGRID database (Oughtred et al., 2021). D) Validation of WRNIP1 as an interactor of HUWE1 by immunoprecipitation and immunoblot. E) Immunofluorescence staining of HUWE1 and WRNIP1 in parental HCT116 cells. Scale bar: 5 µm. F) PLA assay with antibodies to HUWE1 and WRNIP1 in HUWE1-WT and HUWE1-CS cells expressing a control (shCtrl) or HUWE1-targeting (shH1) shRNA (≥70 cells per group). The non-parametric Kruskal-Wallis test followed by Dunn's multiple comparison was used to determine p-values. ****p ≤ 0.0001, ns: not significant. G) Immunoprecipitation of HUWE1 using the indicated cell lines followed by immunoblot with HUWE1 and WRNIP1 antibodies. H) Cycloheximide assay to assess WRNIP1 protein stability in HUWE1-WT and HUWE1-CS cells. This figure was adapted from Einig et al. (2023).*

To identify regions in WRNIP1 that are required for HUWE1 binding, I immunoprecipitated HUWE1 from HCT116 cells expressing WRNIP1 variants encompassing different functional domains. This experiment identified the leucine zipper (LZ) containing domain of WRNIP1 as the region required for HUWE1 binding, since depletion of the LZ domain abolishes co-precipitation and expression of the LZ domain only enables co-precipitation of WRNIP1 variants (Figure 12A, B) (Einig et al., 2023).

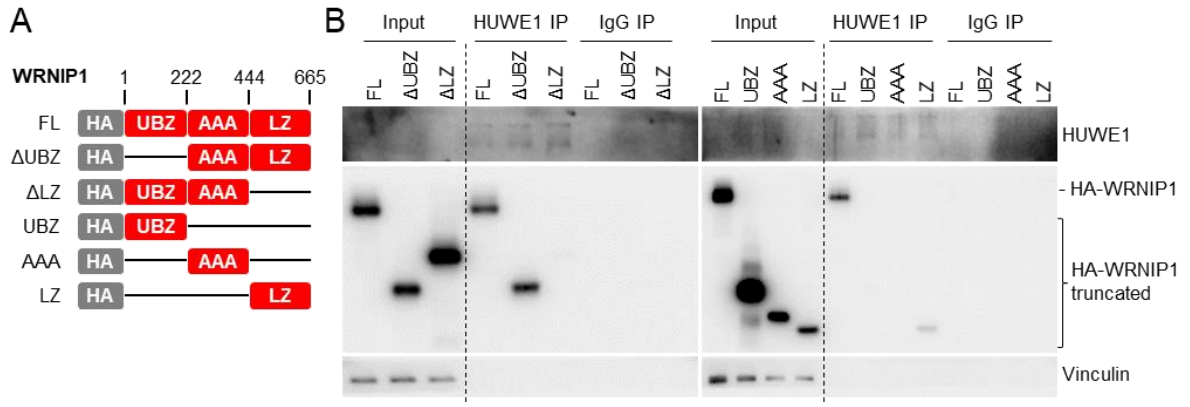


***Figure 12: The WRNIP1 leucine zipper domain is required to bind HUWE1.***

*A) Schematic of WRNIP1 functional domains and HA-tagged truncation variants. FL: Full length; UBZ: Ubiquitin binding zinc finger; LZ: Leucine zipper; AAA: AAA+ ATPase domain. B) Immunoprecipitation of HUWE1 from cells expressing HA-tagged WRNIP1 truncation variants. This figure was adapted from Einig et al. (2023).*

WRNIP1 depletion increased DNA damage response signaling (Figure 13A) and diminished replication-dependent EdU incorporation in HUWE1-WT but not in HUWE1-CS cells (Figure 13B, C). Similar to mutation of HUWE1, depletion of WRNIP1 induced the levels of TRCs, which were dependent on elongation-competent RNAPII, since treatment with the transcription inhibitors DRB or triptolide decreased the levels of TRCs in shWRNIP1 expressing cells (Figure 13D). Interestingly, overexpression of HA-tagged WRNIP1 slightly reduced the level of TRCs, whereas expression of WRNIP1 variants lacking the leucine zipper domain, which is required for HUWE1-binding, lead to higher levels of conflicts (Figure 12, Figure 13E). Both, mutation of HUWE1 and depletion of WRNIP1 induce TRCs, however depletion of WRNIP1 in HUWE1-CS cells rescued the increase of TRCs (Figure 13F).

HUWE1 and WRNIP1 can protect replication forks upon replication stress (Choe et al., 2016, Leuzzi et al., 2016), raising the question whether they associate with replication forks redundantly. Either mutation of HUWE1 or depletion of WRNIP1 increased the association of the other protein with integral components of replication forks such as PCNA and MCM2 (Figure 13G, H) (Einig et al., 2023).

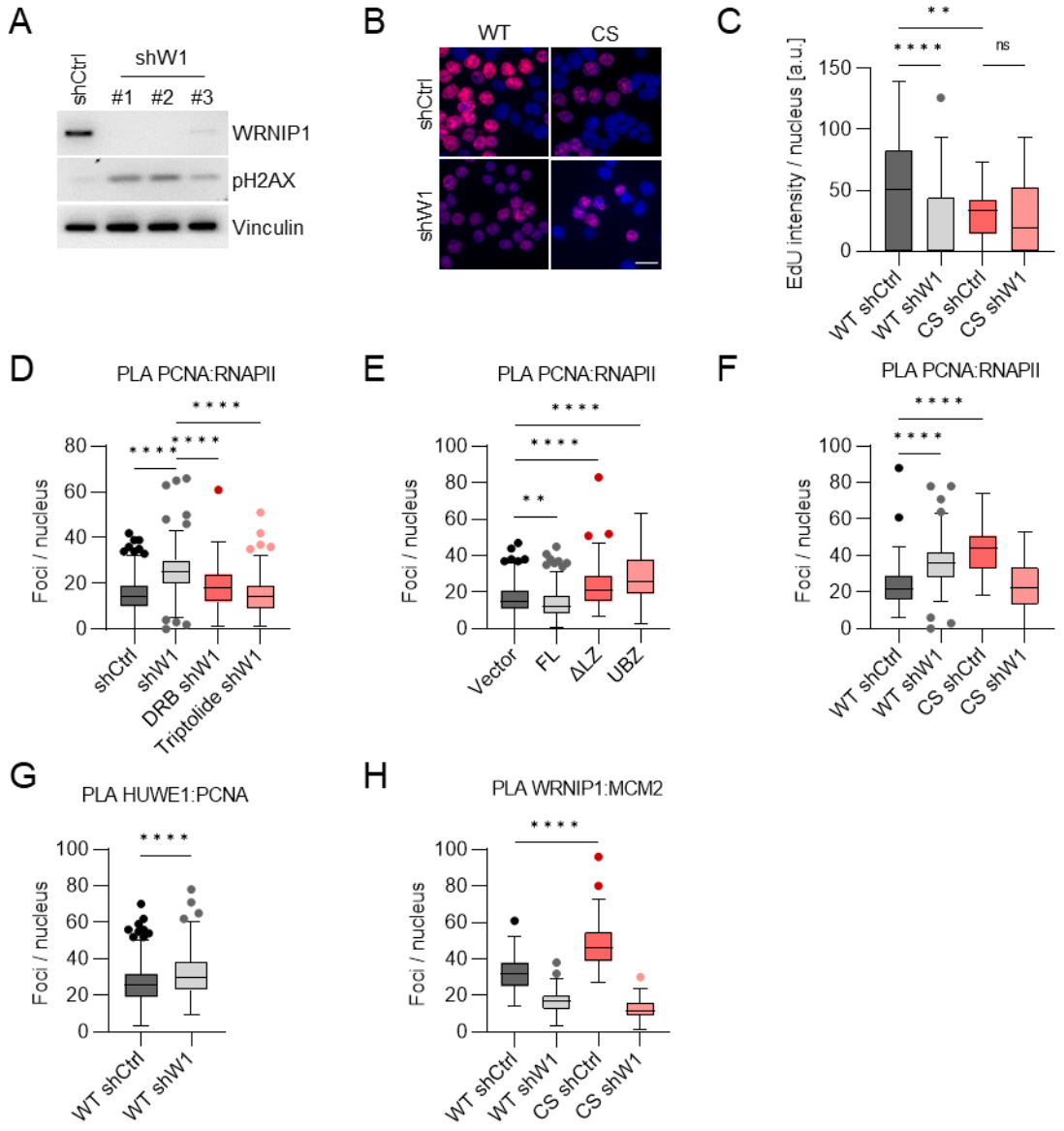


***Figure 13: HUWE1 and WRNIP1 co-regulate DNA replication and TRCs.***

*A) Expression of three different shRNAs targeting WRNIP1 (shW1) followed by immunoblot. Throughout subsequent figures shW1 #1 was used. B) Example images of an EdU incorporation assay in WT or CS cells expressing shCtrl or shWRNIP1 (shW1) Scale bar: 20 µm, Red: EdU, Blue: DAPI. C) Quantification of the EdU incorporation assay shown in B. ≥110 cells per group. D) Quantification of RNAPII-PCNA PLA foci in cells expressing shCtrl or shWRNIP1 and treated with 100 µM DRB or 100 nM triptolide for 6 h (≥100 cells per group). Expression of shRNAs was induced for 7 days with 100 ng/ml doxycycline. E) RNAPII-PCNA PLA foci quantification of cells expressing full-length (FL) HA-WRNIP1, HA-WRNIP1 lacking the leucine zipper domain (ΔLZ) or solely the WRNIP1 UBZ domain (UBZ) (≥130 cells per group). F) Quantification of PLA foci with antibodies to RNAPII and PCNA in HUWE1-WT and HUWE1-CS cells expressing shCtrl or shWRNIP1 (≥170 cells per group). G) PLA with antibodies to HUWE1 and PCNA in shWRNIP1 and shCtrl cells (≥300 cells per group). Significance was determined using the non-parametric Mann-Whitney test. ****p ≤ 0.0001. H) PLA with antibodies to WRNIP1 and MCM2 in*

*HUWE1-WT and HUWE1-CS cells expressing shCtrl or shWRNIP1 (≥80 cells per group). C-F,H) Boxplots represent the median ± quartiles according to the style of tukey. The non-parametric Kruskal-Wallis test followed by Dunn's multiple comparison was used to determine p-values. *p ≤ 0.05, **p ≤ 0.01, ***p ≤ 0.001, ****p ≤ 0.0001, ns: not significant. This figure was adapted from Einig et al. (2023).*

## 6.3 Association of WRNIP1 with RNAPII is controlled by HUWE1

To investigate how HUWE1 may influence whether and where WRNIP1 binds chromatin, ChIPseq and Cut&Run experiments were performed. Indeed, functional HUWE1 promotes WRNIP1 binding to chromatin as shown in both experiments (Figure 14A, B). As expected, depletion of WRNIP1 reduced the ChIPseq coverage, validating the specificity and suitability of the antibody (Figure 14A).

Immunoprecipitation of WRNIP1 from benzonase-treated samples showed that RNAPII is readily co-precipitated, as well as its CTD-phosphorylated proteoforms pS2-RNAPII and pS5-RNAPII (Figure 14C). Therefore, this interaction does not depend on DNA or RNA. Intriguingly, PLA assays revealed that WRNIP1 not only associates with total, pS2- and pS5-RNAPII, but also that mutation of HUWE1 diminished association of WRNIP1 with elongation-competent pS2-RNAPII, reduced the association of WRNIP1 with total RNAPII but did not affect association with paused pS5-RNAPII (Figure 14D). WRNIP1 association with RNAPII required the N-terminal region of WRNIP1 encompassing its ubiquitin-binding domain (Figure 14E) in contrast to HUWE1-WRNIP1 binding, which requires the leucine zipper domain (Figure 12).

Depletion of WRNIP1 and catalytic mutation of HUWE1 lead to elevated levels of pS2-RNAPII in whole cell lysates (Figure 14F). However, this increase was abolished upon depletion of WRNIP1 in HUWE1-CS cells, which correlates with the level of TRCs in the respective cell lines (Figure 13F). Since TRCs were dependent on transcription elongation (Figure 10C, D), the question arises whether elongation-competent RNAPII preferentially encounters the replisome. Immunoprecipitation of RNAPII revealed preferential association of the replication factors MCM2 and MCM5 with pS2-RNAPII rather than pS5-RNAPII in HUWE1-CS cells (Figure 14G). This indicates that TRCs predominantly involve actively transcribing RNAPII (Einig et al., 2023).

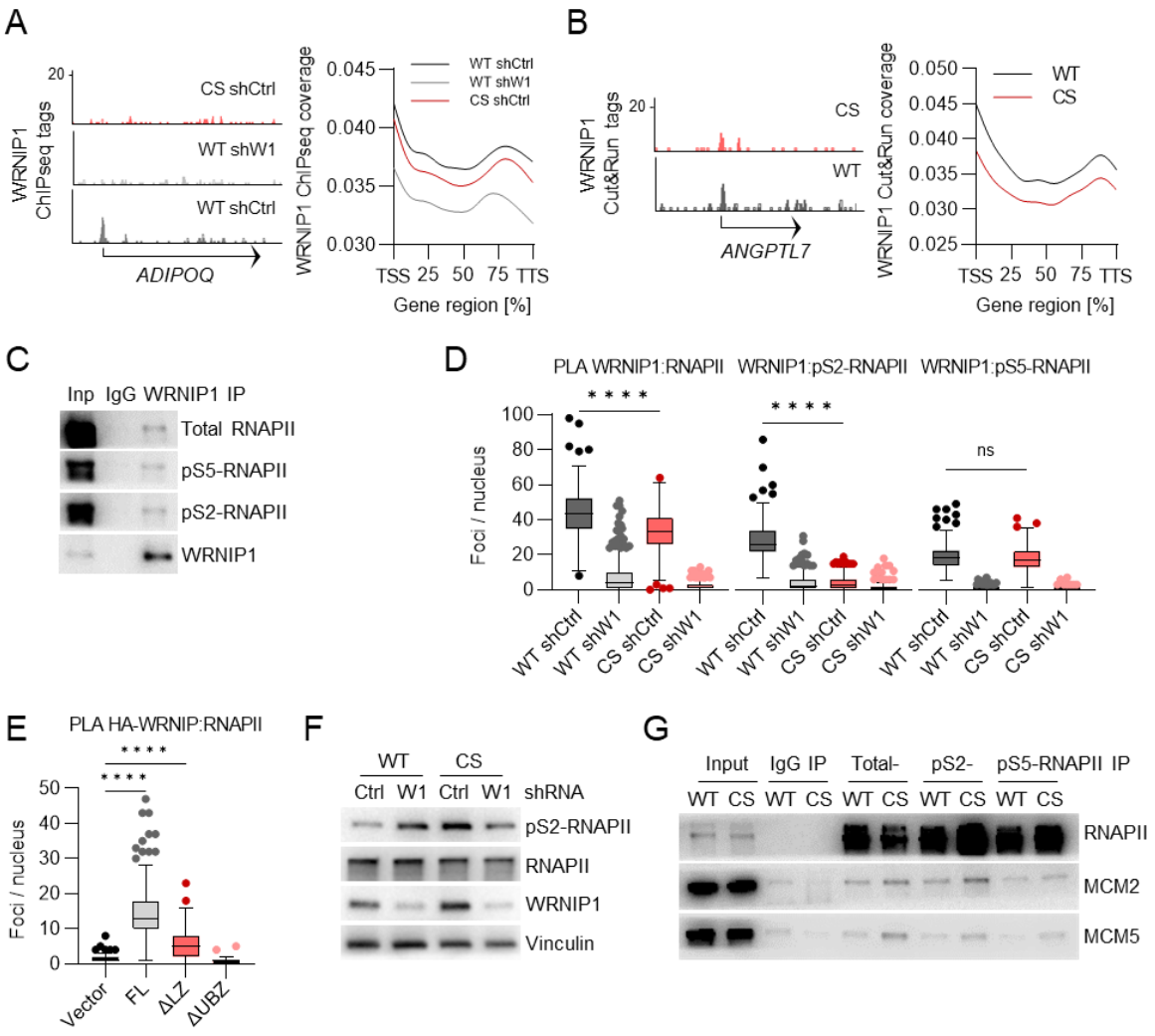


***Figure 14: HUWE1 promotes association of WRNIP1 with elongating RNAPII.***

*A) Example genome browser tracks (left) and global quantification (right) of WRNIP1 ChIPseq signal in HUWE1-WT, HUWE1-CS cells and cells expressing shWRNIP1. WRNIP1 ChIPseq tags were quantified for all genes and displayed as scaled metagenes. B) Example track of Cut&Run analysis using WRNIP1 antibodies in HUWE1-WT and HUWE1-CS cells (left). WRNIP1 Cut&Run tags were quantified for all genes and displayed as scaled metagenes (right). C) Immunoprecipitation of WRNIP1 in benzonase-treated HCT116 lysates, followed by western blot. D) PLA with antibodies to WRNIP1 and RNAPII (≥180 cells), pS2-RNAPII (≥170 cells) and pS5-RNAPII (≥180 cells) in HUWE1-WT and HUWE1-CS cells expressing shWRNIP1 (shW1) or shCtrl. E) PLA with antibodies to RNAPII and HA-tag in cells expressing the indicated HA-tagged WRNIP1 truncation variants. FL: Full length; ΔLZ: Leucine zipper domain is depleted; ΔUBZ: Ubiquitin binding zinc finger domain is depleted. F) Immunoblots of HUWE1-WT and HUWE1-CS cells expressing shCtrl or shWRNIP1. G) Immunoprecipitation of total, pS2-, or pS5-RNAPII in formaldehyde-crosslinked and sonified HUWE1-WT and HUWE1-CS cells. D, E) Boxplots represent the median ± quartiles according to the style of tukey. The non-parametric Kruskal-Wallis test followed by Dunn's multiple comparison was used to determine p-values. ****p ≤ 0.0001, ns: not significant. This figure was adapted from Einig et al. (2023).*

Since pS2-RNAPII levels in whole cell lysates were increased upon depletion of WRNIP1 or mutation of HUWE1, the question arises how pS2-RNAPII is distributed on chromatin. In line with immunoblot analysis, ChIPseq experiments revealed either mutation of HUWE1 or depletion of WRNIP1 induced accumulation of pS2-RNAPII at the 3' regions of gene bodies and transcription termination sites (Figure 15A, B, C). However, depletion of WRNIP1 in HUWE1-CS cells reverted this effect on pS2-RNAPII accumulation. Contrary to transcription termination sites, HUWE1 mutation and WRNIP1 depletion showed opposing effects on pS2-RNAPII accumulation at transcription start sites (Figure 15D). Interestingly, a subset of more than 2200 transcripts at which pS2-RNAPII accumulates upon mutation of HUWE1 or depletion of WRNIP1 does not accumulate in the double mutant cells. Further, these genes show a strong recruitment of WRNIP1 to chromatin that depends on the catalytic activity of HUWE1 (Figure 15E, F). Therefore, HUWE1 promotes association of WRNIP1 with pS2-RNAPII, which suppresses TRCs and pS2-RNAPII accumulation at gene regions close to transcription termination sites (Einig et al., 2023).

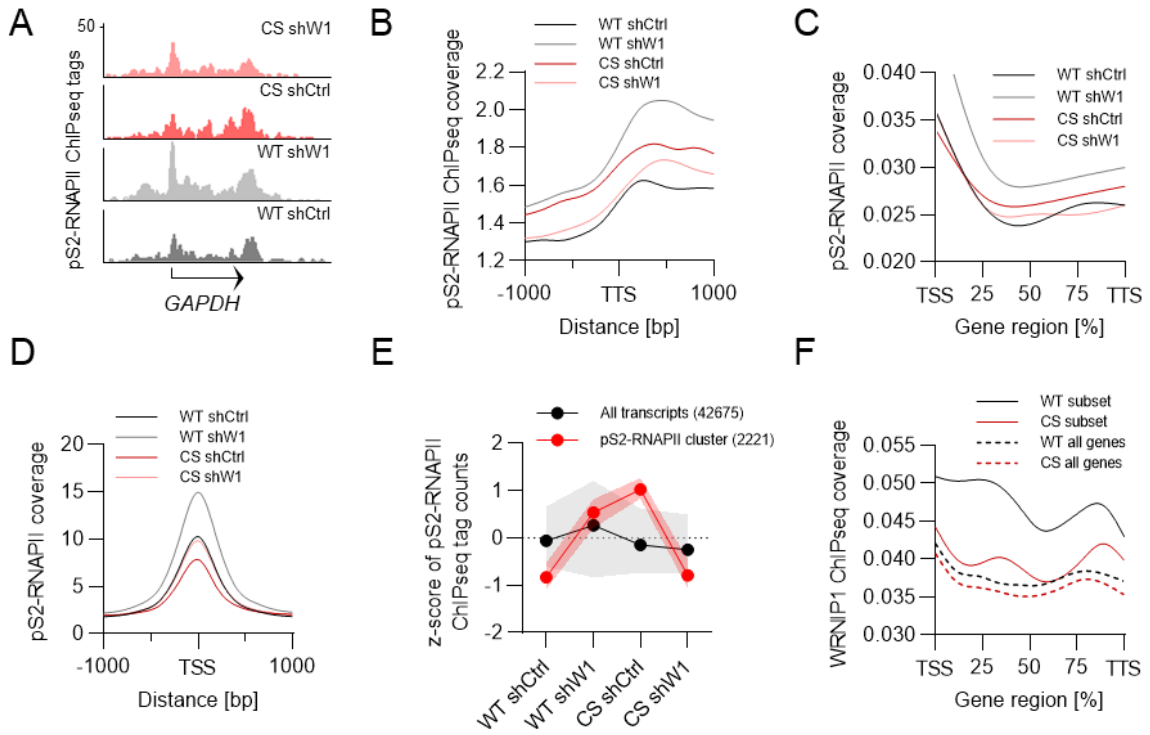


***Figure 15: HUWE1 and WRNIP1 prevent accumulation of pS2-RNAPII at gene regions.***

*A) Representative genome browser tracks showing ChIPseq analysis of pS2-RNAPII in the indicated cell lines. B) Quantification of pS2-RNAPII ChIPseq tag coverage at all transcription termination sites (TTS), C) gene regions scaled as metagenes and D) at transcription start sites (TSS). E) ChIPseq tags of pS2-RNAPII were clustered based on euclidean distance of z-scores for genic areas of all transcripts. A gene cluster with the most pronounced HUWE1- and WRNIP1-dependent pS2-RNAPII accumulation, which was reverted in the double mutant is highlighted in red. Points represent median z-scores of read*

*counts, whereas the shaded areas correspond to the upper and lower quartile respectively. F) ChIPseq analysis of WRNIP1 at gene regions for the same gene subset as in E compared with all genes (dashed lines, see also Figure 14A). This figure was adapted from Einig et al. (2023).*

## 6.4 HUWE1 and WRNIP1 suppress ATM signaling

In line with the observation that TRCs lead to ATM activation (Hamperl et al., 2017), HUWE1-CS cells show higher levels of the phosphorylated ATM targets pKAP1 and histone pH2AX as well as increased levels of phosphorylated ATM compared with HUWE1-WT cells (Figure 16A, B). Histone H2AX is phosphorylated at sites of DNA damage, as well as in the vicinity of stalled replication forks (Gagou et al., 2010, Ward and Chen, 2001, Petermann et al., 2010). Furthermore, depletion of WRNIP1 leads to similar effects on ATM activation (Figure 16A, B). Accordingly, overexpression of WRNIP1 reduced ATM signaling as shown by immunoblot of ATM targets (Figure 16C). However, ATR phosphorylation remained unchanged upon depletion or expression of WRNIP1, as well as phosphorylation of the ATR target pCHK1 upon expression of WRNIP1 (Figure 16A, C), indicating that ATM signaling is not induced due to stalling of replication forks solely (Einig et al., 2023).

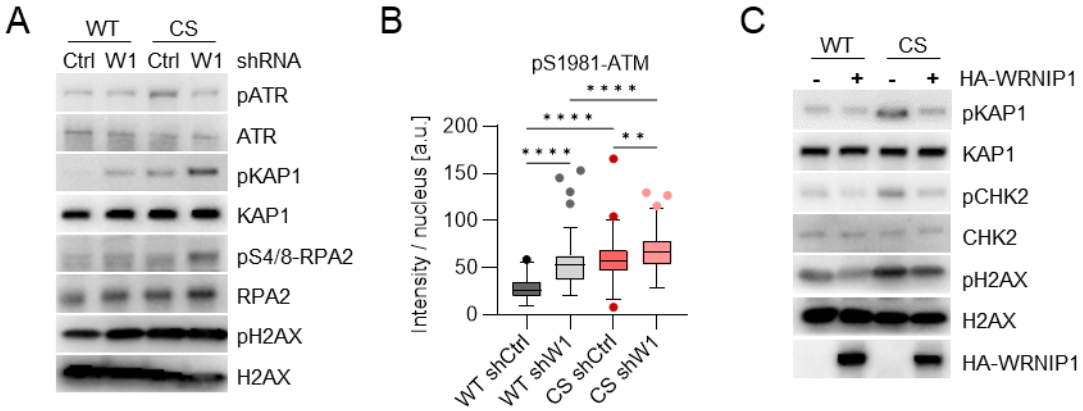


***Figure 16: HUWE1 and WRNIP1 limit ATM activation.***

*A) Immunoblot analysis of HUWE1-WT and HUWE1-CS cells expressing shWRNIP1 or shCtrl. B) Immunofluorescence intensity quantification of pS1981-ATM in HUWE-WT, HUWE1-CS and shWRNIP1 or shCtrl cells (≥105 cells per group). Boxplots represent the median ± quartiles according to the style of tukey. The non-parametric Kruskal-Wallis test followed by Dunn's multiple comparison was used to determine p-values. ****p ≤ 0.0001, **p ≤ 0.01. C) HA-WRNIP1 overexpression followed by immunoblot analysis. This figure was adapted from Einig et al. (2023).*

Accordingly, DNA breakage in shWRNIP1 cells remained unchanged as shown by neutral comet assay, whereas HUWE1-CS cells showed a small increase (1.5-fold) compared with HUWE1-WT cells (Figure 17A). Further, depletion of WRNIP1 in HUWE1-CS cells resulted in a strong increase (3.6-fold) of DNA breakage (Figure 17A), as well as reduced levels of TRCs

as shown previously (Figure 13F). Not only neutral comet assays, but also double strand break sequencing, according to the DSBCapture protocol, showed no increase in shWRNIP1 cells, only a moderate increase for HUWE1-CS and a strong increase of DSBseq tags in the double mutant (Figure 17B). In line with this observation, phosphorylation of S4/8-RPA2, a marker for collapsed replication forks and a target of DNA-PK (Liu et al., 2012), was most pronounced in the double mutant cells (Figure 16A).

Small molecule inhibition of ATM diminished H2AX and KAP1 phosphorylation in HUWE1-CS and shWRNIP1 cells compared with HUWE1-WTcells whereas this effect was only marginal in the double mutant cells (Figure 17C), indicating that this phosphorylation events are ATM independent and may be conducted by other PIKK family members (Lu et al., 2019, Stiff et al., 2004). Induction of DNA damage response signaling with no or only low levels of DNA breakage in shWRNIP1 and HUWE1-CS cells was paralleled with retarded cell proliferation (Figure 17D). Moreover, the strong induction of DNA damage response signaling and high levels of DNA breakage in the double mutant cells correlated with a severe decrease in cell viability (Figure 17D) (Einig et al., 2023).

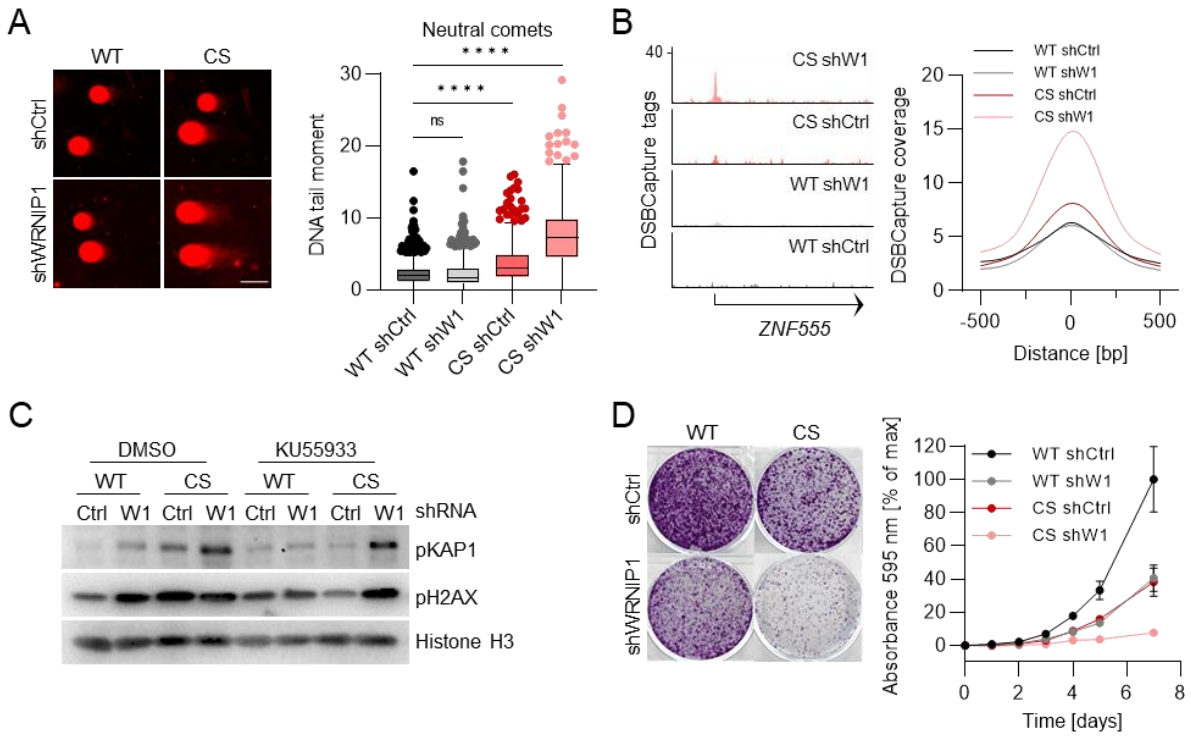


***Figure 17: HUWE1 and WRNIP1 prevent DNA damage, DDR signaling and promote cell proliferation.***

*A) Neutral comet assay with HUWE1-WT and HUWE1-CS cells expressing shWRNIP1 or shCtrl (≥ 660 comets per group, scale bar: 50 µm). Sample preparation was performed by Chao Jin. Boxplots (right) show median ± quartiles according the style of tukey. The non-parametric Kruskal-Wallis test followed by Dunn's multiple comparison was used to determine p-values. ****p ≤ 0.0001, ns: not significant. B) DSBCapture experiment in the indicated cell lines treated with doxycycline for 4 days prior to methanol*

*fixation. Shown are example genome browser tracks (left) and quantification centered at peaks that were identified in all samples. C) Immunoblot of HUWE1-WT and HUWE1-CS cells expressing shCtrl or shWRNIP1, treated with 2.5 µM ATM inhibitor KU-55933 or DMSO for 2 h 30 min. D) Cell proliferation analysis of HUWE1-WT or HUWE1-CS cells with or without WRNIP1 depletion. Cells were stained with crystal violet (left) and respective absorbance was measured at 595 nm (right). This figure was adapted from Einig et al. (2023).*

## 6.5 HUWE1 and WRNIP1 limit ATM activation at RNAPII

ATM signaling in HUWE1-CS cells was diminished after treatment with the transcription inhibitors AZD4573 or triptolide (Figure 18A), correlating with reduced levels of TRCs upon treatment with transcription inhibitors. Following the question, whether elongation-competent RNAPII may promote ATM activation, immunoprecipitation of pS2-RNAPII in benzonase-treated lysates of mouse embryonic fibroblasts (MEFs) was performed, followed by LC-MS/MS analysis. Intriguingly, RAD50 and MRE11 were identified as potential binding partners of pS2-RNAPII in non-transformed fibroblasts (Figure 18B). Both proteins are members of the MRN complex, which recruits ATM to sites of DNA damage (Lee and Paull, 2005). Immunoprecipitation of RAD50 and MRE11 in HCT116 cells resulted in a robust co-precipitation of pS2-RNAPII accordingly, confirming the results obtained in MEFs (Figure 18C). The MRN-RNAPII interaction remained intact, independent of WRNIP1 depletion or HUWE1 mutation (Figure 18D). However, depletion of WRNIP1 or catalytic mutation of HUWE1 induced the association of ATM with RNAPII (Figure 18E, F), likely via its recruitment by the RNAPII-bound MRN complex. This correlates with higher levels of TRCs and ATM signaling in HUWE1-CS and shWRNIP1 cell lines (Figure 13F, Figure 16A).

Antibodies to active pS1981-ATM co-precipitated elongation-competent pS2-RNAPII in HUWE1-CS cells (Figure 18G). Inhibition of RNAPII with triptolide not only reduced the level of TRCs (Figure 10C, D), but also eliminated the ATM-RNAPII interaction in both HUWE1-WT and HUWE1-CS cells (Figure 18F) (Einig et al., 2023).

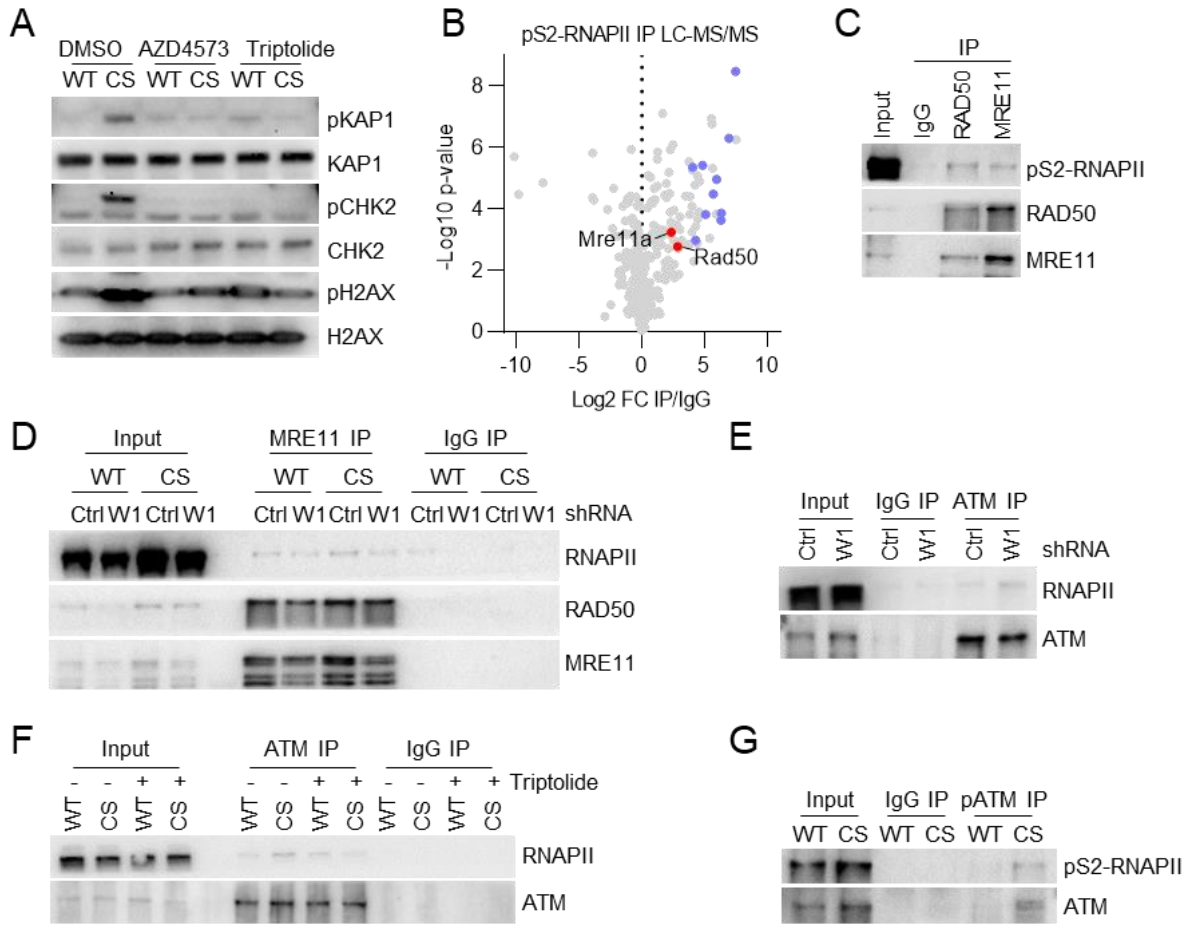


***Figure 18: ATM recruitment by RNAPII depends on HUWE1 and WRNIP1.***

*A) Immunoblot of HUWE1-WT and HUWE1-CS cells treated with 20 nM AZD4573 or 20 nM triptolide for 6 h. B) Immunoprecipitation of pS2-RNAPII in benzonase-treated lysates of mouse embryonic fibroblasts (MEF) followed by LC-MS/MS analysis. MRN complex members are highlighted in red and subunits of the RNAPII complex are highlighted in blue. C) Immunoprecipitation of RAD50 and MRE11 in benzonase-treated lysates of parental HCT116 cells. D) Immunoprecipitation of MRE11 in HUWE1-WT and HUWE1-CS cells, expressing shCtrl or shWRNIP1. E) Immunoprecipitation of ATM in benzonase-treated lysates of cells expressing shWRNIP1 or shCtrl. F) Immunoprecipitation as in D) using HUWE1-WT and HUWE1-CS cells that were treated with DMSO or 20 nM triptolide (+) for 4 h. G) Immunoprecipitation of pS1981-ATM in HUWE1-WT and HUWE1-CS cells. C – G) Panels were provided by Nikita Popov. This figure was adapted from Einig et al. (2023).*

A functional sgRNA library screen targeting genes with gene ontology (GO) terms “Cell cycle”, “DNA replication” and “DNA repair” revealed RAD50 as a gene selectively required for proliferation of HUWE1-CS cells (Figure 19A). Since RAD50 is a member of the MRN complex, which recruits ATM to sites of DNA damage (Lee and Paull, 2005), I tested whether the dependence of HUWE1-CS cells on the presence of RAD50 sensitizes cells to ATM inhibition. Indeed, mutation of HUWE1 lead to reduced cell viability upon ATM inhibition with the small molecule inhibitor KU-55933 (Figure 19B). Moreover, the HUWE1 inhibitor BI8622 acutely

inactivates HUWE1, which synergized with ATM inhibition in HUWE1-WT but not in HUWE1-CS cells (Figure 19C) (Einig et al., 2023).

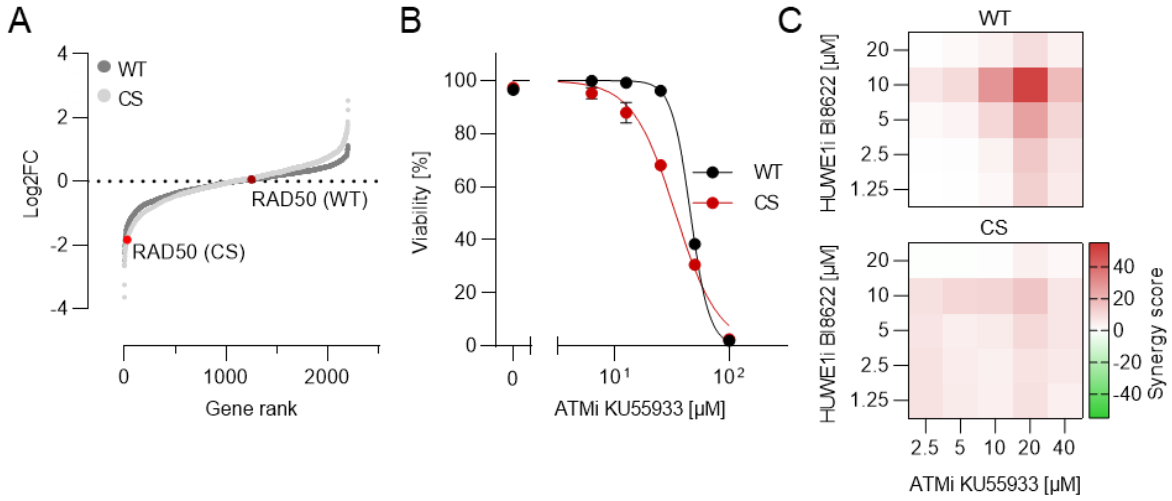


***Figure 19: Loss of HUWE1 function sensitizes cells to ATM inhibition.***

*A) Focused CRISPR-KO screen with an sgRNA library that targets genes with GO terms "Cell cycle", "DNA replication" and "DNA repair" in HUWE1-WT and HUWE1-CS cells. B) Survival of HUWE1-WT and HUWE1-CS cells treated with the ATM inhibitor KU-55933 for 4 days, determined by WST-8 assay. C) Synergy of ATM and HUWE1 inhibitors on growth inhibition of HUWE1-WT and HUWE1-CS cells. Viability was determined by WST-8 assay after 4 days of treatment and synergy scores were calculated with SynergyFinder 2.0. This figure was adapted from Einig et al. (2023).*

## 6.6 HUWE1 and WRNIP1 control RNAPII-dependent ATM activation upon induction of replication stress

Since transcription replication conflicts constitute a replication blockade, I investigated how drug-induced replication stress connects to transcription-dependent TRCs induced by HUWE1 mutation or WRNIP1 depletion. Previous studies established a role of WRNIP1 by recruitment to and stabilization of stalled replication forks upon hydroxyurea (HU) treatment (Leuzzi et al., 2016, Porebski et al., 2019). Consistent with these findings, PLA and immunoprecipitation experiments showed a rapid association of WRNIP1 with the replisome following HU treatment, which was reversible during release from HU treatment (Figure 20A, B). Similar to the WRNIP1-RNAPII interaction, the association of WRNIP1 with the replisome protein MCM2 required the UBZ domain of WRNIP1 (Figure 20C), as reported (Crosetto et al., 2008). Intriguingly, the HU-dependent association of WRNIP1 with the replisome was accompanied by a rapid decrease of WRNIP1-RNAPII association (Figure 20A, B).

Treatment with HU leads to rapid increase of TRCs (Figure 20D), whereas the incidence of TRCs did not further increase in HUWE1-CS or shWRNIP1 upon treatment (Figure 20E). Strikingly, the HU-dependent induction of both total RNAPII or pS2-RNAPII

containing TRCs was eliminated using the transcription inhibitors triptolide and AZD4573 (Figure 20F, G), suggesting that WRNIP1 dissociation from RNAPII upon replication stress underlies the induction of TRCs (Einig et al., 2023).

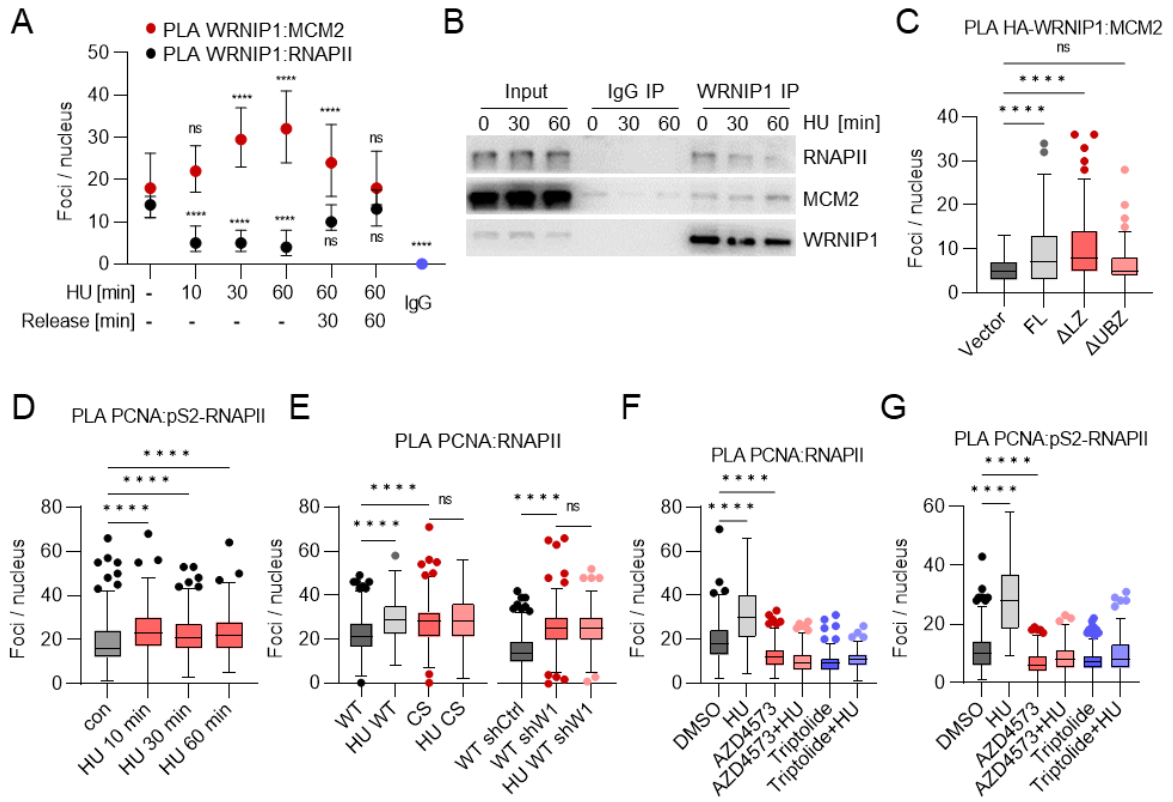


***Figure 20: Replication stress dissociates WRNIP1 from RNAPII and induces transcription-dependent TRCs.***

*A) PLA in parental HCT116 cells with antibodies to WRNIP1 and MCM2 or WRNIP1 and RNAPII. Cells were treated with 1 mM hydroxyurea (HU) for the indicated time or released from treatment. The points represent median values (± quartiles) for the number of proximity pairs in the nuclei of ≥130 cells per group. Asterisks indicate p-values from the comparison of the respective sample with the untreated control sample. B) Immunoprecipitation of WRNIP1 in cells treated with 1 mM hydroxyurea for the indicated time. C) PLA assay with antibodies to HA-tagged WRNIP1 variants and MCM2 in HCT116 cells (≥140 cells). FL: Full length; ΔLZ: Leucine zipper domain is depleted; ΔUBZ: Ubiquitin binding zinc finger domain is depleted. D) PLA assay with antibodies to PCNA and pS2-RNAPII in parental HCT116 cells treated with 1 mM HU for the indicated time (≥190 cells). E) PLA with antibodies to PCNA and RNAPII in HUWE1-WT, HUWE1-CS and shWRNIP1 cells, treated with DMSO or with 1 mM HU for 2 h (≥110 cells). F) PLA with antibodies to PCNA and RNAPII in cells treated with 20 nM AZD4573 or with 100 nM triptolide for 2 h in combination with or without 1 mM HU for additional 4 h (≥160 cells). G) PLA with antibodies to PCNA and pS2-RNAPII in cells treated with 1 mM HU for 4 h with or without 2 h pre-treatment using 20 nM AZD4573 or 100 nM triptolide (≥140 cells). A, C – G) Boxplots represent the median ± quartiles according to the style of tukey. The non-parametric Kruskal-Wallis test followed by Dunn's multiple comparison was used to determine p-values. *p ≤ 0.05, **p ≤ 0.01, ***p ≤ 0.001, ****p ≤ 0.0001, ns: not significant. This figure was adapted from Einig et al. (2023).*

Treatment with hydroxyurea stimulated phosphorylation of the ATM targets KAP1 and CHK2 (Figure 21A). However, treatment with AZD4573 or triptolide strongly reduced the HU-induced ATM signaling. Moreover, HU stimulated the interaction of ATM with RNAPII and the replisome member MCM2, which was diminished by triptolide or AZD4573 (Figure 21B, C), correlating with the effect of HUWE1-CS or WRNIP1 depletion (Figure 18E, F). Transcription inhibitors not only abolished the HU-induced ATM-RNAPII interaction, but also impaired the interaction of ATM with the replisome member MCM2 (Figure 21B, C), indicating that elongation-competent transcription is required for ATM activation at replication forks stalled by hydroxyurea or TRCs. Interestingly, WRNIP1 precipitation in unstressed cells showed an interaction of WRNIP1 with MRE11 and RNAPII, which is rapidly reduced upon treatment with HU (Figure 21D). Together, this may indicate that WRNIP1 antagonizes ATM recruitment to RNAPII by the RNAPII-bound MRN complex (Einig et al., 2023).

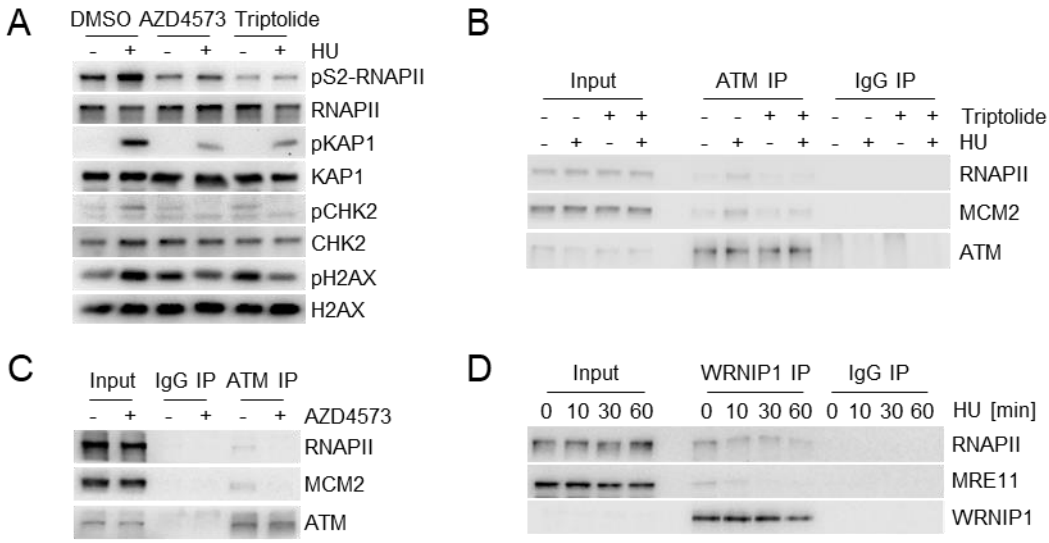


***Figure 21: Replication stress induced ATM signaling requires elongation-competent RNAPII.*** *A) Immunoblot of HCT116 cells treated with 1 mM hydroxyurea for 2 h or in combination with 3 h pre-treatment using 20 nM AZD4573 or with 100 nM triptolide. B) Immunoprecipitation of ATM in cells treated with 1 mM hydroxyurea in combination with or without 20 nM triptolide for 4 h. C) Immunoprecipitation of ATM from benzonase-treated lysates of cells treated with 1 mM HU in combination with or without 20 nM AZD4573 for 4 h. D) Immunoprecipitation of WRNIP1 from HCT116 cells, treated with 1 mM HU for indicated time points. B – D) Panels were provided by Nikita Popov. This figure was adapted from Einig et al. (2023).*

Since transcription inhibition dampens replication stress-induced DNA damage response signaling, the question arises whether the level of damage response signaling reflects the actual level of DNA damage. Therefore, I treated HCT116 cells for 24 h with HU alone or in combination with triptolide or AZD4573 and released the cells in full growth medium for several time points. The levels of the DNA damage marker pH2AX strongly increased upon HU

treatment and decreased in the following 60 minutes of release (Figure 22A). In contrast, cells treated with a combination of HU with AZD4573 or triptolide remained with high levels of pH2AX.

To not only rely on a phosphorylation event to judge actual DNA breakage in cells, accumulation of DNA damage was assessed using a neutral comet assay or DSBCapture (Lensing et al., 2016) followed by next generation sequencing (NGS). Interestingly, both experiments uncovered no or only a small increase of DNA breakage upon single inhibitor treatments, which was exceeded by the combined treatment with HU and AZD4573 (Figure 22B, C). DSBCapture peaks are predominantly localized to gene regions independent of the treatment (Figure 22D).

Treatment with the transcription inhibitors AZD4573 and triptolide in combination with HU strongly reduced cell survival (Figure 22E, F), in agreement with previous studies (Yu et al., 2010). This leads to the idea that RNAPII-localized activation of ATM upon replication stress promotes DNA repair and cell survival (Einig et al., 2023).

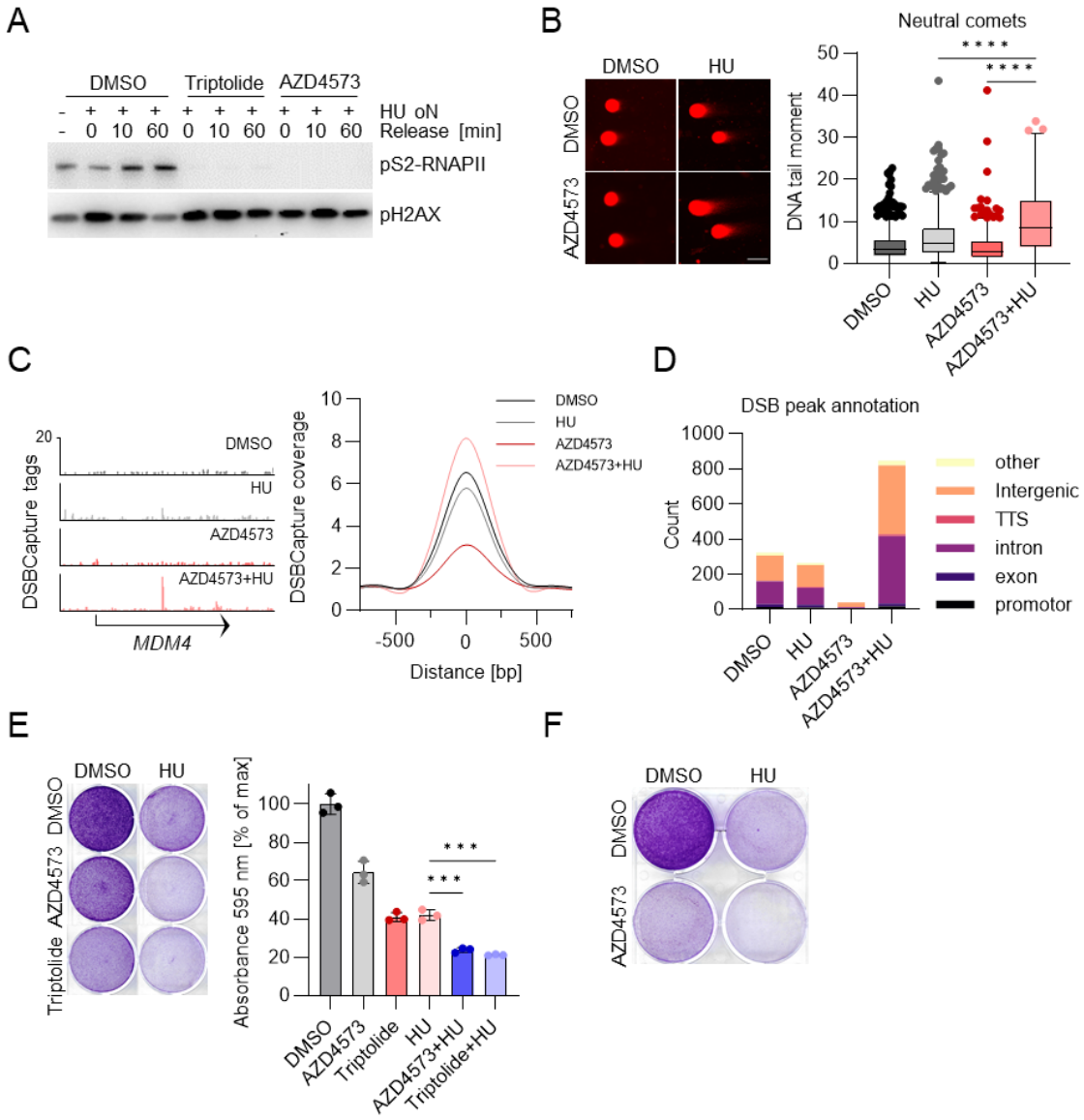


***Figure 22: Elongation-competent RNAPII dampens replication stress induced DNA breakage.*** *A) Immunoblots of HCT116 cells treated with 1 mM HU alone or in combination with 20 nM triptolide or with 20 nM AZD4573 and released for the indicated time. B) Neutral comet assay in HCT116 cells treated with DMSO or 20 nM AZD4573 for 6 h followed by 1 mM HU overnight and 24 h treatment release. Sample preparation was performed by Chao Jin. Scale bar: 50 µm. For quantification, ≥320 cells per group were analyzed. Boxplots show median ± quartiles. The non-parametric Kruskal-Wallis test followed by Dunn's multiple comparison was used to determine p-values. ****p ≤ 0.0001 C) Representative tracks (left) and quantification of DSB capture tag density (right) in HCT116 cells treated with 1 mM HU in combination with or without pre-treatment using 20 nM AZD4573 for 4 h. Cells were released from treatment for 24 h prior to DSBCapture. D) Frequency distribution of peak annotations of DSB capture peaks. E) Crystal violet staining of HCT116 cells treated with 1 nM AZD4573 or 2.5 nM triptolide for 3 h followed by addition of 250 µM HU for 4 days. F) Crystal violet staining of HeLa cells treated with 1 nM AZD4573 or 2.5 nM triptolide for 3 h followed by addition of 250 µM HU for 4 days. This figure was adapted from Einig et al. (2023).*

# 7 Discussion

*Parts of this chapter were adapted from EINIG, E., JIN, C., ANDRIOLETTI, V., MACEK, B. & POPOV, N. 2023. RNAPII-dependent ATM signaling at collisions with replication forks. Nature Communications.*

In this study, I characterize the interaction of the ubiquitin ligase HUWE1 with the ATPase WRNIP1 and its impact on TRCs, DNA damage and DNA damage response signaling (Einig et al., 2023). Catalytic activity of HUWE1 is required for WRNIP1 binding to elongation-competent RNAPII, which prevents conflicts of the transcription machinery (TRCs) with the replisome and therefore limits ATM signaling during an unperturbed cell cycle. Loss of the HUWE1 ubiquitin ligase function, depletion of WRNIP1 protein or expression of WRNIP1 variants incapable of HUWE1 binding induce transcription-dependent TRCs. HUWE1 and WRNIP1 safeguard TRCs to prevent actual DNA breakage. Higher levels of conflicts lead to ATM activation, which depends on elongation-competent RNAPII. Induction of replication stress via nucleotide depletion rapidly induces the transfer of WRNIP1 from RNAPII to the replisome, formation of transcription-dependent TRCs and ATM signaling. Elongating RNAPII promotes localized ATM activation under replication stress and at TRCs to prevent DNA breakage and promote repair (Figure 23).

DNA damage response (DDR) signaling is triggered by DNA damage and conveyed by either ATR, in the case of ssDNA lesions, or ATM and DNA-PK in the case of DNA double strand breaks (DSBs) (Blackford and Jackson, 2017). Recruitment of ATM to sites of DNA lesions requires the MRN complex, which consists of the exonuclease MRE11, the ATPase RAD50 and NBS1 (Marechal and Zou, 2013). Upon replication stress, stalling of DNA replication forks potently induces activation of ATR, as well as ATM, which in turn leads to stabilization, remodeling and restart of replication forks. This facilitates the recovery from replication stress (Schleicher et al., 2022, Trenz et al., 2006).

A proposed mechanism of ATM recruitment to stalled replication forks involves the ATPase WRNIP1 and the ATM-interacting protein ATMIN (Kanu et al., 2016). According to this model, WRNIP1 recruitment to stalled replication forks depends on the WRNIP1 UBZ domain (Crosetto et al., 2008), which binds ubiquitinated PCNA upon replication stress (Hishida et al., 2006). Together with the finding that WRNIP1 binds to ATMIN, WRNIP1 may play a mediator role in recruitment of ATM to stalled replication forks (Kanu et al., 2016). Other known functions of WRNIP1 include the stabilization of stalled replication forks by inhibiting exonuclease activity of the MRN complex. This facilitates replication fork restart after release from drug-induced replication stress (Leuzzi et al., 2016). Supporting this model, experiments in this study show that replication stress triggers recruitment of WRNIP1 to the replisome and this interaction

depends on its UBZ domain (Figure 20A–C). However, WRNIP1 is not essential for ATM activation. Intriguingly, depletion of WRNIP1 triggers ATM activation and ATM-target phosphorylation, whereas overexpression of WRNIP1 shows the opposite effect (Figure 16). This leads to the conclusion that WRNIP1 limits ATM activation during unperturbed cell cycle progression. The model of WRNIP1-independent activation of ATM upon replication stress is supported by the finding that ATM may directly interact with ubiquitinated PCNA at stalled replication forks (Gamper et al., 2012) and ATM activation does not strictly require ATMIN (Liu et al., 2017), further undermining the model that WRNIP1 is crucial to bridge ubiquitinated PCNA with ATMIN for ATM activation. Therefore, the question arises which role WRNIP1 plays for ATM signaling at TRCs.

ChIPseq and Cut&Run experiments show that WRNIP1 broadly associates with transcriptionally active chromatin in the absence of exogenous stress (Figure 14A, B). Moreover, WRNIP1 binds to RNAPII and the phosphorylated pS2-RNAPII (elongation-competent) and pS5-RNAPII (promotor-proximal paused) proteoforms (Figure 14C, D). Similar to the interaction with the replisome (Crosetto et al., 2008), the UBZ domain of WRNIP1 is required for RNAPII association (Figure 14E), leading to a simple model of alternate binding to either the transcription or replication machinery. This model includes the possibility that alternative WRNIP1 binding to the replisome or RNAPII depends on ubiquitination of a member of either complex. Interestingly, WRNIP1 translocates from RNAPII association to the replisome early upon global replication fork stalling following nucleotide depletion by hydroxyurea treatment (Figure 20A–C). Therefore, replication stress may lead to the formation of a high affinity binding site for WRNIP1 at the replisome, which could likely be the ubiquitination of PCNA (Saugar et al., 2012) or the formation of reversed replication forks (Porebski et al., 2019), favoring WRNIP1 recruitment to the replisome over its interaction with RNAPII. DNA replication forks frequently encounter obstacles such as DNA lesions, crosslinked proteins or the transcription machinery. During unperturbed cell cycle, localized transfer of WRNIP1 at transcription replication conflicts may be most efficient. This transfer can be instrumental to coordinate DNA replication with RNAPII-dependent transcription in order to control ATM signaling and maintain genome integrity (Liu et al., 2021, Saponaro, 2022).

The association of WRNIP1 with elongation-competent pS2-RNAPII requires the catalytic activity of the ubiquitin ligase HUWE1, whereas association with pS5-RNAPII remained unchanged upon HUWE1 mutation (Figure 14D), suggesting that HUWE1 promotes WRNIP1 association particularly with elongating RNAPII. This study identifies a robust interaction between WRNIP1 and HUWE1 in numerous cell lines, which is independent of the catalytic activity of HUWE1 (Figure 11A-G). WRNIP1 binds to HUWE1 via its leucine zipper domain (Figure 12), in contrast to its interaction with RNAPII or replisome members via its UBZ

domain. The initial idea that WRNIP1 is targeted by HUWE1 for proteasomal degradation was not confirmed, since WRNIP1 protein stability is independent of HUWE1 ubiquitin ligase activity (Figure 11H).

HUWE1 is a versatile ubiquitin ligase catalyzing K6-, K11-, K48-, and K63-linked poly-ubiquitination as well as mono-ubiquitination. This enables HUWE1 to regulate a multitude of substrates including MYC, MIZ1, MCL1 and TP53, which are regulators of transcription, DNA repair, apoptosis, stress responses, proliferation and differentiation (Kao et al., 2018, Qi et al., 2012, Jäckl et al., 2018). Since HUWE1 plays a broad role in protein regulation networks, the question arises 1) how it affects tumor proliferation and 2) whether WRNIP1 is a HUWE1 effector protein that plays a role in maintaining genome integrity.

On the one hand, HUWE1 is implicated in tumor suppression through degradation of MYC (Myant et al., 2017). Mice develop colonic tumors upon depletion of HUWE1. Contrary to this study, inhibition or depletion of HUWE1 in tumor cells and xenograft mouse models results in growth retardation (Peter et al., 2014), which is in line with diminished cell proliferation in HUWE1-CS cells (Figure 17D). Moreover, global analysis of CRISPR/Cas9 and RNAi screens revealed that the majority of tested cell lines requires HUWE1 for efficient proliferation (Tsherniak et al., 2017, Vazquez and Boehm, 2020, Pacini et al., 2021), rendering the protein a potential drug target for cancer therapy and a handle to modulate non-druggable substrates (Crawford et al., 2020), provided that concerns about its tumor suppressive functions are eliminated. Available small molecule inhibitors may have unknown off-target effects that could compromise the benefit for research purposes. Therefore, to deepen the mechanistic understanding of HUWE1 ubiquitin ligase functions, mutation of the catalytic cysteine (C4341S) in the endogenous HUWE1 locus is a useful and necessary tool (Figure 8).

Previous studies examined that small molecule inhibition or depletion of HUWE1 deregulates the expression of about 700 genes, which show a strong enrichment of MYC target genes (Peter et al., 2014). In contrast, catalytic mutation of HUWE1 in a homozygous genetic background leads to deregulated mRNA expression of more than 1900 genes, in which MYC hallmark gene sets are not strongly enriched (Figure 9C-G). This discrepancy can be addressed by the different cellular systems applied or rather by the nature of how HUWE1 function is altered. To date, it is unclear whether the available HUWE1 inhibitors BI8622 and BI8626 solely bind and inhibit the catalytic center of the HUWE1-HECT domain only, or interfere with its function based on conformational changes at other regions of the protein, such as domains required for target protein binding. In this study, a genetic model of HUWE1 ubiquitin ligase inhibition is employed (Figure 8, Figure 6), which is expected to keep given scaffold functions and interaction domains of the HUWE1 protein intact, while its ubiquitin ligase function is abolished. However, constitutive expression of dysfunctional HUWE1 may allow and force cells to adapt to long term defects. Regarding gene expression profiles, these

results indicate that the HUWE1 ubiquitin ligase function regulates RNAPII-dependent gene expression also via other effectors than MYC.

Mutation of HUWE1 deregulates not only transcription, but also DNA replication. In agreement with previous studies (Choe et al., 2016), catalytic mutation of HUWE1 (HUWE-CS) caused a significant defect in DNA replication fork progression as shown by DNA fiber assays (Figure 9A, B). This result is supported by EdU incorporation assays, which additionally show that depletion of WRNIP1 in HUWE1-WT cells diminish EdU incorporation, but not in HUWE1-CS cells (Figure 13B, C), indicating that HUWE1 and WRNIP1 jointly affect DNA replication.

Since HUWE1-CS cells harbor defects in DNA replication fork progression, as well as dysregulation of transcription, I investigated the effect of HUWE1 on transcription replication conflicts. Interestingly, the level of TRCs is increased in HUWE1-CS cells (Figure 10). Therefore, the question arises of how HUWE1 is capable of coordinating both, transcription and DNA replication. A potential mechanism may include HUWE1-dependent regulation of WRNIP1 at sites of TRCs.

Catalytic mutation of HUWE1 diminishes the association of WRNIP1 with (pS2-) RNAPII, whereas the association with the replisome is induced (Figure 14D; Figure 13H), similar to treatment with hydroxyurea (Figure 20A, B). One possibility is that HUWE1 contributes to the association of WRNIP1 with RNAPII by ubiquitination of a member of the transcription machinery. This model can explain WRNIP1 dissociation upon HUWE1 mutation, since the proposed ubiquitination event is missing. On the other hand, stalled replication forks in HUWE1-CS cells and concomitant post-translational modifications on effector proteins, such as ubiquitination of PCNA, might result in a preferred binding site for WRNIP1. Binding of WRNIP1 to ubiquitinated PCNA has already been proposed for its yeast homolog Mgs1 (Saugar et al., 2012, Ulrich, 2009). Taken together, replication stress induces the transfer of WRNIP1 from RNAPII to the replisome. Hence, transcription does not only shape replication, but also vice versa, hinting at a concomitant coordination of either process.

The transfer of WRNIP1 from the transcription machinery to the replisome could be very efficient at collisions of the transcription machinery with a replisome due to spatial vicinity of both complexes. Mutation of HUWE1 elevates the level of TRCs and based on the known role of WRNIP1 in protecting stalled replication forks from degradation (Leuzzi et al., 2016), I propose that WRNIP1 stabilizes the TRC configuration to prevent its collapse. This is in line with the observation that depletion of WRNIP1 in HUWE1-CS cells lowers the level of TRCs and simultaneously leads to increased DNA breakage (Figure 13F, Figure 17). Interestingly, depletion of WRNIP1 is sufficient to elevate TRC levels that depend on transcription and the catalytic activity of HUWE1 and slightly increase HUWE1 association with the replisome member PCNA (Figure 13D, F, G). Either depletion of WRNIP1 or loss of HUWE1 function

leads to elevated levels of TRCs. Therefore, I conclude that both proteins are required for resolution or prevention of TRCs, whereas either HUWE1 or WRNIP1 are sufficient to stabilize replication forks at transcription replication conflicts when the other protein is dysfunctional.

Beyond being binding partners, HUWE1 and WRNIP1 may regulate a common interaction partner involved in resolution of TRCs. An apparent possibility is the common regulation of PCNA (Choe et al., 2016, Saugar et al., 2012). HUWE1 may ubiquitinate PCNA with single or multiple ubiquitin moieties harboring distinct linkage specificities in the absence of WRNIP1, while the presence of WRNIP1 and its binding to ubiquitinated PCNA may functionally compensate the lack of this modification in HUWE1-CS cells. A similar mechanism could apply to the regulation of linker Histone H1, which compacts nucleosomes and is ubiquitinated by HUWE1 upon induction of DNA damage (Mandemaker et al., 2017, Li et al., 2018, Almeida et al., 2018). Removal of Histone H1 from nucleosomes softens chromatin compaction and facilitates recruitment of repair factors. Further, WRNIP1 may be involved in shaping the substrate specificity or the ubiquitin linkage types generated by HUWE1.

Abolishing the function of both HUWE1 and WRNIP1 reverts the level of TRCs (Figure 13F), which indicates that either fewer conflicts are generated or replication forks at TRCs are instable and likely collapse. A collapse results in the formation of DNA double strand breaks and arises the necessity to repair DNA. Indeed, cells without either protein function show a strong increase in DNA damage levels as shown by neutral comet assays and DSBCapture experiments (Figure 17A, B). Consistent with this idea, the double mutant cells harbor an increase in the DNA-PK-dependent phosphorylation of pS4/8-RPA2 (Figure 16A), which is a marker of collapsed replication forks (Zernik-Kobak et al., 1997, Liu et al., 2012). Moreover, ATM inhibition in the double mutant cells did not decrease the levels of pH2AX, further hinting to preferred DNA-PK-dependent signaling of DSBs, whereas in the single mutant cell lines inhibition of ATM reduced pH2AX levels (Figure 17C). Hence, a TRC may provide a mechanism for replication fork stalling and stabilization in a controlled manner to facilitate rapid recovery from replication stress and to prevent the formation of DSBs. Therefore, stabilized TRCs can be envisioned as rescue event rather than a source of genome instability.

Strong activation of ATM signaling in cells without detectable DNA damage and simultaneously high levels of TRCs suggest that the TRC-dependent protection of DNA integrity is at least partially mediated by induction of ATM signaling. The canonical DSB-dependent induction of ATM signaling (Blackford et al., 2012, Sirbu et al., 2011) is not excluded by this data. However, it appears that the low level of breaks indicate that also other DNA structures may trigger ATM signaling, as for instance stalled forks or transcription replication conflicts. This is supported by the finding that depletion of WRNIP1 does not activate ATR (Figure 16A), showing that replication forks are not collapsed to DSBs, which is supported by the finding that DSB levels remain similar with or without WRNIP1.

Mutation of HUWE1 strongly increases ATM signaling, potentially due to the occurrence of TRCs or due to slightly elevated levels of actual DNA breakage as shown by neutral comet assays and DSBCapture experiments (Figure 16A; Figure 17A, B). Keeping in mind that HUWE1 may serve as a suitable drug target to abolish cancer cell proliferation (Kao et al., 2018), I investigated synthetic lethal interactions with the mutation of HUWE1. Surprisingly, a CRISPR/Cas9-KO screen showed specific depletion of sgRNAs targeting RAD50 in HUWE1-CS cells compared with HUWE1-WT cells. Therefore, RAD50 is identified as candidate for synthetic lethality with HUWE1-inhibition (Figure 19A). As described previously, RAD50 is an integral component of the MRN complex, which is instrumental for ATM activation. Indeed, mutation of HUWE1 sensitized cells to the ATM inhibitor KU55933 and acute HUWE1 inhibition synergized with ATM inhibition in HUWE1-WT cells (Figure 19B, C). This indicates that for coping with defects due to HUWE1-inhibition, tumor cells require RAD50 and ATM signaling in order to limit DNA damage and to proliferate efficiently.

Transcription replication conflicts and replication stress-induced ATM signaling are both dependent on elongation-competent RNAPII (Figure 10C, D; Figure 21A), suggesting that association of the MRN complex with pS2-RNAPII plays a key role in mediating these effects. Indeed, previous studies characterized the interaction of RNAPII with the MRN complex at sites of DSBs, which enables the synthesis of damage induced long non-coding RNA from and towards the DSB site (Michelini et al., 2017, Sharma et al., 2021). Transcription activity at DSBs was shown to be independent of the MRN exonuclease activity and rather depends on the ability to melt DNA ends. The presence of dilncRNAs supports DNA repair mechanisms by recruitment of 53BP1 to damaged sites. However, the association of RNAPII with the MRN complex is not restricted to sites of DNA damage but rather occurs throughout the genome, especially at highly transcribed genes where RNAPII accumulates (Salifou et al., 2021). In line with these observations, immunoprecipitation of elongation-competent pS2-RNAPII reveal an interaction with MRN components and vice versa in unstressed tumor cells and in non-transformed mouse embryonic fibroblasts (Figure 18B-D). This suggests that RNAPII bound MRN may directly recruit ATM for signaling at encounters with the replication machinery.

Indeed, ATM pulldown assays showed increased co-precipitation of RNAPII in WRNIP1-depleted or HUWE1-CS cells (Figure 18E, F). Not only total ATM interaction with RNAPII, but also active pS1981-ATM binding to elongation-competent pS2-RNAPII was elevated in HUWE1-CS cells (Figure 18G), indicating that ATM activation may occur locally at sites of elongation-competent pS2-RNAPII. The ATM interaction with RNAPII further decreases upon inhibition of RNAPII, strengthening this argument (Figure 18F). Likewise, RNAPII inhibition with either AZD4573 or triptolide obliterated ATM target phosphorylation in HUWE1-CS cells (Figure 18A). Therefore, the RNAPII-MRN interaction may represent a poised state for ATM recruitment and signaling at active RNAPII. A possible mechanism of

ATM recruitment to and activation on RNAPII could include WRNIP1 translocation, if WRNIP1 prevents ATM binding to the RNAPII-bound MRN complex for example by sterical hindrance. Indeed, WRNIP1 precipitation showed an interaction with RNAPII and MRE11 in the same samples, which were both reduced already after 10 – 30 minutes of hydroxyurea treatment (Figure 21D), which induces the transfer of WRNIP1 from RNAPII to the replisome.

Hydroxyurea-induced replication stress rapidly induces TRCs (Figure 20D-G), which may trigger ATM signaling at stalled replication forks. Interestingly, hydroxyurea increases the interaction of RNAPII with ATM, which was diminished upon RNAPII inhibition (Figure 21B, C). Moreover, RNAPII inhibition eliminates replication stress-induced TRCs (Figure 20F, G), as well as ATM signaling (Figure 21A) and undermines DNA repair and cell proliferation during exposure to replication stress, while the level of DNA breakage strongly increases (Figure 22B-F). Hydroxyurea-induced phosphorylation of histone H2AX was rescued already one hour after treatment release, whereas pre-treatment with transcription inhibitors obliterated this effect (Figure 22A). Therefore, elongation-competent RNAPII plays an integral role in facilitating the tolerance to replication stress and TRCs by recruitment of ATM. This is in line with previous studies showing a dependency of the RNAPII-CTD kinase CDK9 for cell survival during low levels of replication stress (Shiloh and Ziv, 2013, Yu et al., 2010).

Now the question arises how active RNAPII is involved in the prevention and repair of DNA damage resulting from DNA replication and TRCs. Beyond RNAPII-dependent recruitment of ATM, RNAPII may sustain ATM signaling required for efficient DNA repair via several mechanisms. This includes transcription of dilncRNAs at DSBs, which facilitates 53BP1 foci formation (Michelini et al., 2017). Moreover, ATM signaling may be supported by the generation of DNA-RNA hybrids, termed R-loops, which may arise from RNAPII arrest in a TRC adjacent to proximally stalled replication forks (Aguilera and Garcia-Muse, 2012). In turn, ATM activation facilitates the resolution of R-loops. Furthermore, spatial vicinity of active ATM and RNAPII-associated factors might fuel ATM activation and impact fork stabilization, fork remodeling and DNA repair.

For example, members of the spliceosome complex are associated with pS2-RNAPII and transcriptional pausing or arrest of pS2-RNAPII is sufficient to displace the spliceosome. This may lead to accumulation of R-loops, resulting in a positive feedback loop of ATM signaling, which further displaces the spliceosome (Tresini et al., 2015, Sherill-Rofe et al., 2022). Moreover, the RNAPII-bound DNA helicase RECQ5, which suppresses HR mediated repair, is recruited to DSBs via the MRN complex and activates ATM signaling (Zheng et al., 2009, Aygun et al., 2008). Likewise, the RNA helicase DHX9 is activated by ATM and promotes BRCA1 recruitment to RNAPII and thereby facilitates end resection at DSB sites, enabling DNA repair based on homologous recombination (Chakraborty and Hiom, 2021). Besides BRCA1, the tumor suppressor BRCA2 is not only a key mediator of homologous recombination

dependent DNA repair, but is also implicated in stabilization of stalled replication forks and broadly associates with RNAPII (Lomonosov et al., 2003, Welcsh et al., 2000, Gruber et al., 2019). Beyond these possibilities, pS2-RNAPII may directly support the recruitment of ATM via its binding to the MRN complex, which this study characterizes, and therefore enable ATM signaling as soon as the transcription machinery is perturbed for instance by encounters with the replisome. However, it is likely that depending on the chromatin context these mechanisms overlap and are integrated to support or regulate each other in order to maintain genome stability.

The cellular need to coordinate transcription and DNA replication is most apparent in cells with a very fast proliferation rate, such as tumor cells. Therefore, not only drug-induced replication stress, but also oncogene-dependent replication stress may be tolerated because of the efficient coordination of transcription and DNA replication by HUWE1 and WRNIP1. This is supported by transcription-dependent rescue mechanisms to stabilize DNA replication forks and TRCs, resulting in preemptive ATM signaling. In line with this model, MYC-driven tumors with elevated levels of replication stress are sensitized to inhibition of the kinases CDK7 and CDK9, which are required for activation of RNAPII-dependent transcription (Chipumuro et al., 2014, Huang et al., 2014). While the HUWE1-dependent coordination of genome integrity provides a proliferation benefit for tumor cells by coping with elevated stress levels, long term depletion of HUWE1 function in non-transformed healthy tissue may result in low, but long-lasting, levels of genome instability and therefore eventually in the development of cancer cells over time (Myant et al., 2017). Hence, the identified and discussed implications of HUWE1 may partially explain its previously contradicting role as either tumor suppressor or oncogene. Therefore, novel strategies to exploit HUWE1 as drug target for cancer therapy shall be developed with great care to identify a treatment window in time and dose allowing regression of tumor burden while oncogenesis is prevented.

All in all, this study proposes that contrary to the common model of TRCs being the cause of genome instability, a conflict may represent a rescue event to prevent replication fork collapse, initiate early DNA damage response signaling via ATM and thereby maintain genome integrity (Figure 23). The concert of transcription and DNA replication is tightly controlled by numerous proteins, including HUWE1 and WRNIP1. Abolishing the HUWE1 ubiquitin ligase function or depletion of WRNIP1 elevates levels of TRCs. Transcription replication conflicts harboring pS2-RNAPII are strongly elevated upon drug-induced replication stress and simultaneous inhibition of RNAPII diminishes corresponding ATM activation. This results in high levels of DNA damage that compromise tumor cell survival. Beyond drug-induced replication stress, this system may underlie coping strategies for oncogene-induced replication stress in tumor cells. Therefore, these findings integrate a model of coordinated DNA replication, transcription and ATM signaling. The mechanistic understanding, including the

roles of HUWE1 and WRNIP1, may serve as a rationale to advance combinatorial, antineoplastic therapies.

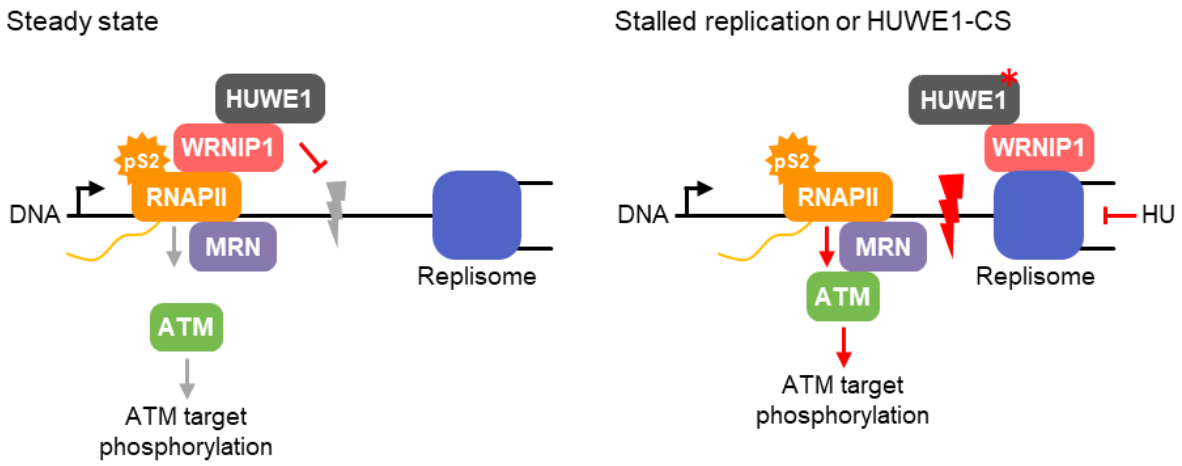


***Figure 23: Proposed model of HUWE1 and WRNIP1 dependent coordination of transcription and replication.***

*Binding of HUWE1 with WRNIP1 prevents transcription-dependent TRCs. WRNIP1 associates with elongation-competent pS2-RNAPII in a HUWE1-dependent manner. Mutation of HUWE1 or drug-induced replication stress lead to transfer of WRNIP1 from RNAPII to the replisome and induction of TRCs. WRNIP1 and HUWE1 stabilize transcription-dependent TRCs redundantly to prevent collapse resulting in DSBs. The RNAPII-bound MRN complex recruits ATM in a pS2-RNAPII-dependent manner to initiate preemptive DNA damage response signaling, facilitate repair and support genome integrity. This figure was adapted from Einig et al. (2023).*

# 8 Conclusions

In this study, I characterize the effect of the HUWE1 ubiquitin ligase on TRCs, and DNA damage and uncover the involvement of WRNIP1, RNAPII and ATM signaling to propose a model of coordinated transcription and replication. This work enables the following conclusions:

1. HUWE1 coordinates transcription, DNA replication and TRCs via WRNIP1.
2. HUWE1 binds WRNIP1 and its ubiquitin ligase function is required for WRNIP1 association with elongation-competent RNAPII.
3. HUWE1 and WRNIP1 prevent DNA damage response signaling and promote cell proliferation. HUWE1 and WRNIP1 jointly prevent DNA double strand breaks. Inactivation of either HUWE1 or WRNIP1 leads to TRCs and preemptive DNA damage response signaling by ATM.
4. ATM recruitment to and activation at elongation-competent RNAPII depends on HUWE1 and WRNIP1.
5. Elongation-competent RNAPII associates with the MRN complex that is instrumental in ATM recruitment to sites of DNA lesions. Active RNAPII is required for induction of ATM signaling upon replication stress or HUWE1 mutation. HUWE1 and WRNIP1 limit RNAPII-dependent ATM activation.
6. HUWE1 inhibition synergizes with ATM inhibition to limit cell viability.
7. Replication stress leads to transcription-dependent TRCs and the transfer of WRNIP1 from RNAPII to the replisome. This transfer may allow RNAPII-dependent, preemptive ATM signaling at sites of collisions to stabilize TRCs prior to DNA breakage. Therefore, TRCs may play an important role to prevent severe DNA breaks, provide time for damage response signaling and recruitment of repair factors.
8. HUWE1 activity promotes tumor cell survival and proliferation, rendering it a potential cancer drug target given that its tumor suppressive functions are maintained.

# 9 References


ADELMAN, K. & LIS, J. T. 2012. Promoter-proximal pausing of RNA polymerase II: emerging roles in metazoans. *Nat Rev Genet,* 13**,** 720-31.

ADHIKARY, S., MARINONI, F., HOCK, A., HULLEMAN, E., POPOV, N., BEIER, R., BERNARD, S., QUARTO, M., CAPRA, M., GOETTIG, S., KOGEL, U., SCHEFFNER, M., HELIN, K. & EILERS, M. 2005. The ubiquitin ligase HectH9 regulates transcriptional activation by Myc and is essential for tumor cell proliferation. *Cell,* 123**,** 409-21.

AGUILERA, A. & GARCIA-MUSE, T. 2012. R loops: from transcription byproducts to threats to genome stability. *Mol Cell,* 46**,** 115-24.

ALABERT, C., BUKOWSKI-WILLS, J. C., LEE, S. B., KUSTATSCHER, G., NAKAMURA, K., DE LIMA ALVES, F., MENARD, P., MEJLVANG, J., RAPPSILBER, J. & GROTH, A. 2014. Nascent chromatin capture proteomics determines chromatin dynamics during DNA replication and identifies unknown fork components. *Nat Cell Biol,* 16**,** 281-93.

ALMEIDA, R., FERNANDEZ-JUSTEL, J. M., SANTA-MARIA, C., CADORET, J. C., CANO-AROCA, L., LOMBRANA, R., HERRANZ, G., AGRESTI, A. & GOMEZ, M. 2018. Chromatin conformation regulates the coordination between DNA replication and transcription. *Nat Commun,* 9**,** 1590.

AUBREY, B. J., STRASSER, A. & KELLY, G. L. 2016. Tumor-Suppressor Functions of the TP53 Pathway. *Cold Spring Harb Perspect Med,* 6**,** a026062.

AWASTHI, P., FOIANI, M. & KUMAR, A. 2015. ATM and ATR signaling at a glance. *J Cell Sci,* 128**,** 4255-62.

AYGUN, O., SVEJSTRUP, J. & LIU, Y. 2008. A RECQ5-RNA polymerase II association identified by targeted proteomic analysis of human chromatin. *Proc Natl Acad Sci U S A,* 105**,** 8580-4.

AZVOLINSKY, A., GIRESI, P. G., LIEB, J. D. & ZAKIAN, V. A. 2009. Highly transcribed RNA polymerase II genes are impediments to replication fork progression in Saccharomyces cerevisiae. *Mol Cell,* 34**,** 722-34.

BAKKENIST, C. J. & KASTAN, M. B. 2003. DNA damage activates ATM through intermolecular autophosphorylation and dimer dissociation. *Nature,* 421**,** 499-506.

BALMAIN, A. 2022. Peto's paradox revisited: black box vs mechanistic approaches to understanding the roles of mutations and promoting factors in cancer. *Eur J Epidemiol***,** 1-8.

BARLAAM, B., CASELLA, R., CIDADO, J., COOK, C., DE SAVI, C., DISHINGTON, A., DONALD, C. S., DREW, L., FERGUSON, A. D., FERGUSON, D., GLOSSOP, S., GREBE, T., GU, C., HANDE, S., HAWKINS, J., HIRD, A. W., HOLMES, J., HORSTICK, J., JIANG, Y., LAMB, M. L., MCGUIRE, T. M., MOORE, J. E., O'CONNELL, N., PIKE, A., PIKE, K. G., PROIA, T., ROBERTS, B., SAN MARTIN, M., SARKAR, U., SHAO, W., STEAD, D., SUMNER, N., THAKUR, K., VASBINDER, M. M., VARNES, J. G., WANG, J., WANG, L., WU, D., WU, L., YANG, B. & YAO, T. 2020. Discovery of AZD4573, a Potent and Selective Inhibitor of CDK9 That Enables Short Duration of Target Engagement for the Treatment of Hematological Malignancies. *J Med Chem,* 63**,** 15564-15590.

BARTEK, J., LUKAS, C. & LUKAS, J. 2004. Checking on DNA damage in S phase. *Nat Rev Mol Cell Biol,* 5**,** 792-804.

BÉKÉS, M., LANGLEY, D. R. & CREWS, C. M. 2022. PROTAC targeted protein degraders: the past is prologue. *Nature Reviews Drug Discovery,* 21**,** 181-200.

BENSAUDE, O. 2011. Inhibiting eukaryotic transcription. Which compound to choose? How to evaluate its activity? Which compound to choose? How to evaluate its activity? *Transcription,* 2**,** 103-108.

BERMEJO, R., LAI, M. S. & FOIANI, M. 2012. Preventing replication stress to maintain genome stability: resolving conflicts between replication and transcription. *Mol Cell,* 45**,** 710-8.

BERTI, M., CORTEZ, D. & LOPES, M. 2020. The plasticity of DNA replication forks in response to clinically relevant genotoxic stress. *Nat Rev Mol Cell Biol,* 21**,** 633-651.

BLACKFORD, A. N. & JACKSON, S. P. 2017. ATM, ATR, and DNA-PK: The Trinity at the Heart of the DNA Damage Response. *Mol Cell,* 66**,** 801-817.

BLACKFORD, A. N., SCHWAB, R. A., NIEMINUSZCZY, J., DEANS, A. J., WEST, S. C. & NIEDZWIEDZ, W. 2012. The DNA translocase activity of FANCM protects stalled replication forks. *Hum Mol Genet,* 21**,** 2005-16.

BLIN, M., LE TALLEC, B., NAHSE, V., SCHMIDT, M., BROSSAS, C., MILLOT, G. A., PRIOLEAU, M. N. & DEBATISSE, M. 2019. Transcription-dependent regulation of replication dynamics modulates genome stability. *Nat Struct Mol Biol,* 26**,** 58-66.

BONDARENKO, V. A., STEELE, L. M., UJVARI, A., GAYKALOVA, D. A., KULAEVA, O. I., POLIKANOV, Y. S., LUSE, D. S. & STUDITSKY, V. M. 2006. Nucleosomes can form a polar barrier to transcript elongation by RNA polymerase II. *Mol Cell,* 24**,** 469-79.

BOURDAIS, R., ROUSSEAU, B., PUJALS, A., BOUSSION, H., JOLY, C., GUILLEMIN, A., BAUMGAERTNER, I., NEUZILLET, C. & TOURNIGAND, C. 2017. Polymerase proofreading domain mutations: New opportunities for immunotherapy in hypermutated colorectal cancer beyond MMR deficiency. *Crit Rev Oncol Hematol,* 113**,** 242-248.

BOUTET-ROBINET, E., TROUCHE, D. & CANITROT, Y. 2013. Neutral comet assay. *Bio-protocol,* 3**,** e915-e915.

BRISON, O., EL-HILALI, S., AZAR, D., KOUNDRIOUKOFF, S., SCHMIDT, M., NAHSE, V., JASZCZYSZYN, Y., LACHAGES, A. M., DUTRILLAUX, B., THERMES, C., DEBATISSE, M. & CHEN, C. L. 2019. Transcription-mediated organization of the replication initiation program across large genes sets common fragile sites genome-wide. *Nat Commun,* 10**,** 5693.

BUISSON, R., BOISVERT, J. L., BENES, C. H. & ZOU, L. 2015. Distinct but Concerted Roles of ATR, DNA-PK, and Chk1 in Countering Replication Stress during S Phase. *Mol Cell,* 59**,** 1011-24.

BURGERS, P. M. J. & KUNKEL, T. A. 2017. Eukaryotic DNA Replication Fork. *Annu Rev Biochem,* 86**,** 417-438.

CAHILL, D. P., KINZLER, K. W., VOGELSTEIN, B. & LENGAUER, C. 1999. Genetic instability and darwinian selection in tumours. *Trends Cell Biol,* 9**,** M57-60.

CHAKRABORTY, A., TAPRYAL, N., VENKOVA, T., HORIKOSHI, N., PANDITA, R. K., SARKER, A. H., SARKAR, P. S., PANDITA, T. K. & HAZRA, T. K. 2016. Classical non-homologous end-joining pathway utilizes nascent RNA for error-free double-strand break repair of transcribed genes. *Nat Commun,* 7**,** 13049.

CHAKRABORTY, P. & HIOM, K. 2021. DHX9-dependent recruitment of BRCA1 to RNA promotes DNA end resection in homologous recombination. *Nat Commun,* 12**,** 4126.

CHEN, D., KON, N., LI, M., ZHANG, W., QIN, J. & GU, W. 2005. ARF-BP1/Mule is a critical mediator of the ARF tumor suppressor. *Cell,* 121**,** 1071-83.

CHEN, Y. H., KEEGAN, S., KAHLI, M., TONZI, P., FENYO, D., HUANG, T. T. & SMITH, D. J. 2019. Transcription shapes DNA replication initiation and termination in human cells. *Nat Struct Mol Biol,* 26**,** 67-77.

CHENG, B. & PRICE, D. H. 2007. Properties of RNA polymerase II elongation complexes before and after the P-TEFb-mediated transition into productive elongation. *J Biol Chem,* 282**,** 21901-12.

CHEUNG, A. C. & CRAMER, P. 2011. Structural basis of RNA polymerase II backtracking, arrest and reactivation. *Nature,* 471**,** 249-53.

CHILKOVA, O., STENLUND, P., ISOZ, I., STITH, C. M., GRABOWSKI, P., LUNDSTROM, E. B., BURGERS, P. M. & JOHANSSON, E. 2007. The eukaryotic leading and lagging strand DNA polymerases are loaded onto primer-ends via separate mechanisms but have comparable processivity in the presence of PCNA. *Nucleic Acids Res,* 35**,** 6588-97.

CHIPUMURO, E., MARCO, E., CHRISTENSEN, C. L., KWIATKOWSKI, N., ZHANG, T., HATHEWAY, C. M., ABRAHAM, B. J., SHARMA, B., YEUNG, C., ALTABEF, A., PEREZ-ATAYDE, A., WONG, K. K., YUAN, G. C., GRAY, N. S., YOUNG, R. A. &

GEORGE, R. E. 2014. CDK7 inhibition suppresses super-enhancer-linked oncogenic transcription in MYCN-driven cancer. *Cell,* 159**,** 1126-1139.

CHO, E. J., KOBOR, M. S., KIM, M., GREENBLATT, J. & BURATOWSKI, S. 2001. Opposing effects of Ctk1 kinase and Fcp1 phosphatase at Ser 2 of the RNA polymerase II C-terminal domain. *Genes Dev,* 15**,** 3319-29.

CHOE, K. N., NICOLAE, C. M., CONSTANTIN, D., IMAMURA KAWASAWA, Y., DELGADO-DIAZ, M. R., DE, S., FREIRE, R., SMITS, V. A. & MOLDOVAN, G. L. 2016. HUWE1 interacts with PCNA to alleviate replication stress. *EMBO Rep,* 17**,** 874-86.

CLAY, S. L., FONSECA-PEREIRA, D. & GARRETT, W. S. 2022. Colorectal cancer: the facts in the case of the microbiota. *J Clin Invest,* 132**,** e155101.

COMPE, E. & EGLY, J.-M. 2012. TFIIH: when transcription met DNA repair. *Nature reviews Molecular cell biology,* 13**,** 343-354.

CONTI, B. A. & SMOGORZEWSKA, A. 2020. Mechanisms of direct replication restart at stressed replisomes. *DNA Repair (Amst),* 95**,** 102947.

COSTANZO, V., SHECHTER, D., LUPARDUS, P. J., CIMPRICH, K. A., GOTTESMAN, M. & GAUTIER, J. 2003. An ATR- and Cdc7-dependent DNA damage checkpoint that inhibits initiation of DNA replication. *Mol Cell,* 11**,** 203-13.

COUCH, F. B., BANSBACH, C. E., DRISCOLL, R., LUZWICK, J. W., GLICK, G. G., BETOUS, R., CARROLL, C. M., JUNG, S. Y., QIN, J., CIMPRICH, K. A. & CORTEZ, D. 2013. ATR phosphorylates SMARCAL1 to prevent replication fork collapse. *Genes Dev,* 27**,** 1610-23.

COX, J., NEUHAUSER, N., MICHALSKI, A., SCHELTEMA, R. A., OLSEN, J. V. & MANN, M. 2011. Andromeda: a peptide search engine integrated into the MaxQuant environment. *J Proteome Res,* 10**,** 1794-805.

CRAMER, P., BUSHNELL, D. A. & KORNBERG, R. D. 2001. Structural basis of transcription: RNA polymerase II at 2.8 angstrom resolution. *Science,* 292**,** 1863-76.

CRAWFORD, L. J., CAMPBELL, D. C., MORGAN, J. J., LAWSON, M. A., DOWN, J. M., CHAUHAN, D., MCAVERA, R. M., MORRIS, T. C., HAMILTON, C., KRISHNAN, A., RAJALINGAM, K., CHANTRY, A. D. & IRVINE, A. E. 2020. The E3 ligase HUWE1 inhibition as a therapeutic strategy to target MYC in multiple myeloma. *Oncogene,* 39**,** 5001-5014.

CROSETTO, N., BIENKO, M., HIBBERT, R. G., PERICA, T., AMBROGIO, C., KENSCHE, T., HOFMANN, K., SIXMA, T. K. & DIKIC, I. 2008. Human Wrnip1 is localized in replication factories in a ubiquitin-binding zinc finger-dependent manner. *J Biol Chem,* 283**,** 35173-85.

CROSSLEY, M. P., BOCEK, M. & CIMPRICH, K. A. 2019. R-Loops as Cellular Regulators and Genomic Threats. *Mol Cell,* 73**,** 398-411.

CUADRADO, M., MARTINEZ-PASTOR, B., MURGA, M., TOLEDO, L. I., GUTIERREZ-MARTINEZ, P., LOPEZ, E. & FERNANDEZ-CAPETILLO, O. 2006. ATM regulates ATR chromatin loading in response to DNA double-strand breaks. *J Exp Med,* 203**,** 297-303.

CYBULLA, E. & VINDIGNI, A. 2023. Leveraging the replication stress response to optimize cancer therapy. *Nat Rev Cancer,* 23**,** 6-24.

DAMSMA, G. E. & CRAMER, P. 2009. Molecular basis of transcriptional mutagenesis at 8-oxoguanine. *J Biol Chem,* 284**,** 31658-63.

DARWIN, C. 1859. On the origin of species by means of natural selection, or the preservation of favoured races in the struggle for life. *London: John Murray*.

DAVIDSON, L., MUNIZ, L. & WEST, S. 2014. 3' end formation of pre-mRNA and phosphorylation of Ser2 on the RNA polymerase II CTD are reciprocally coupled in human cells. *Genes Dev,* 28**,** 342-56.

DESCOSTES, N., HEIDEMANN, M., SPINELLI, L., SCHULLER, R., MAQBOOL, M. A., FENOUIL, R., KOCH, F., INNOCENTI, C., GUT, M., GUT, I., EICK, D. & ANDRAU, J. C. 2014. Tyrosine phosphorylation of RNA polymerase II CTD is associated with antisense promoter transcription and active enhancers in mammalian cells. *Elife,* 3**,** e02105.

DOBIN, A., DAVIS, C. A., SCHLESINGER, F., DRENKOW, J., ZALESKI, C., JHA, S., BATUT, P., CHAISSON, M. & GINGERAS, T. R. 2013. STAR: ultrafast universal RNA-seq aligner. *Bioinformatics,* 29**,** 15-21.

DOMINGUEZ-BRAUER, C., KHATUN, R., ELIA, A. J., THU, K. L., RAMACHANDRAN, P., BANIASADI, S. P., HAO, Z., JONES, L. D., HAIGHT, J., SHENG, Y. & MAK, T. W. 2017. E3 ubiquitin ligase Mule targets beta-catenin under conditions of hyperactive Wnt signaling. *Proc Natl Acad Sci U S A,* 114**,** E1148-E1157.

DUAN, S. & PAGANO, M. 2021. Ubiquitin ligases in cancer: Functions and clinical potentials. *Cell Chem Biol,* 28**,** 918-933.

DUFFY, M. J., O'GRADY, S., TANG, M. & CROWN, J. 2021. MYC as a target for cancer treatment. *Cancer Treat Rev,* 94**,** 102154.

EATON, J. D. & WEST, S. 2020. Termination of Transcription by RNA Polymerase II: BOOM! *Trends Genet,* 36**,** 664-675.

EDGAR, R., DOMRACHEV, M. & LASH, A. E. 2002. Gene Expression Omnibus: NCBI gene expression and hybridization array data repository. *Nucleic Acids Res,* 30**,** 207-10.

EGLOFF, S. 2021. CDK9 keeps RNA polymerase II on track. *Cell Mol Life Sci,* 78**,** 5543-5567.

EICK, D. & GEYER, M. 2013. The RNA polymerase II carboxy-terminal domain (CTD) code. *Chem Rev,* 113**,** 8456-90.

EINIG, E., JIN, C., ANDRIOLETTI, V., MACEK, B. & POPOV, N. 2023. RNAPII-dependent ATM signaling at collisions with replication forks. *Nature Communications*.

ELIAS, J. E. & GYGI, S. P. 2007. Target-decoy search strategy for increased confidence in large-scale protein identifications by mass spectrometry. *Nat Methods,* 4**,** 207-14.

ENDRES, T., SOLVIE, D., HEIDELBERGER, J. B., ANDRIOLETTI, V., BALUAPURI, A., ADE, C. P., MUHAR, M., EILERS, U., VOS, S. M., CRAMER, P., ZUBER, J., BELI, P., POPOV, N., WOLF, E., GALLANT, P. & EILERS, M. 2021. Ubiquitylation of MYC couples transcription elongation with double-strand break repair at active promoters. *Mol Cell,* 81**,** 830-844 e13.

FORGO, E., GOMEZ, A. J., STEINER, D., ZEHNDER, J. & LONGACRE, T. A. 2020. Morphological, immunophenotypical and molecular features of hypermutation in colorectal carcinomas with mutations in DNA polymerase epsilon (POLE). *Histopathology,* 76**,** 366-374.

FRANCETTE, A. M., TRIPPLEHORN, S. A. & ARNDT, K. M. 2021. The Paf1 Complex: A Keystone of Nuclear Regulation Operating at the Interface of Transcription and Chromatin. *J Mol Biol,* 433**,** 166979.

FRANCO, I. & ERIKSSON, M. 2022. Reverting to old theories of ageing with new evidence for the role of somatic mutations. *Nat Rev Genet,* 23**,** 645-646.

GAGOU, M. E., ZUAZUA-VILLAR, P. & MEUTH, M. 2010. Enhanced H2AX phosphorylation, DNA replication fork arrest, and cell death in the absence of Chk1. *Mol Biol Cell,* 21**,** 739-52.

GAILLARD, H., GARCIA-MUSE, T. & AGUILERA, A. 2015. Replication stress and cancer. *Nat Rev Cancer,* 15**,** 276-89.

GAMPER, A. M., CHOI, S., MATSUMOTO, Y., BANERJEE, D., TOMKINSON, A. E. & BAKKENIST, C. J. 2012. ATM protein physically and functionally interacts with proliferating cell nuclear antigen to regulate DNA synthesis. *J Biol Chem,* 287**,** 12445-54.

GARCIA-MUSE, T. & AGUILERA, A. 2019. R Loops: From Physiological to Pathological Roles. *Cell,* 179**,** 604-618.

GARCÍA-MUSE, T. & AGUILERA, A. 2016. Transcription–replication conflicts: how they occur and how they are resolved. *Nature reviews Molecular cell biology,* 17**,** 553.

GERBER, J. K., GOGEL, E., BERGER, C., WALLISCH, M., MULLER, F., GRUMMT, I. & GRUMMT, F. 1997. Termination of mammalian rDNA replication: polar arrest of replication fork movement by transcription termination factor TTF-I. *Cell,* 90**,** 559-67.

GIMPLE, R. C. & WANG, X. 2019. RAS: Striking at the Core of the Oncogenic Circuitry. *Front Oncol,* 9**,** 965.

GONG, X., DU, D., DENG, Y., ZHOU, Y., SUN, L. & YUAN, S. 2020. The structure and regulation of the E3 ubiquitin ligase HUWE1 and its biological functions in cancer. *Invest New Drugs,* 38**,** 515-524.

GONZALEZ-MAGANA, A. & BLANCO, F. J. 2020. Human PCNA Structure, Function and Interactions. *Biomolecules,* 10**,** 570.

GRAHAM, T. G., WALTER, J. C. & LOPARO, J. J. 2016. Two-Stage Synapsis of DNA Ends during Non-homologous End Joining. *Mol Cell,* 61**,** 850-8.

GROELLY, F. J., FAWKES, M., DAGG, R. A., BLACKFORD, A. N. & TARSOUNAS, M. 2023. Targeting DNA damage response pathways in cancer. *Nat Rev Cancer,* 23**,** 78-94.

GRUBER, J. J., CHEN, J., GELLER, B., JAGER, N., LIPCHIK, A. M., WANG, G., KURIAN, A. W., FORD, J. M. & SNYDER, M. P. 2019. Chromatin Remodeling in Response to BRCA2-Crisis. *Cell Rep,* 28**,** 2182-2193 e6.

GUHA, S. & BHAUMIK, S. R. 2022. Transcription-coupled DNA double-strand break repair. *DNA Repair (Amst),* 109**,** 103211.

GUINNEY, J., DIENSTMANN, R., WANG, X., DE REYNIES, A., SCHLICKER, A., SONESON, C., MARISA, L., ROEPMAN, P., NYAMUNDANDA, G., ANGELINO, P., BOT, B. M., MORRIS, J. S., SIMON, I. M., GERSTER, S., FESSLER, E., DE SOUSA, E. M. F., MISSIAGLIA, E., RAMAY, H., BARRAS, D., HOMICSKO, K., MARU, D., MANYAM, G. C., BROOM, B., BOIGE, V., PEREZ-VILLAMIL, B., LADERAS, T., SALAZAR, R., GRAY, J. W., HANAHAN, D., TABERNERO, J., BERNARDS, R., FRIEND, S. H., LAURENT-PUIG, P., MEDEMA, J. P., SADANANDAM, A., WESSELS, L., DELORENZI, M., KOPETZ, S., VERMEULEN, L. & TEJPAR, S. 2015. The consensus molecular subtypes of colorectal cancer. *Nat Med,* 21**,** 1350-6.

GYORI, B. M., VENKATACHALAM, G., THIAGARAJAN, P. S., HSU, D. & CLEMENT, M. V. 2014. OpenComet: an automated tool for comet assay image analysis. *Redox Biol,* 2**,** 457-65.

HAFFNER, M. C., ARYEE, M. J., TOUBAJI, A., ESOPI, D. M., ALBADINE, R., GUREL, B., ISAACS, W. B., BOVA, G. S., LIU, W., XU, J., MEEKER, A. K., NETTO, G., DE MARZO, A. M., NELSON, W. G. & YEGNASUBRAMANIAN, S. 2010. Androgen-induced TOP2B-mediated double-strand breaks and prostate cancer gene rearrangements. *Nat Genet,* 42**,** 668-75.

HAMPERL, S., BOCEK, M. J., SALDIVAR, J. C., SWIGUT, T. & CIMPRICH, K. A. 2017. Transcription-Replication Conflict Orientation Modulates R-Loop Levels and Activates Distinct DNA Damage Responses. *Cell,* 170**,** 774-786 e19.

HAMPERL, S. & CIMPRICH, K. A. 2016. Conflict Resolution in the Genome: How Transcription and Replication Make It Work. *Cell,* 167**,** 1455-1467.

HANAHAN, D. 2022. Hallmarks of Cancer: New Dimensions. *Cancer Discov,* 12**,** 31-46.

HANAHAN, D. & WEINBERG, R. A. 2000. The hallmarks of cancer. *Cell,* 100**,** 57-70.

HANAHAN, D. & WEINBERG, R. A. 2011. Hallmarks of cancer: the next generation. *Cell,* 144**,** 646-74.

HANAWALT, P. C. & SPIVAK, G. 2008. Transcription-coupled DNA repair: two decades of progress and surprises. *Nat Rev Mol Cell Biol,* 9**,** 958-70.

HANTSCHEL, O. & SUPERTI-FURGA, G. 2004. Regulation of the c-Abl and Bcr-Abl tyrosine kinases. *Nat Rev Mol Cell Biol,* 5**,** 33-44.

HE, Q. L., TITOV, D. V., LI, J., TAN, M., YE, Z., ZHAO, Y., ROMO, D. & LIU, J. O. 2015. Covalent modification of a cysteine residue in the XPB subunit of the general transcription factor TFIIH through single epoxide cleavage of the transcription inhibitor triptolide. *Angew Chem Int Ed Engl,* 54**,** 1859-63.

HE, Y., ZHOU, J. & WAN, Q. 2021. The E3 ligase HUWE1 mediates TGFBR2 ubiquitination and promotes gastric cancer cell proliferation, migration, and invasion. *Invest New Drugs,* 39**,** 713-723.

HEIDEMANN, M., HINTERMAIR, C., VOSS, K. & EICK, D. 2013. Dynamic phosphorylation patterns of RNA polymerase II CTD during transcription. *Biochim Biophys Acta,* 1829**,** 55-62.

HELLER, R. C., KANG, S., LAM, W. M., CHEN, S., CHAN, C. S. & BELL, S. P. 2011. Eukaryotic origin-dependent DNA replication in vitro reveals sequential action of DDK and S-CDK kinases. *Cell,* 146**,** 80-91.

HISHIDA, T., OHYA, T., KUBOTA, Y., KAMADA, Y. & SHINAGAWA, H. 2006. Functional and physical interaction of yeast Mgs1 with PCNA: impact on RAD6-dependent DNA damage tolerance. *Mol Cell Biol,* 26**,** 5509-17.

HOELLER, D. & DIKIC, I. 2009. Targeting the ubiquitin system in cancer therapy. *Nature,* 458**,** 438-44.

HUANG, C. H., LUJAMBIO, A., ZUBER, J., TSCHAHARGANEH, D. F., DORAN, M. G., EVANS, M. J., KITZING, T., ZHU, N., DE STANCHINA, E., SAWYERS, C. L., ARMSTRONG, S. A., LEWIS, J. S., SHERR, C. J. & LOWE, S. W. 2014. CDK9-mediated transcription elongation is required for MYC addiction in hepatocellular carcinoma. *Genes Dev,* 28**,** 1800-14.

HUNKELER, M., JIN, C. Y., MA, M. W., MONDA, J. K., OVERWIJN, D., BENNETT, E. J. & FISCHER, E. S. 2021. Solenoid architecture of HUWE1 contributes to ligase activity and substrate recognition. *Mol Cell,* 81**,** 3468-3480 e7.

HUSTEDT, N. & DUROCHER, D. 2016. The control of DNA repair by the cell cycle. *Nat Cell Biol,* 19**,** 1-9.

IANEVSKI, A., GIRI, A. K. & AITTOKALLIO, T. 2020. SynergyFinder 2.0: visual analytics of multi-drug combination synergies. *Nucleic Acids Res,* 48**,** W488-W493.

JÄCKL, M., STOLLMAIER, C., STROHÄKER, T., HYZ, K., MASPERO, E., POLO, S. & WIESNER, S. 2018. β-Sheet augmentation is a conserved mechanism of priming HECT E3 ligases for ubiquitin ligation. *Journal of molecular biology,* 430**,** 3218-3233.

JACKSON, D. A. & POMBO, A. 1998. Replicon clusters are stable units of chromosome structure: evidence that nuclear organization contributes to the efficient activation and propagation of S phase in human cells. *J Cell Biol,* 140**,** 1285-95.

JACKSON, S. P. & BARTEK, J. 2009. The DNA-damage response in human biology and disease. *Nature,* 461**,** 1071-8.

JIMÉNEZ-MARTÍN, A., SAUGAR, I., JOSEPH, C. R., MAYER, A., LEHMANN, C. P., SZAKAL, B., BRANZEI, D. & TERCERO, J. A. 2020. The Mgs1/WRNIP1 ATPase is required to prevent a recombination salvage pathway at damaged replication forks. *Science Advances,* 6**,** eaaz3327.

JOUNG, J., KONERMANN, S., GOOTENBERG, J. S., ABUDAYYEH, O. O., PLATT, R. J., BRIGHAM, M. D., SANJANA, N. E. & ZHANG, F. 2017. Genome-scale CRISPR-Cas9 knockout and transcriptional activation screening. *Nat Protoc,* 12**,** 828-863.

KANU, N., ZHANG, T., BURRELL, R. A., CHAKRABORTY, A., CRONSHAW, J., DACOSTA, C., GRÖNROOS, E., PEMBERTON, H. N., ANDERTON, E. & GONZALEZ, L. 2016. RAD18, WRNIP1 and ATMIN promote ATM signalling in response to replication stress. *Oncogene,* 35**,** 4009-4019.

KAO, S. H., WU, H. T. & WU, K. J. 2018. Ubiquitination by HUWE1 in tumorigenesis and beyond. *J Biomed Sci,* 25**,** 67.

KEMIHA, S., POLI, J., LIN, Y. L., LENGRONNE, A. & PASERO, P. 2021. Toxic R-loops: Cause or consequence of replication stress? *DNA Repair (Amst),* 107**,** 103199.

KEMPEN, R. P., DABAS, P. & ANSARI, A. Z. 2023. The Phantom Mark: Enigmatic roles of phospho-Threonine 4 modification of the C-terminal domain of RNA polymerase II. *Wiley Interdiscip Rev RNA***,** e1771.

KESKIN, H., SHEN, Y., HUANG, F., PATEL, M., YANG, T., ASHLEY, K., MAZIN, A. V. & STORICI, F. 2014. Transcript-RNA-templated DNA recombination and repair. *Nature,* 515**,** 436-9.

KOMANDER, D., CLAGUE, M. J. & URBE, S. 2009. Breaking the chains: structure and function of the deubiquitinases. *Nat Rev Mol Cell Biol,* 10**,** 550-63.

KOMANDER, D. & RAPE, M. 2012. The ubiquitin code. *Annu Rev Biochem,* 81**,** 203-29.

KOMARNITSKY, P., CHO, E. J. & BURATOWSKI, S. 2000. Different phosphorylated forms of RNA polymerase II and associated mRNA processing factors during transcription. *Genes Dev,* 14**,** 2452-60.

KONTOMANOLIS, E. N., KOUTRAS, A., SYLLAIOS, A., SCHIZAS, D., MASTORAKI, A., GARMPIS, N., DIAKOSAVVAS, M., ANGELOU, K., TSATSARIS, G., PAGKALOS, A., NTOUNIS, T. & FASOULAKIS, Z. 2020. Role of Oncogenes and Tumor-suppressor Genes in Carcinogenesis: A Review. *Anticancer Res,* 40**,** 6009-6015.

KOTSANTIS, P., PETERMANN, E. & BOULTON, S. J. 2018. Mechanisms of Oncogene-Induced Replication Stress: Jigsaw Falling into Place. *Cancer Discov,* 8**,** 537-555.

KOTSANTIS, P., SILVA, L. M., IRMSCHER, S., JONES, R. M., FOLKES, L., GROMAK, N. & PETERMANN, E. 2016. Increased global transcription activity as a mechanism of replication stress in cancer. *Nat Commun,* 7**,** 13087.

KUNZ, V., BOMMERT, K. S., KRUK, J., SCHWINNING, D., CHATTERJEE, M., STUHMER, T., BARGOU, R. & BOMMERT, K. 2020. Targeting of the E3 ubiquitin-protein ligase HUWE1 impairs DNA repair capacity and tumor growth in preclinical multiple myeloma models. *Sci Rep,* 10**,** 18419.

LALONDE, M., TRAUNER, M., WERNER, M. & HAMPERL, S. 2021. Consequences and Resolution of Transcription-Replication Conflicts. *Life (Basel),* 11**,** 637.

LANS, H., HOEIJMAKERS, J. H. J., VERMEULEN, W. & MARTEIJN, J. A. 2019. The DNA damage response to transcription stress. *Nat Rev Mol Cell Biol,* 20**,** 766-784.

LAUKIEN, F. H. 2021. The evolution of evolutionary processes in organismal and cancer evolution. *Prog Biophys Mol Biol,* 165**,** 43-48.

LEE, J.-H. & PAULL, T. T. 2005. ATM activation by DNA double-strand breaks through the Mre11-Rad50-Nbs1 complex. *Science,* 308**,** 551-554.

LEE, J. S. & MENDELL, J. T. 2020. Antisense-Mediated Transcript Knockdown Triggers Premature Transcription Termination. *Mol Cell,* 77**,** 1044-1054 e3.

LENSING, S. V., MARSICO, G., HANSEL-HERTSCH, R., LAM, E. Y., TANNAHILL, D. & BALASUBRAMANIAN, S. 2016. DSBCapture: in situ capture and sequencing of DNA breaks. *Nat Methods,* 13**,** 855-7.

LEROY, G., OKSUZ, O., DESCOSTES, N., AOI, Y., GANAI, R. A., KARA, H. O., YU, J. R., LEE, C. H., STAFFORD, J., SHILATIFARD, A. & REINBERG, D. 2019. LEDGF and HDGF2 relieve the nucleosome-induced barrier to transcription in differentiated cells. *Sci Adv,* 5**,** eaay3068.

LEUZZI, G., MARABITTI, V., PICHIERRI, P. & FRANCHITTO, A. 2016. WRNIP 1 protects stalled forks from degradation and promotes fork restart after replication stress. *The EMBO journal,* 35**,** 1437-1451.

LI, W., XU, H., XIAO, T., CONG, L., LOVE, M. I., ZHANG, F., IRIZARRY, R. A., LIU, J. S., BROWN, M. & LIU, X. S. 2014. MAGeCK enables robust identification of essential genes from genome-scale CRISPR/Cas9 knockout screens. *Genome Biol,* 15**,** 554.

LI, Z., LI, Y., TANG, M., PENG, B., LU, X., YANG, Q., ZHU, Q., HOU, T., LI, M. & LIU, C. 2018. Destabilization of linker histone H1. 2 is essential for ATM activation and DNA damage repair. *Cell research,* 28**,** 756-770.

LING, S., HU, Z., YANG, Z., YANG, F., LI, Y., LIN, P., CHEN, K., DONG, L., CAO, L., TAO, Y., HAO, L., CHEN, Q., GONG, Q., WU, D., LI, W., ZHAO, W., TIAN, X., HAO, C., HUNGATE, E. A., CATENACCI, D. V., HUDSON, R. R., LI, W. H., LU, X. & WU, C. I. 2015. Extremely high genetic diversity in a single tumor points to prevalence of non-Darwinian cell evolution. *Proc Natl Acad Sci U S A,* 112**,** E6496-505.

LIU, R., KING, A., HOCH, N. C., CHANG, C., KELLY, G. L., DEANS, A. J. & HEIERHORST, J. 2017. ASCIZ/ATMIN is dispensable for ATM signaling in response to replication stress. *DNA Repair (Amst),* 57**,** 29-34.

LIU, S., OPIYO, S. O., MANTHEY, K., GLANZER, J. G., ASHLEY, A. K., AMERIN, C., TROKSA, K., SHRIVASTAV, M., NICKOLOFF, J. A. & OAKLEY, G. G. 2012. Distinct roles for DNA-PK, ATM and ATR in RPA phosphorylation and checkpoint activation in response to replication stress. *Nucleic Acids Res,* 40**,** 10780-94.

LIU, Y., AI, C., GAN, T., WU, J., JIANG, Y., LIU, X., LU, R., GAO, N., LI, Q., JI, X. & HU, J. 2021. Transcription shapes DNA replication initiation to preserve genome integrity. *Genome Biol,* 22**,** 176.

LOMONOSOV, M., ANAND, S., SANGRITHI, M., DAVIES, R. & VENKITARAMAN, A. R. 2003. Stabilization of stalled DNA replication forks by the BRCA2 breast cancer susceptibility protein. *Genes Dev,* 17**,** 3017-22.

LONGO, P. A., KAVRAN, J. M., KIM, M.-S. & LEAHY, D. J. 2013. Transient mammalian cell transfection with polyethylenimine (PEI). *Methods in enzymology.* Elsevier.

LOPEZ-CONTRERAS, A. J., SPECKS, J., BARLOW, J. H., AMBROGIO, C., DESLER, C., VIKINGSSON, S., RODRIGO-PEREZ, S., GREEN, H., RASMUSSEN, L. J., MURGA, M., NUSSENZWEIG, A. & FERNANDEZ-CAPETILLO, O. 2015. Increased Rrm2 gene dosage reduces fragile site breakage and prolongs survival of ATR mutant mice. *Genes Dev,* 29**,** 690-5.

LU, H., SAHA, J., BECKMANN, P. J., HENDRICKSON, E. A. & DAVIS, A. J. 2019. DNA-PKcs promotes chromatin decondensation to facilitate initiation of the DNA damage response. *Nucleic Acids Res,* 47**,** 9467-9479.

LYONS, D. E., MCMAHON, S. & OTT, M. 2020. A combinatorial view of old and new RNA polymerase II modifications. *Transcription,* 11**,** 66-82.

MA, J. & WANG, M. D. 2016. DNA supercoiling during transcription. *Biophys Rev,* 8**,** 75-87.

MACHERET, M. & HALAZONETIS, T. D. 2018. Intragenic origins due to short G1 phases underlie oncogene-induced DNA replication stress. *Nature,* 555**,** 112-116.

MADAAN, K., KAUSHIK, D. & VERMA, T. 2012. Hydroxyurea: a key player in cancer chemotherapy. *Expert Rev Anticancer Ther,* 12**,** 19-29.

MANASANCH, E. E. & ORLOWSKI, R. Z. 2017. Proteasome inhibitors in cancer therapy. *Nat Rev Clin Oncol,* 14**,** 417-433.

MANDEMAKER, I. K., VAN CUIJK, L., JANSSENS, R. C., LANS, H., BEZSTAROSTI, K., HOEIJMAKERS, J. H., DEMMERS, J. A., VERMEULEN, W. & MARTEIJN, J. A. 2017. DNA damage-induced histone H1 ubiquitylation is mediated by HUWE1 and stimulates the RNF8-RNF168 pathway. *Sci Rep,* 7**,** 15353.

MANSOUR, M. A. 2018. Ubiquitination: Friend and foe in cancer. *Int J Biochem Cell Biol,* 101**,** 80-93.

MARCHAL, C., SIMA, J. & GILBERT, D. M. 2019. Control of DNA replication timing in the 3D genome. *Nat Rev Mol Cell Biol,* 20**,** 721-737.

MARECHAL, A. & ZOU, L. 2013. DNA damage sensing by the ATM and ATR kinases. *Cold Spring Harb Perspect Biol,* 5**,** a012716.

MARK, K. G. & RAPE, M. 2021. Ubiquitin-dependent regulation of transcription in development and disease. *EMBO Rep,* 22**,** e51078.

MARMOL, I., SANCHEZ-DE-DIEGO, C., PRADILLA DIESTE, A., CERRADA, E. & RODRIGUEZ YOLDI, M. J. 2017. Colorectal Carcinoma: A General Overview and Future Perspectives in Colorectal Cancer. *Int J Mol Sci,* 18**,** 197.

MARTIN, R. D., HEBERT, T. E. & TANNY, J. C. 2020. Therapeutic Targeting of the General RNA Polymerase II Transcription Machinery. *Int J Mol Sci,* 21**,** 3354.

MARTINCORENA, I., ROSHAN, A., GERSTUNG, M., ELLIS, P., VAN LOO, P., MCLAREN, S., WEDGE, D. C., FULLAM, A., ALEXANDROV, L. B., TUBIO, J. M., STEBBINGS, L., MENZIES, A., WIDAA, S., STRATTON, M. R., JONES, P. H. & CAMPBELL, P. J. 2015. Tumor evolution. High burden and pervasive positive selection of somatic mutations in normal human skin. *Science,* 348**,** 880-6.

MARTINEZ-JIMENEZ, F., MUINOS, F., SENTIS, I., DEU-PONS, J., REYES-SALAZAR, I., ARNEDO-PAC, C., MULARONI, L., PICH, O., BONET, J., KRANAS, H., GONZALEZ-PEREZ, A. & LOPEZ-BIGAS, N. 2020. A compendium of mutational cancer driver genes. *Nat Rev Cancer,* 20**,** 555-572.

MASUDA, Y. & MASUTANI, C. 2019. Spatiotemporal regulation of PCNA ubiquitination in damage tolerance pathways. *Crit Rev Biochem Mol Biol,* 54**,** 418-442.

MAZOUZI, A., VELIMEZI, G. & LOIZOU, J. I. 2014. DNA replication stress: causes, resolution and disease. *Exp Cell Res,* 329**,** 85-93.

MEERS, M. P., BRYSON, T. D., HENIKOFF, J. G. & HENIKOFF, S. 2019. Improved CUT&RUN chromatin profiling tools. *Elife,* 8.

MENDEZ, R. & BANERJEE, S. 2017. Proximal Ligation Assay (PLA) on Lung Tissue and Cultured Macrophages to Demonstrate Protein-protein Interaction. *Bio Protoc,* 7.

MERYET-FIGUIERE, M., ALAEI-MAHABADI, B., ALI, M. M., MITRA, S., SUBHASH, S., PANDEY, G. K., LARSSON, E. & KANDURI, C. 2014. Temporal separation of replication and transcription during S-phase progression. *Cell Cycle,* 13**,** 3241-8.

MICHELINI, F., PITCHIAYA, S., VITELLI, V., SHARMA, S., GIOIA, U., PESSINA, F., CABRINI, M., WANG, Y., CAPOZZO, I., IANNELLI, F., MATTI, V., FRANCIA, S., SHIVASHANKAR, G. V., WALTER, N. G. & D'ADDA DI FAGAGNA, F. 2017. Damage-induced lncRNAs control the DNA damage response through interaction with DDRNAs at individual double-strand breaks. *Nat Cell Biol,* 19**,** 1400-1411.

MURGA, M., CAMPANER, S., LOPEZ-CONTRERAS, A. J., TOLEDO, L. I., SORIA, R., MONTANA, M. F., ARTISTA, L., SCHLEKER, T., GUERRA, C., GARCIA, E., BARBACID, M., HIDALGO, M., AMATI, B. & FERNANDEZ-CAPETILLO, O. 2011. Exploiting oncogene-induced replicative stress for the selective killing of Myc-driven tumors. *Nat Struct Mol Biol,* 18**,** 1331-1335.

MYANT, K. B., CAMMARERI, P., HODDER, M. C., WILLS, J., VON KRIEGSHEIM, A., GYORFFY, B., RASHID, M., POLO, S., MASPERO, E., VAUGHAN, L., GURUNG, B., BARRY, E., MALLIRI, A., CAMARGO, F., ADAMS, D. J., IAVARONE, A., LASORELLA, A. & SANSOM, O. J. 2017. HUWE1 is a critical colonic tumour suppressor gene that prevents MYC signalling, DNA damage accumulation and tumour initiation. *EMBO Mol Med,* 9**,** 181-197.

NIEMINUSZCZY, J., SCHWAB, R. A. & NIEDZWIEDZ, W. 2016. The DNA fibre technique - tracking helicases at work. *Methods,* 108**,** 92-8.

OLCINA, M. M., FOSKOLOU, I. P., ANBALAGAN, S., SENRA, J. M., PIRES, I. M., JIANG, Y., RYAN, A. J. & HAMMOND, E. M. 2013. Replication stress and chromatin context link ATM activation to a role in DNA replication. *Mol Cell,* 52**,** 758-66.

OSMAN, S. & CRAMER, P. 2020. Structural Biology of RNA Polymerase II Transcription: 20 Years On. *Annu Rev Cell Dev Biol,* 36**,** 1-34.

OUGHTRED, R., RUST, J., CHANG, C., BREITKREUTZ, B. J., STARK, C., WILLEMS, A., BOUCHER, L., LEUNG, G., KOLAS, N., ZHANG, F., DOLMA, S., COULOMBE-HUNTINGTON, J., CHATR-ARYAMONTRI, A., DOLINSKI, K. & TYERS, M. 2021. The BioGRID database: A comprehensive biomedical resource of curated protein, genetic, and chemical interactions. *Protein Sci,* 30**,** 187-200.

PACINI, C., DEMPSTER, J. M., BOYLE, I., GONCALVES, E., NAJGEBAUER, H., KARAKOC, E., VAN DER MEER, D., BARTHORPE, A., LIGHTFOOT, H., JAAKS, P., MCFARLAND, J. M., GARNETT, M. J., TSHERNIAK, A. & IORIO, F. 2021. Integrated cross-study datasets of genetic dependencies in cancer. *Nat Commun,* 12**,** 1661.

PANIER, S. & BOULTON, S. J. 2014. Double-strand break repair: 53BP1 comes into focus. *Nat Rev Mol Cell Biol,* 15**,** 7-18.

PARUA, P. K., KALAN, S., BENJAMIN, B., SANSO, M. & FISHER, R. P. 2020. Distinct Cdk9-phosphatase switches act at the beginning and end of elongation by RNA polymerase II. *Nat Commun,* 11**,** 4338.

PENG, X., WU, J., BRUNMEIR, R., KIM, S. Y., ZHANG, Q., DING, C., HAN, W., XIE, W. & XU, F. 2015. TELP, a sensitive and versatile library construction method for next-generation sequencing. *Nucleic Acids Res,* 43**,** e35.

PEREZ-ARNAIZ, P., BRUCK, I. & KAPLAN, D. L. 2016. Mcm10 coordinates the timely assembly and activation of the replication fork helicase. *Nucleic Acids Res,* 44**,** 315-29.

PEREZ-RIVEROL, Y., BAI, J., BANDLA, C., GARCIA-SEISDEDOS, D., HEWAPATHIRANA, S., KAMATCHINATHAN, S., KUNDU, D. J., PRAKASH, A., FRERICKS-ZIPPER, A., EISENACHER, M., WALZER, M., WANG, S., BRAZMA, A. & VIZCAINO, J. A. 2022. The PRIDE database resources in 2022: a hub for mass spectrometry-based proteomics evidences. *Nucleic Acids Res,* 50**,** D543-D552.

PETER, S., BULTINCK, J., MYANT, K., JAENICKE, L. A., WALZ, S., MULLER, J., GMACHL, M., TREU, M., BOEHMELT, G., ADE, C. P., SCHMITZ, W., WIEGERING, A., OTTO, C., POPOV, N., SANSOM, O., KRAUT, N. & EILERS, M. 2014. Tumor cell-specific

inhibition of MYC function using small molecule inhibitors of the HUWE1 ubiquitin ligase. *EMBO Mol Med,* 6**,** 1525-41.

PETERLIN, B. M. & PRICE, D. H. 2006. Controlling the elongation phase of transcription with P-TEFb. *Mol Cell,* 23**,** 297-305.

PETERMANN, E., ORTA, M. L., ISSAEVA, N., SCHULTZ, N. & HELLEDAY, T. 2010. Hydroxyurea-stalled replication forks become progressively inactivated and require two different RAD51-mediated pathways for restart and repair. *Mol Cell,* 37**,** 492-502.

PFISTER, S. X., MARKKANEN, E., JIANG, Y., SARKAR, S., WOODCOCK, M., ORLANDO, G., MAVROMMATI, I., PAI, C. C., ZALMAS, L. P., DROBNITZKY, N., DIANOV, G. L., VERRILL, C., MACAULAY, V. M., YING, S., LA THANGUE, N. B., D'ANGIOLELLA, V., RYAN, A. J. & HUMPHREY, T. C. 2015. Inhibiting WEE1 Selectively Kills Histone H3K36me3-Deficient Cancers by dNTP Starvation. *Cancer Cell,* 28**,** 557-568.

POLI, J., GERHOLD, C. B., TOSI, A., HUSTEDT, N., SEEBER, A., SACK, R., HERZOG, F., PASERO, P., SHIMADA, K., HOPFNER, K. P. & GASSER, S. M. 2016. Mec1, INO80, and the PAF1 complex cooperate to limit transcription replication conflicts through RNAPII removal during replication stress. *Genes Dev,* 30**,** 337-54.

POMMIER, Y., SUN, Y., HUANG, S. N. & NITISS, J. L. 2016. Roles of eukaryotic topoisomerases in transcription, replication and genomic stability. *Nat Rev Mol Cell Biol,* 17**,** 703-721.

POREBSKI, B., WILD, S., KUMMER, S., SCAGLIONE, S., GAILLARD, P. L. & GARI, K. 2019. WRNIP1 Protects Reversed DNA Replication Forks from SLX4-Dependent Nucleolytic Cleavage. *iScience,* 21**,** 31-41.

PRIMO, L. M. F. & TEIXEIRA, L. K. 2019. DNA replication stress: oncogenes in the spotlight. *Genet Mol Biol,* 43**,** e20190138.

PUNDIR, S., MARTIN, M. J. & O'DONOVAN, C. 2017. UniProt protein knowledgebase. *Protein Bioinformatics.* Springer.

QI, C. F., KIM, Y. S., XIANG, S., ABDULLAEV, Z., TORREY, T. A., JANZ, S., KOVALCHUK, A. L., SUN, J., CHEN, D., CHO, W. C., GU, W. & MORSE III, H. C. 2012. Characterization of ARF-BP1/HUWE1 interactions with CTCF, MYC, ARF and p53 in MYC-driven B cell neoplasms. *Int J Mol Sci,* 13**,** 6204-6219.

QI, L., XU, X. & QI, X. 2022. The giant E3 ligase HUWE1 is linked to tumorigenesis, spermatogenesis, intellectual disability, and inflammatory diseases. *Front Cell Infect Microbiol,* 12**,** 905906.

QIU, H., HU, C., GAUR, N. A. & HINNEBUSCH, A. G. 2012. Pol II CTD kinases Bur1 and Kin28 promote Spt5 CTR-independent recruitment of Paf1 complex. *EMBO J,* 31**,** 3494-505.

QU, H., LIU, H., JIN, Y., CUI, Z. & HAN, G. 2018. HUWE1 upregulation has tumor suppressive effect in human prostate cancer cell lines through c-Myc. *Biomedicine & Pharmacotherapy,* 106**,** 309-315.

RAMANATHAN, A., ROBB, G. B. & CHAN, S. H. 2016. mRNA capping: biological functions and applications. *Nucleic Acids Res,* 44**,** 7511-26.

RAN, F. A., HSU, P. D., WRIGHT, J., AGARWALA, V., SCOTT, D. A. & ZHANG, F. 2013. Genome engineering using the CRISPR-Cas9 system. *Nat Protoc,* 8**,** 2281-2308.

RAPPSILBER, J., MANN, M. & ISHIHAMA, Y. 2007. Protocol for micro-purification, enrichment, pre-fractionation and storage of peptides for proteomics using StageTips. *Nat Protoc,* 2**,** 1896-906.

RICKMAN, K. & SMOGORZEWSKA, A. 2019. Advances in understanding DNA processing and protection at stalled replication forks. *J Cell Biol,* 218**,** 1096-1107.

RIPLEY, B. M., GILDENBERG, M. S. & WASHINGTON, M. T. 2020. Control of DNA Damage Bypass by Ubiquitylation of PCNA. *Genes (Basel),* 11**,** 138.

RIVERA-MULIA, J. C. & GILBERT, D. M. 2016. Replication timing and transcriptional control: beyond cause and effect-part III. *Curr Opin Cell Biol,* 40**,** 168-178.

ROBINSON, M. D., MCCARTHY, D. J. & SMYTH, G. K. 2010. edgeR: a Bioconductor package for differential expression analysis of digital gene expression data. *Bioinformatics,* 26**,** 139-40.

ROBISON, J. G., ELLIOTT, J., DIXON, K. & OAKLEY, G. G. 2004. Replication protein A and the Mre11.Rad50.Nbs1 complex co-localize and interact at sites of stalled replication forks. *J Biol Chem,* 279**,** 34802-10.

RONCO, C., MARTIN, A. R., DEMANGE, L. & BENHIDA, R. 2017. ATM, ATR, CHK1, CHK2 and WEE1 inhibitors in cancer and cancer stem cells. *Medchemcomm,* 8**,** 295-319.

SALIFOU, K., BURNARD, C., BASAVARAJAIAH, P., GRASSO, G., HELSMOORTEL, M., MAC, V., DEPIERRE, D., FRANCKHAUSER, C., BEYNE, E., CONTRERAS, X., DEJARDIN, J., ROUQUIER, S., CUVIER, O. & KIERNAN, R. 2021. Chromatin-associated MRN complex protects highly transcribing genes from genomic instability. *Sci Adv,* 7**,** eabb2947.

SANJANA, N. E., SHALEM, O. & ZHANG, F. 2014. Improved vectors and genome-wide libraries for CRISPR screening. *Nat Methods,* 11**,** 783-784.

SAPONARO, M. 2022. Transcription-Replication Coordination. *Life (Basel),* 12**,** 108.

SAUGAR, I., PARKER, J. L., ZHAO, S. & ULRICH, H. D. 2012. The genome maintenance factor Mgs1 is targeted to sites of replication stress by ubiquitylated PCNA. *Nucleic Acids Res,* 40**,** 245-57.

SAXENA, S. & ZOU, L. 2022. Hallmarks of DNA replication stress. *Mol Cell,* 82**,** 2298-2314.

SCHAUB, F. X., DHANKANI, V., BERGER, A. C., TRIVEDI, M., RICHARDSON, A. B., SHAW, R., ZHAO, W., ZHANG, X., VENTURA, A., LIU, Y., AYER, D. E., HURLIN, P. J., CHERNIACK, A. D., EISENMAN, R. N., BERNARD, B., GRANDORI, C. & CANCER GENOME ATLAS, N. 2018. Pan-cancer Alterations of the MYC Oncogene and Its Proximal Network across the Cancer Genome Atlas. *Cell Syst,* 6**,** 282-300 e2.

SCHIER, A. C. & TAATJES, D. J. 2020. Structure and mechanism of the RNA polymerase II transcription machinery. *Genes Dev,* 34**,** 465-488.

SCHINDELIN, J., ARGANDA-CARRERAS, I., FRISE, E., KAYNIG, V., LONGAIR, M., PIETZSCH, T., PREIBISCH, S., RUEDEN, C., SAALFELD, S., SCHMID, B., TINEVEZ, J. Y., WHITE, D. J., HARTENSTEIN, V., ELICEIRI, K., TOMANCAK, P. & CARDONA, A. 2012. Fiji: an open-source platform for biological-image analysis. *Nat Methods,* 9**,** 676-82.

SCHLEICHER, E. M., DHOONMOON, A., JACKSON, L. M., KHATIB, J. B., NICOLAE, C. M. & MOLDOVAN, G. L. 2022. The TIP60-ATM axis regulates replication fork stability in BRCA-deficient cells. *Oncogenesis,* 11**,** 33.

SCHMITT, E., PAQUET, C., BEAUCHEMIN, M. & BERTRAND, R. 2007. DNA-damage response network at the crossroads of cell-cycle checkpoints, cellular senescence and apoptosis. *Journal of Zhejiang University Science B,* 8**,** 377-397.

SHAO, X., JOERGENSEN, A. M., HOWLETT, N. G., LISBY, M. & OESTERGAARD, V. H. 2020. A distinct role for recombination repair factors in an early cellular response to transcription-replication conflicts. *Nucleic Acids Res,* 48**,** 5467-5484.

SHARMA, S., ANAND, R., ZHANG, X., FRANCIA, S., MICHELINI, F., GALBIATI, A., WILLIAMS, H., RONATO, D. A., MASSON, J. Y., ROTHENBERG, E., CEJKA, P. & D'ADDA DI FAGAGNA, F. 2021. MRE11-RAD50-NBS1 Complex Is Sufficient to Promote Transcription by RNA Polymerase II at Double-Strand Breaks by Melting DNA Ends. *Cell Rep,* 34**,** 108565.

SHEN, M., YOUNG, A. & AUTEXIER, C. 2021. PCNA, a focus on replication stress and the alternative lengthening of telomeres pathway. *DNA Repair (Amst),* 100**,** 103055.

SHERILL-ROFE, D., RABAN, O., FINDLAY, S., RAHAT, D., UNTERMAN, I., SAMIEI, A., YASMEEN, A., KAISER, Z., KUASNE, H., PARK, M., FOULKES, W. D., BLOCH, I., ZICK, A., GOTLIEB, W. H., TABACH, Y. & ORTHWEIN, A. 2022. Multi-omics data integration analysis identifies the spliceosome as a key regulator of DNA double-strand break repair. *NAR Cancer,* 4**,** zcac013.

SHILATIFARD, A., CONAWAY, R. C. & CONAWAY, J. W. 2003. The RNA polymerase II elongation complex. *Annu Rev Biochem,* 72**,** 693-715.

SHILOH, Y. & ZIV, Y. 2013. The ATM protein kinase: regulating the cellular response to genotoxic stress, and more. *Nat Rev Mol Cell Biol,* 14**,** 197-210.

SIMS, R. J., 3RD, BELOTSERKOVSKAYA, R. & REINBERG, D. 2004. Elongation by RNA polymerase II: the short and long of it. *Genes Dev,* 18**,** 2437-68.

SIRBU, B. M., COUCH, F. B., FEIGERLE, J. T., BHASKARA, S., HIEBERT, S. W. & CORTEZ, D. 2011. Analysis of protein dynamics at active, stalled, and collapsed replication forks. *Genes Dev,* 25**,** 1320-7.

SKOURTI-STATHAKI, K., KAMIENIARZ-GDULA, K. & PROUDFOOT, N. J. 2014. R-loops induce repressive chromatin marks over mammalian gene terminators. *Nature,* 516**,** 436-9.

SKOURTI-STATHAKI, K. & PROUDFOOT, N. J. 2014. A double-edged sword: R loops as threats to genome integrity and powerful regulators of gene expression. *Genes Dev,* 28**,** 1384-96.

SLUIMER, J. & DISTEL, B. 2018. Regulating the human HECT E3 ligases. *Cell Mol Life Sci,* 75**,** 3121-3141.

STEWART, S. A., DYKXHOORN, D. M., PALLISER, D., MIZUNO, H., YU, E. Y., AN, D. S., SABATINI, D. M., CHEN, I. S., HAHN, W. C., SHARP, P. A., WEINBERG, R. A. & NOVINA, C. D. 2003. Lentivirus-delivered stable gene silencing by RNAi in primary cells. *RNA,* 9**,** 493-501.

STIFF, T., O'DRISCOLL, M., RIEF, N., IWABUCHI, K., LOBRICH, M. & JEGGO, P. A. 2004. ATM and DNA-PK function redundantly to phosphorylate H2AX after exposure to ionizing radiation. *Cancer Res,* 64**,** 2390-6.

SUBRAMANIAN, A., TAMAYO, P., MOOTHA, V. K., MUKHERJEE, S., EBERT, B. L., GILLETTE, M. A., PAULOVICH, A., POMEROY, S. L., GOLUB, T. R., LANDER, E. S. & MESIROV, J. P. 2005. Gene set enrichment analysis: a knowledge-based approach for interpreting genome-wide expression profiles. *Proc Natl Acad Sci U S A,* 102**,** 15545-50.

SUNG, H., FERLAY, J., SIEGEL, R. L., LAVERSANNE, M., SOERJOMATARAM, I., JEMAL, A. & BRAY, F. 2021. Global Cancer Statistics 2020: GLOBOCAN Estimates of Incidence and Mortality Worldwide for 36 Cancers in 185 Countries. *CA Cancer J Clin,* 71**,** 209-249.

SWATEK, K. N. & KOMANDER, D. 2016. Ubiquitin modifications. *Cell Res,* 26**,** 399-422.

SYDOW, J. F. & CRAMER, P. 2009. RNA polymerase fidelity and transcriptional proofreading. *Curr Opin Struct Biol,* 19**,** 732-9.

SYED, A. & TAINER, J. A. 2018. The MRE11-RAD50-NBS1 Complex Conducts the Orchestration of Damage Signaling and Outcomes to Stress in DNA Replication and Repair. *Annu Rev Biochem,* 87**,** 263-294.

TENNYSON, C. N., KLAMUT, H. J. & WORTON, R. G. 1995. The human dystrophin gene requires 16 hours to be transcribed and is cotranscriptionally spliced. *Nat Genet,* 9**,** 184-90.

TICAU, S., FRIEDMAN, L. J., IVICA, N. A., GELLES, J. & BELL, S. P. 2015. Single-molecule studies of origin licensing reveal mechanisms ensuring bidirectional helicase loading. *Cell,* 161**,** 513-525.

TITOV, D. V., GILMAN, B., HE, Q. L., BHAT, S., LOW, W. K., DANG, Y., SMEATON, M., DEMAIN, A. L., MILLER, P. S., KUGEL, J. F., GOODRICH, J. A. & LIU, J. O. 2011. XPB, a subunit of TFIIH, is a target of the natural product triptolide. *Nat Chem Biol,* 7**,** 182-8.

TOLEDO, L. I., ALTMEYER, M., RASK, M. B., LUKAS, C., LARSEN, D. H., POVLSEN, L. K., BEKKER-JENSEN, S., MAILAND, N., BARTEK, J. & LUKAS, J. 2014. ATR Prohibits Replication Catastrophe by Preventing Global Exhaustion of RPA (vol 155, pg 1088, 2013). *Cell,* 156**,** 374-374.

TRENZ, K., SMITH, E., SMITH, S. & COSTANZO, V. 2006. ATM and ATR promote Mre11 dependent restart of collapsed replication forks and prevent accumulation of DNA breaks. *EMBO J,* 25**,** 1764-74.

TRESINI, M., WARMERDAM, D. O., KOLOVOS, P., SNIJDER, L., VROUWE, M. G., DEMMERS, J. A., VAN, I. W. F., GROSVELD, F. G., MEDEMA, R. H., HOEIJMAKERS, J. H., MULLENDERS, L. H., VERMEULEN, W. & MARTEIJN, J. A. 2015. The core

spliceosome as target and effector of non-canonical ATM signalling. *Nature,* 523**,** 53-8.

TROTTER, K. W., KING, H. A. & ARCHER, T. K. 2015. Glucocorticoid Receptor Transcriptional Activation via the BRG1-Dependent Recruitment of TOP2beta and Ku70/86. *Mol Cell Biol,* 35**,** 2799-817.

TSHERNIAK, A., VAZQUEZ, F., MONTGOMERY, P. G., WEIR, B. A., KRYUKOV, G., COWLEY, G. S., GILL, S., HARRINGTON, W. F., PANTEL, S., KRILL-BURGER, J. M., MEYERS, R. M., ALI, L., GOODALE, A., LEE, Y., JIANG, G., HSIAO, J., GERATH, W. F. J., HOWELL, S., MERKEL, E., GHANDI, M., GARRAWAY, L. A., ROOT, D. E., GOLUB, T. R., BOEHM, J. S. & HAHN, W. C. 2017. Defining a Cancer Dependency Map. *Cell,* 170**,** 564-576 e16.

TYANOVA, S., TEMU, T. & COX, J. 2016a. The MaxQuant computational platform for mass spectrometry-based shotgun proteomics. *Nat Protoc,* 11**,** 2301-2319.

TYANOVA, S., TEMU, T., SINITCYN, P., CARLSON, A., HEIN, M. Y., GEIGER, T., MANN, M. & COX, J. 2016b. The Perseus computational platform for comprehensive analysis of (prote)omics data. *Nat Methods,* 13**,** 731-40.

UI, A., CHIBA, N. & YASUI, A. 2020. Relationship among DNA double-strand break (DSB), DSB repair, and transcription prevents genome instability and cancer. *Cancer Sci,* 111**,** 1443-1451.

ULRICH, H. D. 2009. Regulating post-translational modifications of the eukaryotic replication clamp PCNA. *DNA Repair (Amst),* 8**,** 461-9.

VAZQUEZ, F. & BOEHM, J. S. 2020. The Cancer Dependency Map enables drug mechanism-of-action investigations. *Mol Syst Biol,* 16**,** e9757.

VIDAKOVIĆ, A. T., MITTER, R., KELLY, G. P., NEUMANN, M., HARREMAN, M., RODRÍGUEZ-MARTÍNEZ, M., HERLIHY, A., WEEMS, J. C., BOEING, S. & ENCHEVA, V. 2020. Regulation of the RNAPII pool is integral to the DNA damage response. *Cell,* 180**,** 1245-1261. e21.

VOS, S. M., FARNUNG, L., URLAUB, H. & CRAMER, P. 2018. Structure of paused transcription complex Pol II-DSIF-NELF. *Nature,* 560**,** 601-606.

WALMACQ, C., WANG, L., CHONG, J., SCIBELLI, K., LUBKOWSKA, L., GNATT, A., BROOKS, P. J., WANG, D. & KASHLEV, M. 2015. Mechanism of RNA polymerase II bypass of oxidative cyclopurine DNA lesions. *Proc Natl Acad Sci U S A,* 112**,** E410-9.

WANG, D., BUSHNELL, D. A., HUANG, X., WESTOVER, K. D., LEVITT, M. & KORNBERG, R. D. 2009. Structural basis of transcription: backtracked RNA polymerase II at 3.4 angstrom resolution. *Science,* 324**,** 1203-6.

WANG, L., ZHOU, Y., XU, L., XIAO, R., LU, X., CHEN, L., CHONG, J., LI, H., HE, C., FU, X. D. & WANG, D. 2015. Molecular basis for 5-carboxycytosine recognition by RNA polymerase II elongation complex. *Nature,* 523**,** 621-5.

WANG, W., WALMACQ, C., CHONG, J., KASHLEV, M. & WANG, D. 2018. Structural basis of transcriptional stalling and bypass of abasic DNA lesion by RNA polymerase II. *Proc Natl Acad Sci U S A,* 115**,** E2538-E2545.

WANG, W., XU, L., HU, L., CHONG, J., HE, C. & WANG, D. 2017. Epigenetic DNA Modification N(6)-Methyladenine Causes Site-Specific RNA Polymerase II Transcriptional Pausing. *J Am Chem Soc,* 139**,** 14436-14442.

WARD, I. M. & CHEN, J. 2001. Histone H2AX is phosphorylated in an ATR-dependent manner in response to replicational stress. *J Biol Chem,* 276**,** 47759-62.

WEBER, A. M. & RYAN, A. J. 2015. ATM and ATR as therapeutic targets in cancer. *Pharmacol Ther,* 149**,** 124-38.

WEBER, J., POLO, S. & MASPERO, E. 2019. HECT E3 Ligases: A Tale With Multiple Facets. *Front Physiol,* 10**,** 370.

WEI, R., LIU, X., YU, W., YANG, T., CAI, W., LIU, J., HUANG, X., XU, G. T., ZHAO, S., YANG, J. & LIU, S. 2015. Deubiquitinases in cancer. *Oncotarget,* 6**,** 12872-89.

WELCSH, P. L., OWENS, K. N. & KING, M. C. 2000. Insights into the functions of BRCA1 and BRCA2. *Trends Genet,* 16**,** 69-74.

WEST, S., GROMAK, N. & PROUDFOOT, N. J. 2004. Human 5' --> 3' exonuclease Xrn2 promotes transcription termination at co-transcriptional cleavage sites. *Nature,* 432**,** 522-5.

WHITESIDE, T. L. 2008. The tumor microenvironment and its role in promoting tumor growth. *Oncogene,* 27**,** 5904-12.

WIEDERSCHAIN, D., WEE, S., CHEN, L., LOO, A., YANG, G., HUANG, A., CHEN, Y., CAPONIGRO, G., YAO, Y. M., LENGAUER, C., SELLERS, W. R. & BENSON, J. D. 2009. Single-vector inducible lentiviral RNAi system for oncology target validation. *Cell Cycle,* 8**,** 498-504.

WIESE, K. E., HAIKALA, H. M., VON EYSS, B., WOLF, E., ESNAULT, C., ROSENWALD, A., TREISMAN, R., KLEFSTRÖM, J. & EILERS, M. 2015. Repression of SRF target genes is critical for M yc-dependent apoptosis of epithelial cells. *The EMBO journal,* 34**,** 1554-1571.

WOOD, A., SCHNEIDER, J., DOVER, J., JOHNSTON, M. & SHILATIFARD, A. 2003. The Paf1 complex is essential for histone monoubiquitination by the Rad6-Bre1 complex, which signals for histone methylation by COMPASS and Dot1p. *J Biol Chem,* 278**,** 34739-42.

YADAV, B., WENNERBERG, K., AITTOKALLIO, T. & TANG, J. 2015. Searching for Drug Synergy in Complex Dose-Response Landscapes Using an Interaction Potency Model. *Comput Struct Biotechnol J,* 13**,** 504-13.

YAMADA, T., YAMAGUCHI, Y., INUKAI, N., OKAMOTO, S., MURA, T. & HANDA, H. 2006. P-TEFb-mediated phosphorylation of hSpt5 C-terminal repeats is critical for processive transcription elongation. *Mol Cell,* 21**,** 227-37.

YANG, D., CHENG, D., TU, Q., YANG, H., SUN, B., YAN, L., DAI, H., LUO, J., MAO, B., CAO, Y., YU, X., JIANG, H. & ZHAO, X. 2018. HUWE1 controls the development of non-small cell lung cancer through down-regulation of p53. *Theranostics,* 8**,** 3517-3529.

YANG, J., XU, Z. P., HUANG, Y., HAMRICK, H. E., DUERKSEN-HUGHES, P. J. & YU, Y. N. 2004. ATM and ATR: sensing DNA damage. *World J Gastroenterol,* 10**,** 155-60.

YANG, X. H. & ZOU, L. 2009. Dual functions of DNA replication forks in checkpoint signaling and PCNA ubiquitination. *Cell Cycle,* 8**,** 191-4.

YASUHARA, T., KATO, R., HAGIWARA, Y., SHIOTANI, B., YAMAUCHI, M., NAKADA, S., SHIBATA, A. & MIYAGAWA, K. 2018. Human Rad52 Promotes XPG-Mediated R-loop Processing to Initiate Transcription-Associated Homologous Recombination Repair. *Cell,* 175**,** 558-570 e11.

YU, D. S., ZHAO, R., HSU, E. L., CAYER, J., YE, F., GUO, Y., SHYR, Y. & CORTEZ, D. 2010. Cyclin-dependent kinase 9-cyclin K functions in the replication stress response. *EMBO Rep,* 11**,** 876-82.

YU, M., YANG, W., NI, T., TANG, Z., NAKADAI, T., ZHU, J. & ROEDER, R. G. 2015. RNA polymerase II-associated factor 1 regulates the release and phosphorylation of paused RNA polymerase II. *Science,* 350**,** 1383-6.

ZENKIN, N., YUZENKOVA, Y. & SEVERINOV, K. 2006. Transcript-assisted transcriptional proofreading. *Science,* 313**,** 518-20.

ZERNIK-KOBAK, M., VASUNIA, K., CONNELLY, M., ANDERSON, C. W. & DIXON, K. 1997. Sites of UV-induced phosphorylation of the p34 subunit of replication protein A from HeLa cells. *J Biol Chem,* 272**,** 23896-904.

ZHANG, H., RIGO, F. & MARTINSON, H. G. 2015. Poly (A) signal-dependent transcription termination occurs through a conformational change mechanism that does not require cleavage at the poly (A) site. *Molecular cell,* 59**,** 437-448.

ZHAO, H. & PIWNICA-WORMS, H. 2001. ATR-mediated checkpoint pathways regulate phosphorylation and activation of human Chk1. *Mol Cell Biol,* 21**,** 4129-39.

ZHENG, L., KANAGARAJ, R., MIHALJEVIC, B., SCHWENDENER, S., SARTORI, A. A., GERRITS, B., SHEVELEV, I. & JANSCAK, P. 2009. MRE11 complex links RECQ5 helicase to sites of DNA damage. *Nucleic Acids Res,* 37**,** 2645-57.

ZHENG, N. & SHABEK, N. 2017. Ubiquitin Ligases: Structure, Function, and Regulation. *Annu Rev Biochem,* 86**,** 129-157.

ZHONG, Q., GAO, W., DU, F. & WANG, X. 2005. Mule/ARF-BP1, a BH3-only E3 ubiquitin ligase, catalyzes the polyubiquitination of Mcl-1 and regulates apoptosis. *Cell,* 121**,** 1085-95.

ZOU, L. & ELLEDGE, S. J. 2003. Sensing DNA damage through ATRIP recognition of RPA-ssDNA complexes. *Science,* 300**,** 1542-8.

ZOU, T. & LIN, Z. 2021. The Involvement of Ubiquitination Machinery in Cell Cycle Regulation and Cancer Progression. *Int J Mol Sci,* 22**,** 5754.

ZUO, Z., ZHOU, Z., CHANG, Y., LIU, Y., SHEN, Y., LI, Q. & ZHANG, L. 2022. Ribonucleotide reductase M2 (RRM2): Regulation, function and targeting strategy in human cancer. *Genes & Diseases*.

# 10 Appendix

## 10.1 Acknowledgements

First of all, I want to thank Prof. Dr. Nikita Popov for enabling this work, for his constant guidance and the many opportunities to learn novel skills. Plenty of fruitful discussions and solid support contributed to my motivation to strive for new discoveries. Thank you, Nikita! Further, I want to express my gratitude towards Prof. Dr. Boris Maček for his interest in this thesis and being the primary referee. Thanks to the training in mass spectrometry related techniques and access to the machines in the laboratory of Prof. Dr. Boris Maček, I could generate valuable data early upon starting this project. Thank you, Boris, for this opportunity! Moreover, I want to thank the other members of my thesis committee, Prof. Dr. Jennifer Ewald and Prof. Dr. Matthias Gehringer, for the chance to present my work and for their effort in its evaluation.

What would science be without great colleagues? Therefore, I want to thank the members of the Popov group for generating a supportive work atmosphere, especially Valentina Andrioletti for her initial work, Dr. Vanessa Rousseau and Ravi Babu Kollampally for teaching methods and Kseniya Popova, as well as Chao Jin for their support. Moreover, I want to thank the members of the Proteome Center Tübingen including Dr. Katharina Zittlau, Dr. Ana Velic, Dr. Philipp Spät, Dr. Nicolas Nalpas, Irina Droste-Borel, Dr. Mirita Franz-Wachtel and Uli Grammig. During the daily lab life, I spent a substantial part of my time together with members of the group of Prof. Dr. Lars Zender and therefore I want to thank you for discussions and support during lab meetings and for sharing thoughts, difficulties and hopes with each other. This includes, but is not limited to Stefan Zwirner, Pascal Wölffing, Dr. Omelyan Trompak, Svenja Schütte, Jorge Macedo, Aylin Heinrich, Dr. Daniel Dauch and Prof. Dr. Lars Zender. Thanks to the work and interest of Prof. Dr. Matthias Gehringer and Xiaojun Julia Liang, I was able to test preliminary inhibitors to pharmacologically target HUWE1.

Moreover, I want to thank the lady at the cafeteria counter for providing tasty chocolate muffins whenever needed. Helpful advice and criticism from my friends and my family contributed to shape my perspective on solutions rather than problems. From the bottom of my heart I want to thank Dr. Ulrike Harant for the biggest present a person may receive and that she is able to always place a broad smile on my face, which I am happy to distribute further. Thank you.

At last, I want to thank you, the reader of this thesis, for the time, interest in reading and determination in understanding this work.

## 10.2 List of authorships

**EINIG, E.**, JIN, C., ANDRIOLETTI, V., MACEK, B. & POPOV, N. 2023. RNAPII-dependent ATM signaling at collisions with replication forks. *Nature Communications*.

JIN, C., **EINIG, E.**, KOLLAMPALLY, R. B., XU, W., SCHLOSSER, A., FLENTJE, M. & POPOV, N. (under revision). The dimeric deubiquitinase Usp28 integrates 53bp1 and Myc functions to control DNA replication.

MAIER, C. R., HARTMANN, O., PRIETO-GARCIA, C., AL-SHAMI, K. M., SCHLICKER, L., VOGEL, F. C. E., HAID, S., KLANN, K., BUCK, V., MUNCH, C., SCHMITZ, W., **EINIG, E.**, KRENZ, B., CALZADO, M. A., EILERS, M., POPOV, N., ROSENFELDT, M. T., DIEFENBACHER, M. E. & SCHULZE, A. 2023. USP28 controls SREBP2 and the mevalonate pathway to drive tumour growth in squamous cancer. *Cell Death Differ***,** 1-16.

ROUSSEAU, V., **EINIG, E.**, JIN, C., HORN, J., RIEBOLD, M., POTH, T., JARBOUI, M. A., FLENTJE, M. & POPOV, N. 2023. Trim33 masks a non-transcriptional function of E2f4 in replication fork progression. *Nature Communications,* 14**,** 5143.

RUDALSKA, R., HARBIG, J., SNAEBJORNSSON, M. T., KLOTZ, S., ZWIRNER, S., TARANETS, L., HEINZMANN, F., KRONENBERGER, T., FORSTER, M., CUI, W., D'ARTISTA, L., **EINIG, E.**, HINTERLEITNER, M., SCHMITZ, W., DYLAWERSKA, A., KANG, T. W., POSO, A., ROSENFELDT, M. T., MALEK, N. P., BITZER, M., LAUFER, S., PICHLER, B. J., POPOV, N., SCHULZE, A., ZENDER, L. & DAUCH, D. 2021. LXRalpha activation and Raf inhibition trigger lethal lipotoxicity in liver cancer. *Nat Cancer,* 2**,** 201-217.

SANDRI, T. L., ANDRADE, F. A., LIDANI, K. C. F., **EINIG, E.**, BOLDT, A. B. W., MORDMULLER, B., ESEN, M. & MESSIAS-REASON, I. J. 2019. Human collectin-11 (COLEC11) and its synergic genetic interaction with MASP2 are associated with the pathophysiology of Chagas Disease. *PLoS Negl Trop Dis,* 13**,** e0007324.

WANG, L., ALBERT, M., **EINIG, E.**, FURST, U., KRUST, D. & FELIX, G. 2016. The pattern-recognition receptor CORE of Solanaceae detects bacterial cold-shock protein. *Nat Plants,* 2**,** 16185.

WANG, L., **EINIG, E.**, ALMEIDA-TRAPP, M., ALBERT, M., FLIEGMANN, J., MITHOFER, A., KALBACHER, H. & FELIX, G. 2018. The systemin receptor SYR1 enhances resistance of tomato against herbivorous insects. *Nat Plants,* 4**,** 152-156.

## 10.3 Statement of contributions

**Elias Einig** conceptualized, planned and analyzed experiments and conducted experimental work including all cell culture work, cloning and transfection of vector constructs, biochemical assays, proteomic experiments and sample preparation for NGS analysis, if not stated otherwise. Acquired data was processed, analyzed, displayed and interpreted by Elias Einig, if not stated otherwise. Elias Einig authored the dissertation.

**Nikita Popov** supervised and conceptualized this study, developed the central research idea and supported experiments with valuable discussions. Nikita Popov provided funding and resources, performed experiments, analyzed data, in particular NGS data, interpreted data and gave advice on data presentation and many aspects of conducting solid research.

**Valentina Andrioletti** generated the HUWE1-WT and HUWE1-CS cell lines and validated the correct gene targeting by Sanger sequencing. Valentina Andrioletti cloned the sgRNA library into the pLentiCRISPR_V2 vector backbone.

**Chao Jin** performed neutral comet assays.

**Boris Maček** provided the mass spectrometry instrumentation, materials for LC-MS/MS sample preparation and feedback on the conceptualization of mass spectrometry experiments.

## 10.4 List of Abbreviations

***Table 11: List of abbreviations.***

| Symbol | Name | Symbol | Name |
|---|---|---|---|
| kg | kilogram | DSB | DNA double strand break |
| g | gram | DSIF | DRB-sensitivity inhibitory factor |
| mg | milligram | DUB | Deubiquitinase |
| µg | microgram | GSEA | Gene set enrichment analysis |
| ng | nanogram | GTF | General transcription factor |
| l | liter | HR | Homology directed repair |
| ml | milliliter | HECT | Homologous to E6AP C terminus |
| µl | microliter | HU | Hydroxyurea |
| nl | nanoliter | HUWE1 | HECT, UBA, and WWE domain containing protein 1 |
| d | days | IP | Immunoprecipitation |
| h | hours | LZ | Leucine zipper |
| min | minutes | MEF | Mouse embryonic fibroblasts |
| s | seconds | MSI | Microsatellite instability |
| M | molar | NELF | Negative elongation factor |
| mM | millimolar | PAF1c | Polymerase associated factor 1 complex |
| µM | micromolar | PAS | Polyadenylation signal |
| nM | nanomolar | PIC | Pre-initiation complex |
| mm | millimeter | PLA | Proximity ligation assay |
| kb | kilo bases | PTM | Post-translational modification |
| bp | base pairs | RBR | RING-between-RING |
| °C | degree celsius | RING | Really interesting new genes |
| ppm | parts per million | RNAPII | RNA polymerase II |
| U | units | TC-NER | Transcription-coupled nucleotide excision repair |
| CDK | cyclin dependent kinase | TLS | Translesion synthesis |
| CIMP | CpG island methylator phenotype | TRC | Transcription replication conflict |
| CIN | Chromosomal instability | TSS | Transcription start site |
| CTD | Carboxyl-terminal domain | TTS | Transcription termination site |
| DDR | DNA damage response | UBD | Ubiquitin binding domain |
| dilncRNA | damage induced long non-coding RNA | UBZ | Ubiquitin zinc finger |
| DRB | 5,6-dichloro-1-beta-D-ribofuranosylbenzimidazole | WRNIP1 | Werner helicase interacting protein 1 |